RESPONSE TRANSMISSIBILITY FOR LOAD IDENTIFICATION IMPROVED BY OPTIMAL SENSOR LOCATIONS

by

Hana'a Mohammad Alqam

A Dissertation Submitted in

Partial Fulfillment of the

Requirements for the Degree of

Doctor of Philosophy

in Engineering

at

The University of Wisconsin – Milwaukee

August 2019

ABSTRACT

RESPONSE TRANSMISSIBILITY FOR LOAD IDENTIFICATION IMPROVED BY OPTIMAL SENSOR LOCATIONS

by

Hana'a M. Alqam

The University of Wisconsin - Milwaukee, 2019

Under the Supervision of Professor Anoop K. Dhingra

A knowledge of loads acting on a structure is important for analysis and design. There are many applications in which it is difficult to measure directly the dynamic loads acting on a component. In such situations, it may be possible to estimate the imposed loads through a measurement of the system output response. Load identification through output response measurement is an inverse problem that is not only ill-conditioned, but in general leads to multiple solutions. Therefore, additional information, such as number and locations of the imposed loads must be provided ahead of time in order to allow for a unique solution. This dissertation focuses on cases where such information is not readily accessible and presents a method for identification of loads applied to a structure using the concept of response transmissibility. The solution approach is divided into two phases that involve finding the number and location of forces first followed by a reconstruction of the load vector. To achieve the first phase, a complete description of the structure in terms of degrees of freedom needs to be specified and a numerical model, usually a finite element model is built. In order to determine the number of forces and their locations, the proposed algorithm combines the dynamic responses measured

experimentally along with the transmissibility matrices obtained from the numerical model. Once the number of loads and their locations are known, a regeneration of the load vector is achieved during the second phase by combining the measured dynamic responses with the transmissibility matrix from the numerical model.

In this dissertation, identification of loads through measurement of structural response at a finite number of optimally selected locations is also investigated. Optimum sensor locations are identified using the D-optimal design algorithm. Two different types of measurements are considered, acceleration measurements using accelerometers and the strain measurements using strain gages.

A series of simulated results on multi-degree of freedom (MDOF) discrete and continuous systems are presented to illustrate the load identification technique based on response transmissibility. One of the factors that affects the accuracy of load reconstruction is the number of vibration modes included in the analysis, which can be a large number. Improvements using model order reduction, not only help reconstruct the input forces accurately, but it also reduces the computational burden significantly.

The developed algorithms are implemented using the finite element tool ANSYS in conjunction with MATLAB software. Numerical sensitivity analysis is also implemented to examine the effect of presence of uncertainties (noise) in experimental data. The results obtained confirm that the techniques presented are robust even in the presence of simulated noise; it is seen that the applied loads are recovered accurately.

To

my parents, my loving husband

and

my children

TABLE OF CONTENTS

LIST OF FIGURES

LIST OF TABLES

ACKNOWLEDGEMENTS

First of all, I would like to thank the Almighty Allah, who helped me in every step and gave me courage to complete this dissertation. It is with deep appreciation. I would like to thank my respected advisor Dr. Anoop Dhingra for his support and guidance. It would have been an impossible task for me if I had not been guided by him. The light of his valuable guidance has led me to complete this dissertation.

I would like to express greatest gratitude to my Ph.D. committee members-Dr. Ronald Perez, Dr. Ilya Avdeev, Dr. Devendra Misra and Dr. Wilkistar Otieno for their ideas, comments and suggestions.

Acknowledgement will be incomplete if I do not mention the moral support, encouragement, patience and cooperation of my loving husband Kamil Samara and the love and support of my mother. My very special thanks go to all my lab colleagues for their comments and suggestions, whenever needed, at various stages of my dissertation.

Chapter 1 - Introduction

1.1 Load Identification Problem

The process of determining applied loading (locations and magnitudes) from response measurements is not a new concept. However, while indirect measurement of loads has a lot of potential, but it also has lot of problems. It is, in fact, the basis for every type of load transducer ever devised, such as those used for measurement of cutting forces on a machine tool, reaction forces in engine mounts, and supporting forces on bearings. So, for a reliable and cost effective design and analysis of structures or engineering equipment, it is desirable to know at the design stage the locations and magnitudes of the external loads transmitted to the structure. These loads may be static or time varying dynamic loads. The stresses induced in the structure are a function of the applied loads. Knowledge of the loads early in the design process is vital for design optimization and effective analysis that ensures the structural integrity of the product. Accurate prediction of the loads leads to greater confidence in numerical simulation such as finite element analysis which, in turn, significantly reduces the reliance on expensive and time consuming experimental testing.

1.2 Restrictions of Load Transducers

There are some situations where the direct measurement of loads using load transducers is difficult or even impossible. For example, it is not feasible to place load cells for certain types of loads imposed on the structure such as aerodynamic loads,

seismic loads, etc. or when the loads which are not in direct contact with the structure. Furthermore, the inaccessibility of load transferring locations may restrict the user from introducing a load transducer which makes the direct method difficult to use. Under these circumstances, indirect identification of input loads from dynamic responses of the structure offers a valuable alternative as such response can generally be easily acquired.

1.3 Indirect Load Identification

The basic idea of the indirect load identification problem is to determine the system input via the knowledge of system output. The system input can be various forms of loads with time or frequency variant characteristics while several types of sensors can be used to detect the system response as shown in Fig.1.1. When the structure is subject to an unknown load, a knowledge of the mathematical model to represent the structure and the measured response due to the unknown load is essential so as to develop the load prediction model for determining the load contents. In general, the load contents can be the magnitude, direction and location of imposed loads. The external loads can be divided into three groups. One is the spatial-variant type such as point loads and distributed loads. Another load type is the time-variant form such as impact, harmonic, periodic and random loads. The time history or the frequency spectra of the load may be of interest. The third load type is the spatial- and time-variant form such as moving loads.

The mathematical model of the structure is required in order to predict the load contents. The modelling process can be treated in different points of views. First, in terms of the representation of system response, the time- or the frequency-domain model can be adopted. For time-domain approach, the convolution integral equation that correlates

the input load and output response can generally be formulated. While Green's function is mainly used for the propagation wave response, impulse-response function (IRF) can be of interest for structural vibration. For frequency-domain approach, frequency-response function (FRF) can be obtained. In some circumstances, the modal approach, i.e. where the system response is expressed in terms of modal parameters, can also be developed to determine the system response. Second, solution methods for the system equations of motion can be done using finite element method, state-space equation approach or dynamic programming, convolution and deconvolution methods and modal analysis. A measurement of the system response due to the load excitation is also needed for force prediction models. Various kinds of sensors have been used, such as strain gages, accelerometers, slope sensors, laser vibrometer and piezoelectric sensors. Normally, the adoption of different types of sensors and mathematical models as well as the solution techniques will result in different approaches for load-prediction.

It is important to mention at this point that the type of loads to be identified (static or time varying dynamic) plays a major role on the procedures adopted to get good load estimates. Basically, for given input time varying loads, structure response can be easily obtained by using principles of elasticity and equations from dynamics. This is known as the "forward problem." In theory, the other way should then be possible to determine the input forces from a measurement of structure response. This is known as the "inverse problem." Unfortunately, solving the inverse problem in most cases encounters numerous difficulties and tends to be highly ill-conditioned, i.e., even very small variations (noise) in the response measurement can cause large errors in the force estimation.

When it comes to solving the forward problem, the excitation forces are concentrated at a few locations on the structure and therefore, information about the forces is well known all over the structure. On the other hand, in the inverse problem, although a non-zero response is present over most of the structure, they can only be measured at a finite number of selected locations, with the response at the rest of the locations left untapped. Therefore, the forward problem can be solved directly for the response, while the inverse problem poses significant challenges to solve for the input forces. Since a combination of different loads at different locations can result in the same level of response, the solution to the inverse problem, still, may not be unique.

Various research works in this area have been developed and proposed to counter the challenges posed by the inverse problem which will be discussed in Chapter 2. The present work is another attempt to develop techniques to identify the number, locations and the magnitudes of the input loads applied to a structure from its measured response, i.e., to solve the inverse problem. In this dissertation, the terms loads and forces are used interchangeably. Similarly, estimation, identification and recovery mean the same in the context of this document.

1.4 Organization of the Dissertation

Chapter 1 explains the significance of this dissertation and presents a brief introduction of the load identification problem along with the challenges involved to address it.

Chapter 2 presents a literature review that gives detailed summary of the available work done by other researchers on the recovery of the number of loads, their locations and their magnitudes in frequency, modal and time domains, and discusses the strength and the drawbacks for each technique. All algorithms have advantages and disadvantages of their own and the need for a new algorithm for load identification is clearly explained under this chapter.

Chapter 3 presents an optimization approach that can predict simultaneously the amplitude and location of a harmonic force acting on a component. Different cases have been presented along with a discussion to address the limitations of this approach.

In Chapter 4, the transmissibility concepts for multi-degrees of freedom systems and its application in the estimation of the applied loads are explained. Furthermore, to help improve the load identification using the motion transmissibility concept, a novel approach is presented which utilizes the D-optimal design algorithm in conjunction with finite element method to determine the optimum sensor locations.

Chapter 5 develops another technique based on transmissibility concept for identifying dynamic load components exciting a structure from measured response. This technique uses strain measurements at a finite number of optimally placed strain gages on the structure.

In Chapter 6, three techniques based on frequency response and optimum locations of sensors have been presented and compared numerically for load identification problem. Different cases have been implemented to study the effect of sensor type along with the number of modes retained in the accuracy of load estimation.

Chapter 7 presents a comprehensive technique for load identification based on transmissibility concept that utilizes the D-optimal algorithm to determine optimum sensor locations, and the technique of model order reduction to keep the computational cost low without compromising on the accuracy. This is especially useful when finite element modeling is used to study dynamics of continuous system.

Finally, Chapter 8 presents some concluding remarks on this research. In addition, potential areas of future research on this topic are also identified.

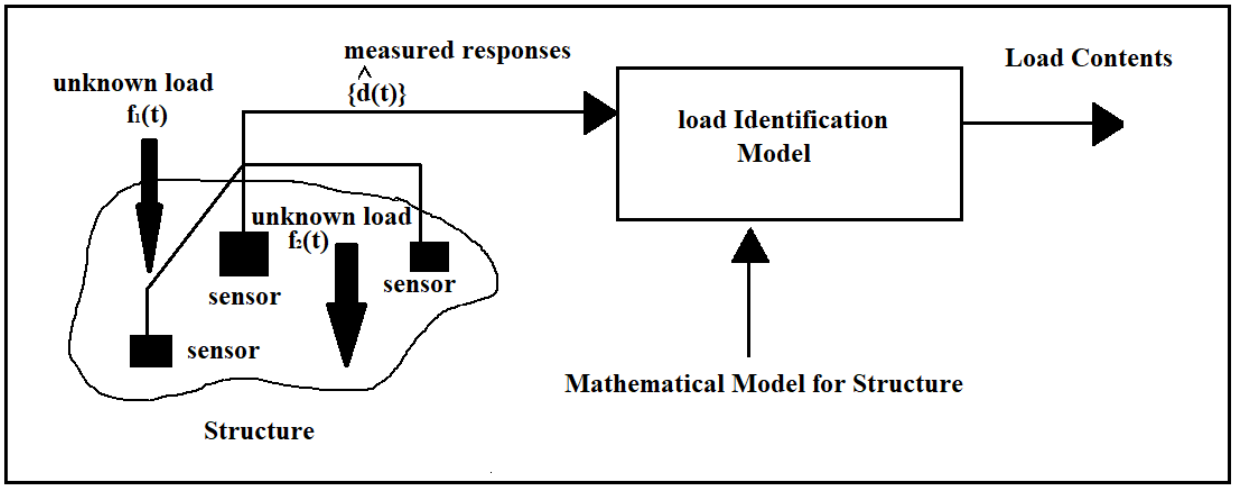

Figure 1.1 Basic Ideas of Force-Prediction Problem

Chapter 2 – Literature Review

Because the estimation of the excitation loads is an important issue in the dynamic analysis of structures, several methods have been developed that can estimate the forces acting on the structure from its measured response without the use of intermediate load cells. There are several aspects of input force estimation from measured responses (e.g., acceleration, displacement, or strain) that have been explored to arrive at an efficient and accurate load estimation technique. In general, the force contents can be the magnitude, direction and location of the imposed load. The external forces can be categorized into three forms. One is the spatial-variant type such as point forces or distributed forces. Another is the time-variant type such as impact, harmonic, periodic and random forces. The time history or the frequency spectra of the force may be of interest. The other is the spatial- and time-variant type such as moving forces. Therefore, many approaches have been proposed in the literature dealing with the force identification problems for different kinds of forces but there is no general model suitable for all kinds of problems encountered in practice. A brief overview of many of the load estimation techniques is presented in this chapter.

2.1 Load Magnitude Identification Literature

In the literature, most of the inverse problems for force identification assume that the load locations are known ahead of time. This information is needed to determine a unique solution in an otherwise general case, and the problem type is usually referred to as indirect force measurement.

Hillary and Ewins (1984) used accelerometers and strain gages to measure the frequency response function (FRF) and estimated two simultaneous sinusoidal input forces on a uniform cantilever beam as test piece by employing the least-squares technique. They found that the strain related model gave more accurate results than the acceleration related model because the strain responses are more influenced by the higher modes at low frequencies; therefore, they capture the effect of higher modes better than the acceleration responses.

The process of indirect load identification in the frequency domain, using the FRF, yields a linear relationship between the measured response and the excitation load. However, the FRF matrix is nearly singular and ill-conditioned. Starkey and Merrill (1989) investigated the reasons for errors encountered in predicting the forces using the inverse method. They concluded that inverse method suffers from ill-conditioning because the (FRF) matrix is frequently near singular with the worst condition number near the natural frequencies of the system. The FRF matrix tends to be dominated by rank-one component corresponding to the dominant mode near resonance.

Lee and Park (1995) present an error analysis that shows that frequencies close to a resonance or an antiresonance frequency are prone to result in an inaccurate determination of force magnitude. In the former case the stability problem is caused by inaccuracies in the frequency response function (FRF) matrix, while at antiresonance problems arise from rank deficiency of the FRF submatrix. Numerical results that conform to this error analysis may be found in Okubo *et al*. (1985).

Carne *et al*. (1992) proposed a technique referred to as the Sum of Weighted Acceleration Technique (SWAT) that estimates the input forces by summing the weight

scaled measured accelerations. The weighting factors can be determined either from inverting the modal matrix or from the free-decay response of the structure. They successfully applied this technique to estimate the impact force applied by the nose of a weapon mockup to the weapon body. This technique suffers with a drawback that only sum of the input forces can be determined without any estimation of the applied individual loads.

Bateman et al. (1992) and Carne *et al*. (1992) determined the forces on an unsupported structure subjected to an impact, from calculated eigen modes and measured accelerations. In this case the load location is either known or without interest, and the evaluated magnitudes are those of the load resultants.

Karlsson (1996) assumed the force spatial distribution available a priori and predicted the complex amplitudes of harmonic forces. Ma and Lin (1997) applied the Kalman filter with a recursive estimator to determine the harmonic forces of an equipment isolator.

2.2 Load Magnitude and Location Identification Literature

The knowledge of locations of loads under investigation is not always available in several examples which leads many researchers to work on simultaneous determination of load magnitudes and load location prediction.

D'Cruz *et al.* (1992) studied a rectangular viscoelastic plate with a single transverse harmonic point load and showed that it is sufficient to measure the transverse displacement at three discrete points to determine the magnitude, phase, and location of

the force. It is of some interest to note that in an earlier paper D'Cruz *et al.* (1991) concluded that with an *elastic* plate, it takes at least four displacement readings to calculate the force location and magnitude.

Choi and Chang (1996) determined the location and magnitude of an impact load on a beam in a nested loop algorithm. In the outer loop, the load location is estimated by minimizing a nonlinear function with a quasi-Newton method, while the load magnitude is calculated in the inner loop.

Shih *et al*. (1989) and Zhang *et al*. (1990) use the "Best Approximation Subspace" technique, described by Zhang *et al*. (1988) to locate a given number of incoherent forces. It is noted that this approach presumes that the number of sources is known and that there is a candidate set of points for their locations.

Moller (1999) tentatively gave the spatial shape and position of the harmonic point load and applied Betti reciprocal theorem with a reference load case to calculate the magnitude and match the load location.

Wang (2002) developed an optimization approach for both time- and frequency domain to predict the unknown force amplitude and location simultaneously for an arbitrary structure subject to impact and harmonic forces.

2.3 Transmissibility in Load Identification Literature

Prior to 1998, the concept of transmissibility was largely limited to single degree of freedom (SDOF) systems and generally denotes the relationship between the input and the output displacements. Since 1998, the concept of transmissibility has been extended

to multi degree of freedom (MDOF) systems by several researchers such as Riberio *et al.* (2000), and Liu and Ewins (1998). Varoto and McConnell (1998) discussed motion transmissibility concepts in the context of industrial applications and developed a matrix to characterize transmissibility of MDOF systems. In a multi degree of freedom system, there are many input and output responses. Therefore, the transmissibility matrix is not unique for MDOF systems. This means that for MDOF systems, the number of generalized forces and their locations must be equal. Such a generalization can be and has been not only developed in terms of a relation between two sets of harmonic responses for a given loading, but also between applied harmonic forces and corresponding reactions. Extensions to comply with random motions and random forces have also been achieved. From the establishment of the various formulations, it was possible to deduce and understand several important properties, which allow for diverse applications that have been envisaged, such as evaluation of unmeasured frequency response functions (FRFs), estimation of reaction forces and detection of damage in structure.

An application where the transmissibility seems of great interest is when in field service one cannot measure the response at some coordinates of the structure. If the transmissibility could be evaluated in the laboratory or theoretically (numerically) beforehand, then by measuring some responses in service one would be able to estimate the responses at inaccessible coordinates.

Several studies done by Maia and his collaborators (1999-2014) have focused on an estimation of location, number, and magnitude of loads imposed on multi-degree of freedom systems using the concept of transmissibility. The reconstruction of loads is done

in two successive phases. In the first phase, the location and number of applied loads are estimated by using a transmissibility model. In the second phase, the load vector is reconstructed by multiplying the inverse of the structural FRF matrix with the system's measured response. This approach uses system response, such as accelerations, to predict the load magnitudes and locations. While this technique provides promising results, the question of sensor placement was not addressed and was left as user's choice.

2.4 Optimum Location of Sensors

Practically, there are many locations on a structure where the accelerometers or strain gages can be mounted for measurement of the system response. Due to financial constraints and/or restrictions on potential sensor locations, the number and the locations of sensors are limited. In previous as well as recent works that use the concept of transmissibility for load prediction, the number of sensors used was addressed, but little attention was paid to their locations. The placements of sensors were left to the engineering experience or judgement of the user. According to Masroor and Zachary (1991), the accuracy of load estimation is strongly influenced by location of sensors. They showed that a random placement of sensors increases problem ill-conditioning whereas a proper selection of sensor locations decreases problem ill-conditioning and improves the accuracy of load estimation.

Recently, Gupta and Dhingra (2013) used the D-optimal algorithm to identify accelerometer locations to estimate magnitudes of dynamic loads. Based on the D-

optimal criteria developed by Mitchell (1974), Galil (1980) and Johnson *et al.* (1983). D-optimal (Determinant-optimal) methods utilize sequential exchange on k-exchange algorithms to select optimum sensor locations. By using these algorithms for location selection, the best sensor locations are identified from all available locations. However, since the approach presented by Gupta and Dhingra assumes that the load locations are known in advance, their method is limited to certain applications.

The limitation of the approach mentioned above is that the number of loads and their locations are assumed to be known ahead of time. The only unknowns are load magnitudes.

2.5 Motivation for this Dissertation

Load identification has received considerable attention for design, control and health monitoring of structures. A number of studies focused on determining the load magnitudes; in these cases, the locations and the number of the applied loads are assumed to be known in advance. Some studies addressed finding the loads magnitudes and location simultaneously assuming the knowledge of the type of the load applied such harmonic or impact loads.

Some recent works based on the concept of motion transmissibility addressed estimation of locations, number and magnitudes of loads for multi degree of freedom systems. This technique uses system responses such accelerations to predict the loads magnitudes and locations. In these studies, the number of sensors were addressed but not their locations. Since the locations of the sensors have a very important effect on the

prediction accuracy of the load locations and magnitudes, therefore, it is important to locate these sensors at the optimum locations.

The main novelty of this dissertation lies in the fact that using the concept of response transmissibility, we can solve the load identification problem wherein all three load components: number of applied loads, load locations, and load magnitudes are unknown. We also provide an answer to the question of sensor placement for improved load prediction. This is especially important when multiple loads are applied to the structure. It is seen that the efficacy of load estimation is improved when sensors are placed at optimum locations. These optimum sensor locations are determined using the D-optimization technique.

Furthermore, the transmissibility concepts presented in the literature are based on using the displacement responses and the displacement frequency response functions. On the other hand, previous studies have suggested that by using strain gages for measurement of vibration response, more accurate force identification results have been reported compared to traditionally used accelerometers. Therefore, in this dissertation, an effort towards overcoming this gap will be studied and the use of strain frequency response functions and the strain gages to achieve improvements in the problem of load identification using the transmissibility concept.

Another factor along with the type and locations of sensors on the structure which affects the precision of load estimates is the accuracy of the frequency response function that is obtained from the finite element model. Implementing the response transmissibility on complex systems requires larger models that lead to a large number of calculations and more computational times. As a result, Model Order Reduction (MOR) techniques

are commonly used to reduce the full finite element model. In this dissertation a MOR technique will be presented to reduce the number of degrees of freedom in a model without changing the systems dynamic characteristics significantly so that the applied load locations and magnitudes can be predicted accurately while improving the overall computational time efficiency.

Chapter 3 - Prediction of Harmonic Forces

Many mechanical components are subject to harmonic excitation conditions, in particular, rotating machinery. Such harmonically excited forces, for example may be due to imbalance or hydraulic flow, cannot measured easily but their magnitudes are crucial for structural design or analysis. Some researchers worked on identification of harmonic loads. By measuring the transverse displacement, D'Cruz *et al.* (1992) were able to determine not only the magnitude but also the location and the phase of a transverse harmonic point load applied on a viscoelastic plate. Karlsson (1996) presented the prediction of complex amplitudes of harmonic force by assuming the force spatial distribution available apriori.

An application of Betti reciprocal theorem with a reference load case to estimate the magnitude and location for an assumed spatial load shape of the harmonic point load was presented by Moller (1999). Based on an optimization approach that can be implemented in time or frequency domain, Wang and Chiu (2004) simultaneously predicted the amplitude and location of load applied on an arbitrary structure subjected to impact and harmonic loading.

Wang (2002) developed an optimization method for predicting the unknown impact and harmonic forces acting on arbitrary structures. The force contents including the force amplitude and its location can be determined simultaneously. This chapter is an initial attempt in the determination of location and magnitude of a harmonic force acting on a simple beam system. The following section will introduce the theoretical background of the beam response analysis and the development of harmonic response. Then the

sections after that describe the implementation of prediction program and the numerical prediction results that demonstrate the feasibility of the developed force prediction model.

3.1 Theoretical Analysis

Beam Response Analysis

A uniform cantilever beam is considered and shown in Fig. 3.1. The beam is subjected to a harmonic force whose location is unknown. The equation of motion for lateral vibration analysis for the system can be written:

$$Y_b I_b \frac{\partial^4 u(x,t)}{\partial x^4} + B_b \frac{\partial u(x,t)}{\partial t} + \rho_b A_b \frac{\partial^2 u(x,t)}{\partial t^2} = F(x,t) \quad (3.1)$$

where Y_b is Young's Modulus of beam, I_b is the cross-sectional moment of inertia of the beam, $u(x,t)$ is the beam lateral displacement, B_b damping coefficient of beam, ρ_b is the beam density and A_b is the cross-sectional area of beam.

Assuming a harmonic force is acting at location $x = x_n$ so the force function can be stated:

$$F(x,t) = F_n \, \delta(x - x_n) \, e^{i\omega_s t} \quad (3.2)$$

where the harmonic force location is represented as delta function $\delta(x - x_n)$. Using Modal expansion theorem or Principle of Modal Superposition, which represents the basis of all Modal Analysis procedures for linear mechanical systems, the beam response can be expressed as:

$$u(x,t) = \sum_{j=1}^{\infty} \phi_j(x) \, q_j(t) = \sum_{j=1}^{\infty} \phi_j(x) \, Q_j \, e^{i\omega_s t} \quad (3.3)$$

where $\phi_j(x)$ is the j^{th} displacement mode shape of beam, $q_j(t)$ is modal coordinate.

By substituting Eqn. (3.3) into Eqn. (3.1), the beam displacement at location $x = x_k$ can be derived:

$$u(x,t) = \sum_{j=1}^{\infty} \phi_j(x) Q_j e^{i\omega_s t} = e^{i\omega_s t} \sum_{j=1}^{\infty} \frac{F_n \phi_j(x_j) \phi_j(x_k)}{\left(\omega_j^2 - \omega_s^2\right) + i(2\xi_j \omega_j \omega_s)} \tag{3.4}$$

It is easy to notice that beam displacement is a function of modal parameters, i.e., ω_j , ξ_j and ϕ_j as well as the harmonic force amplitude F_n, excitation frequency ω_s and force location x_n. The beam acceleration can also be found:

$$a(x_k,t) = a_k(t) = Ae^{i\omega_s t} \tag{3.5}$$

where

$$A = -\omega_s^2 \sum_{j=1}^{\infty} \frac{F_n \, \phi_j(x_n) \, \phi_j(x_k)}{\left(\omega_j^2 - \omega_s^2\right) + i(2\xi_j \omega_j \omega_s)} \tag{3.6}$$

In numerical simulation a limited number of m modes are included to calculate the beam acceleration.

3.2 Harmonic Load Prediction Model

The prediction model for harmonic load is described in Fig. 3.2. A structure is subjected to unknown harmonic load; the input to the prediction model is the structural response that can be obtained by sensors as accelerometers. Along with the system modal parameters which can be obtained experimentally or numerically the force

contents, including force amplitude and its location can be determined simultaneously. The optimization problem to predict the unknown harmonic force is formulated as follows,

Objective Function and Design Variables:

The objective function Q_t is defined as the sum of square errors between the measured acceleration $\widehat{a_k}(t_r)$ and the predicted acceleration $a_k(t_r)$ over the time range from t_1 to t_{Nt} as shown in Eqn. (3.7):

$$Q_t = \sum_{r=1}^{N_t}[a_k(t_r) - \widehat{a_k}(t_r)]^2 = \sum_{r=1}^{N_t}\left[-\omega_s^2 \sum_{j=1}^{\infty} \frac{F_n \phi_j(x_n)\phi_j(x_k)}{\left(\omega_j^2 - \omega_s^2\right) + i(2\xi_j \omega_j \omega_s)} e^{i\omega_s t} - \widehat{a_k}(t_r)\right]^2 \qquad (3.7)$$

where the predicted acceleration $a_k(t_r)$ is a function of structural modal parameters and force contents as shown in Eqn. (3.5). Structural modal parameters, including natural frequencies, damping ratios and mode shapes can be obtained by modal analysis. The unknown force contents are the force amplitude F_n and its location x_n. The design variables for the objective function are the force amplitude F_n and its location index n.

When $n = 1$, ϕ_j (x_n) equal to ϕ_j (x_1), j=1,2,...,N, and etc. The index n related to the location x_n will result in ϕ_j (x_n), j = 1,2,...,N . By formulating the force determination problem as an optimization problem, the unknown harmonic force amplitude and its location index n can be determined simultaneously. The objective of the optimization problem is, therefore, to find F_n and n so as to minimize the sum of square errors between $\widehat{a_k}(t_r)$ and $a_k(t_r)$.

3.3 Prediction Program

The load prediction program was developed in MATLAB. The optimization subroutine *Patternsearch* based on direct search complex algorithm was used to solve general optimization problem for the design variables, the force amplitude F_n and its location index *n.* With the help of ANSYS software, a finite element model of the beam was assembled to get the modal parameters and generate the beam acceleration response to represent the measured response $\widehat{a_k}(t_r)$.

Simulation Setup

In order to perform the simulation, ANSYS-APDL software is employed to design the cantilever beam and then to extract the acceleration data. The material used was steel with material properties listed in Table. 3.1. The thickness of the beam, 0.0394 *m* is constant throughout the length of 0.3 *m.* The beam height is 0.0016 *m,* and is considered isotropic in nature, i.e. the material has uniform properties in all the three coordinate directions. The structure shown in Fig. 3.3 is map meshed with Solid45 element in ANSYS. A modal analysis is carried out to obtain the beam modal parameters. The first five natural frequencies of bending modes are listed in Table 3.2.

3.4 Results and Discussion

3.4.1 Theoretical Prediction Results

This section presents the results obtained using the algorithm described previously. The measured acceleration is replaced by the numerically generated response using ANSYS to validate the prediction model and to simulate the real-world

scenario where the accelerations are measured experimentally and measurement errors maybe present, each element in $\widehat{a_k}(t_r)$ was corrupted with normally distributed random errors with zero mean and standard deviation of 10% of its value. Tables 3.3, 3.4, 3.5 and 3.6 show the prediction results for different cases to check the effects of different force amplitudes, locations on the prediction model also the effect of the sensor location. The excitation frequency is chosen to be fs=28 Hz, between the first and second natural frequencies. *i.e.* close to the first natural frequency. Both harmonic force amplitude and its location index converge to the actual values very well too. The force prediction model works well for different force amplitudes and force locations as well as different sensor locations.

3.4.2 Example: Cantilevered Beam

Case1: Prediction of a harmonic load using different sensor locations.

Table 3.3 shows the results for the harmonic load amplitude and location prediction using different locations for sensor. For example, the load is applied on node (81) $f_{81}(t) = -1\cos(2\pi 28t)$ that has location index=15 and the prediction algorithm tested once when sensor is placed on location node number 96 which has index 14. The algorithm is also tested by placing the sensor on different location such as on node 89 which has index 7. Both results show the force prediction model works well for different sensor locations.

Case 2: Prediction of a harmonic load for different load location.

Table 3.4 shows the results for the harmonic load amplitude and location prediction using different load locations. For example, the sensor location is fixed on node 96 that has index (14) and the prediction algorithm tested once when load is applied on location

node number 81 which has index 15. The load is also applied on different location such as on node 88 which has index 6. Both results show the force prediction model works well for different load locations.

Case 3: Prediction of a harmonic load for different load amplitudes and different sensor locations.

Table 3.5 shows the results for the harmonic load amplitude and location prediction using different load amplitudes and different sensor locations. For example, the sensor location is fixed on node 89 that has index (7) and the prediction algorithm tested once when load is applied on location node number 3 which has index (16) with amplitude = -10 then with different amplitude = -1. Finally, the algorithm is tested for the load with amplitude -10 but this time by placing the sensor on node 84 which has index (2). All results show the force prediction model works well for different load amplitudes and different sensor locations.

Case 4: Prediction of a harmonic load for different load amplitudes and different locations but fixed sensor location.

Table 3.6 show the results for different force amplitudes and different force locations, but the sensor location is fixed on node 88 which has index (6). All results show the force prediction model works well for different load amplitudes and fixed sensor locations.

3.5 Conclusions and Summary

This chapter presented the harmonic force prediction algorithm applied to a cantilever beam structure. The algorithm presented can predict the harmonic force amplitude and its location simultaneously. Some conclusions are made as follows:

1. The prediction model is validated through numerical simulation and successfully predicts the harmonic force amplitude and its location.
2. The effects of different force amplitudes, locations on the prediction model are also studied with the proper selection of sensor location. It is seen that the prediction model works well.
3. The drawback of this algorithm is its limitation for one kind of harmonic loads with fixed amplitude and one excitation frequency which leads the research to look for other algorithm to predict the load magnitudes and locations.

Table 3.1 Material Property of Cantilever Beam

Material Property	Value (SI Unit)
Young's Modulus	207 GPa
Poisson's ratio	0.292
Density	7870

Table 3.2 Natural Frequencies of Cantilever Beam

Mode	Natural Frequency (Hz)
1	15.074
2	95.158
3	248.78
4	273.49
5	361.39

Table 3.3 Prediction of a Harmonic Load Using Different Sensor Locations

Sensor location (index)	Predicted Force Amplitude	Predicted Force Location
96 (14)	-0.9896	15
89 (7)	-0.9911	15

Table 3.1 Prediction of a Harmonic Load for Different Load Locations

Load location (index)	Predicted Force Amplitude	Predicted Force Location
88 (6)	-0.9877	6
81 (15)	-0.9896	15

Table 3.4 Prediction of a Harmonic Load for Different Load Amplitudes and Different Sensor Locations

Sensor location (index)	Applied Force Amplitude	Predicted Force Amplitude	Predicted Force Location
89 (7)	-10	-9.87366	16
89 (7)	-1	-0.99116	16
84 (2)	-10	-9.8426	16

Table 3.5 Prediction of a Harmonic Load for Different Load Amplitudes and Different Locations but Fixed Sensor Location

Applied force	Applied Force location (index)	Predicted Force Amplitude	Predicted Force Location
$f(t) = -0.9\cos(2\pi 30t)$	84 (2)	-0.8998	2
$f(t) = 0.7\cos(2\pi 30t)$	92 (10)	0.6925	10
$f(t) = 0.9\cos(2\pi 30t)$	81(15)	0.8877	15

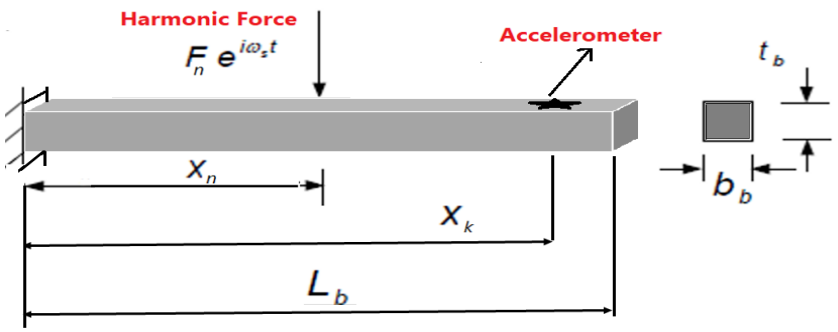

Figure 3.1 Cantilever Beam System

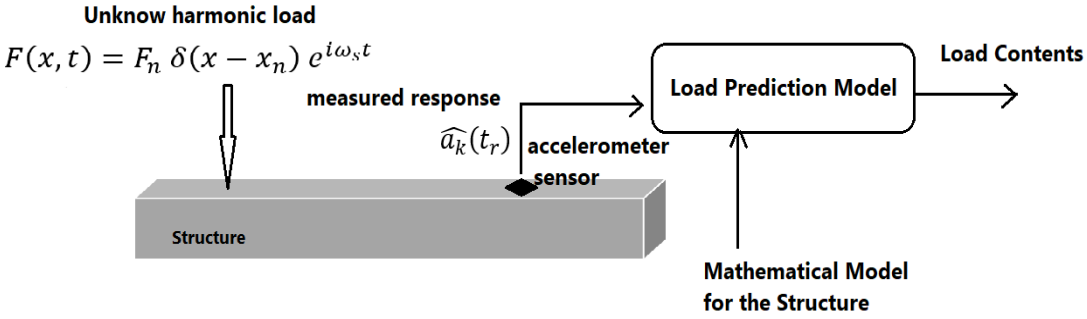

Figure 3. 2 Conceptual Diagram for Force Prediction

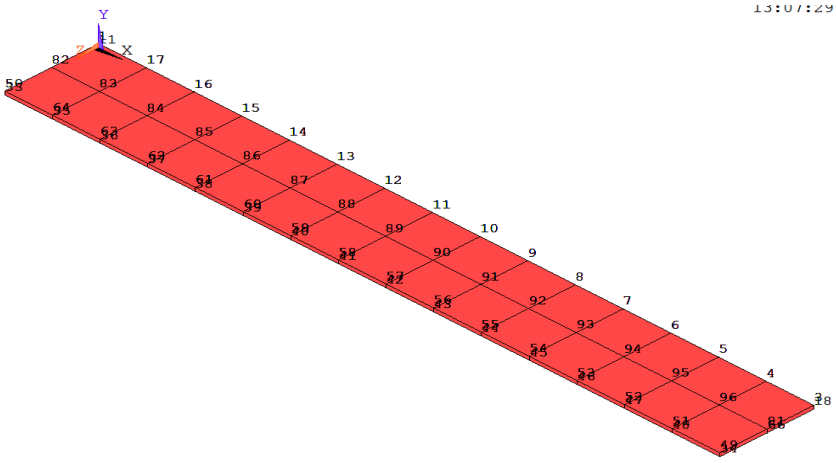

Figure 3. 3 Finite Element Model of Cantilever Beam

Chapter 4 - Force Identification Using Motion Transmissibility

The algorithm discussed in the previous chapter was limited to identification of two of the load's contents (amplitude and location) for simple harmonic loads with one excitation frequency. However, the solution for the force identification problem may require identifying more of the load's contents such as; the number, magnitude, direction and location. To overcome this limitation, this chapter presents a general overview on the concept of transmissibility and its potential application and limitations in the context of a force identification problem.

The notion of transmissibility is discussed in almost every textbook on vibrations. It is explained in the context of a single degree-of-freedom system when the system base is moving harmonically. As mentioned earlier in chapter 2, the transmissibility denotes the relationship between the input and the output response. Based on that; two types of transmissibility can be defined; the transmissibility of motion and the transmissibility of forces. The transmissibility of motion is defined as the ratio between the modulus of the response amplitude and the modulus of the imposed amplitude of motion. Usually, the transmissibility of forces, defined as the ratio between the modulus of the transmitted force magnitude to the ground and the modulus of the imposed force magnitude, is also deduced and the conclusion is that the mathematical formula of the transmissibility of forces is exactly the same as for the transmissibility of displacements. As will be explained in this chapter, this is not the case for multiple degree of freedom systems. The question that arises is how to extend the idea of transmissibility to a system with N degrees-of-freedom, i.e., how to relate a set of unknown responses to another set of known responses, for a given set of applied forces, or how to evaluate a set of reaction forces

from a set of applied ones. It is worthwhile to mention the first time that a general answer to the problem has been given was in 1998, by Ribeiro (1998).

In a multi degree of freedom system, there are many input and output responses. Therefore, the transmissibility matrix is not unique for MDOF systems. This means that for MDOF systems, the number of generalized forces and their locations must be equal. Such a generalization can be and has been not only developed in terms of a relation between two sets of harmonic responses for a given loading, but also between applied harmonic forces and corresponding reactions. Extensions to comply with random motions and random forces have also been achieved. From the establishment of the various formulations, it was possible to deduce and understand several important properties, which allow for diverse applications that have been envisaged, such as evaluation of unmeasured frequency response functions (FRFs), estimation of reaction forces and detection of damage in structure.

So for MDOF systems, the relationships among the responses at various co-ordinates will depend on the number and coordinates of the applied forces. This is a minimum mathematical requirement, as can be appreciated from the formulation presented Sec.4.1.

Several researchers as Maia and his collaborators (1999-2014) have focused on an estimation of location, number, and magnitude of loads imposed on multi-degree of freedom systems using the concept of transmissibility. The reconstruction of loads is done in two successive phases. In the first phase, the location and number of applied loads are estimated by using a transmissibility model. In the second phase, the load vector is reconstructed by multiplying the inverse of the structural FRF matrix with the system's

measured response. This approach uses system response, such as accelerations, to predict the load magnitudes and locations. While this technique provides promising results, the question of sensor placement was not addressed and was left as user's choice.

The main purpose of this chapter is to improve the use of the transmissibility concepts in conjunction with a two-step methodology for determination of force number, locations and magnitudes.

4.1 Transmissibility of Motion in MDOF Systems

In this section and next sub-sections, the main definitions, properties and applications of the transmissibility of motion in multi degree of freedom system will be presented.

4.1.1 Fundamental Formulation

The transmissibility function is traditionally defined as the ratio of two different output spectra. For a MDOF system, it is better to divide the system coordinates into three groups as shown in Fig. 4.1. Here P coordinates correspond to locations where the forces F_P could be applied to the structure whereas *I* coordinates are locations where the displacement responses D_I are known or measured. The *J* coordinates are locations where the displacement responses D_J are unknown.

One of the approaches to determine the transmissibility of motion for MDOF systems is based on a use of (FRF) matrix $[H^d(\omega)]$ which relates the dynamic

displacement amplitudes *D* to the applied force amplitudes *F***.** This matrix is also known as receptance frequency response matrix.

The receptance frequency response matrix $[H^d(\omega)]$ relates the dynamic displacement amplitudes *D* with the external force amplitudes *F* as (using harmonic excitation, in steady-state conditions) as in Eqn. (4.1):

$$\{D(\omega)\} = [H^d(\omega)]\{F(\omega)\} \leftrightarrow \{D(\omega)\} = [([K] - \omega^2[M] + i\omega[C])]^{-1}\{F(\omega)\} \quad (4.1)$$

Here $[K]$, $[M]$ and $[C]$ are the stiffness, mass and damping matrices respectively and can be generated from the finite element model of the structure. $[H^d(\omega)]$ includes all the degrees of freedom in which the system is discretized. It may be noted that the mass-normalized orthogonality properties are observed here:

$$[\phi]^T[M][\phi] = [I] \quad (4.2)$$

$$[\phi]^T[K][\phi] = diag(\omega_r^2) \quad (4.3)$$

In case of damped system with proportional damping, $C = \alpha K + \beta M$ could be assumed and therefore,

$$\{D(\omega)\} = [\phi][diag(\omega_r^2 - \omega^2) + i\omega(\alpha diag(\omega_r^2) + \beta I)]^{-1}[\phi]^T\{F(\omega)\} \quad (4.4)$$

where $[\phi]$ is the mode shape matrix, ω_r is the r^{th} natural frequency and α and β are constants.

From Eqn. (4.1) it is easy to understand that if the response $\{D(\omega)\}$ at the discretization points are known, then the force reconstruction (in frequency-domain) would be given by:

$$\{F(\omega)\} = [H^d(\omega)]^{-1}\{D(\omega)\} \quad (4.5)$$

4.1.2 Transmissibility of Motion in Terms of FRFs

Based on harmonically applied forces at coordinates P, one may establish that displacements at coordinates J and I are related to the applied forces at coordinates P by the following relationships:

$$\{D(\omega)\}_J = [H^d(\omega)]_{JP}\{F(\omega)\}_P \tag{1.6}$$

$$\{D(\omega)\}_I = [H^d(\omega)]_{IP}\{F(\omega)\}_P \tag{4.7}$$

From Eqn. (4.7), using $\{F(\omega)\}_P = [H^d(\omega)]_{IP}{}^{+}\{D(\omega)\}_I$ and substituting in Eqn. (4.6) yields:

$$\{D(\omega)\}_J = [H^d(\omega)]_{JP}[H^d(\omega)]_{IP}^{+}\{D(\omega)\}_I = [T_d(\omega)]_{JI}^{P}\{D(\omega)\}_I \tag{4.8}$$

where $[H(\omega)]_{IP}^{+}$ denotes the pseudo-inverse of the FRF matrix and the transmissibility matrix which relates both sets of displacements is defined as:

$$[T_d(\omega)]_{JI}^{P} = [H^d(\omega)]_{JP}[H^d(\omega)]_{IP}^{+} \tag{4.9}$$

The sub-matrix $[H^d(\omega)]_{IP}$ and can be obtained experimentally or analytically. The only required condition for the pseudo inverse to exist in Eqn. (4.9) is the number of response measurements at *I* coordinates should be greater than or equal to the number of applied point loads at *P* coordinates, i.e. $N_I \geq N_P$.

An important property of the transmissibility matrix to be used here is that it does not depend on the magnitude of the involved forces and only requires the knowledge of a set of coordinates that include all the coordinates where the forces are applied.

4.1.3 Transmissibility of Motion in Terms of Dynamic Stiffness

There exists another method to obtain the transmissibility matrix for the displacements, using the dynamic stiffness matrices. Assuming again harmonic loading and defining two subsets, *A* and *B*, *A* being the set where the dynamic loads may be applied and *B* the set formed by the remaining coordinates, where no forces are applied ($\{F(\omega)\}_B$ = 0), one can obtain (after grouping adequately the degrees of freedom of the problem):

$$\begin{bmatrix}[Z(\omega)]_{AI} & [Z(\omega)]_{AJ}\\ [Z(\omega)]_{BI} & [Z(\omega)]_{BJ}\end{bmatrix}\begin{Bmatrix}D(\omega)_I\\ D(\omega)_J\end{Bmatrix} = \begin{Bmatrix}\{F(\omega)\}_A\\ 0\end{Bmatrix} \tag{4.10}$$

Developing Eqn. (4.10), it follows that

$$[Z(\omega)]_{AI}\{D(\omega)\}_I + [Z(\omega)]_{AJ}\{D(\omega)\}_J = \{F(\omega)\}_A \tag{4.10a}$$

$$[Z(\omega)]_{BI}\{D(\omega)\}_I + [Z(\omega)]_{BJ}\{D(\omega)\}_J = 0 \tag{4.10b}$$

From Eqn. (4.10b) one obtains the transmissibility in term of the dynamic stiffnesses:

$$\{D(\omega)\}_J = -[Z(\omega)]^+_{BJ}[Z(\omega)]_{BI}\{D(\omega)\}_I = [T_d(\omega)]^A_{JI}\{D(\omega)\}_I \tag{4.11}$$

where $[Z(\omega)]^+_{BJ}$ is the pseudo-inverse of $[Z(\omega)]_{BJ}$.

From Eqn. (4.11) it is possible to obtain the response at the unknown coordinates *J*, as long as the pseudo-inverse is feasible, which requires that N_B is greater or equal to N_J.

Indeed, the conditions from the two formulations can be summarized as:

$$[T_d(\omega)]_{JI}^{A} = -[Z(\omega)]_{BJ}^{+}[Z(\omega)]_{BI} = [H^d(\omega)]_{JA}\,[H^d(\omega)]_{IA}^{+} \quad N_B \geq N_J \; and \; N_I \geq N_A \qquad (4.12)$$

4.2 Transmissibility of Forces in MDOF Systems

To present the transmissibility of forces for MDOF systems a similar procedure is followed to the one used in the previous sub-sections. The problem now consists of relating the set of known applied forces to a set of unknown reactions (or the other way around), relating the set of known applied forces (set *I*) with a set of unknown reaction forces (set *J*), which are illustrated in Fig. 4.1. For set *J* it will be assumed that $\{D(\omega)\}_J$ equals 0. In general, there will be other coordinates, where neither there are any applied forces nor there are any reactions that shall constitute the set *K*.

4.2.1 Transmissibility of Forces in Terms of FRFs

With the definition of the new sets *I*, *J* and *K*, the problem may be defined in the following way:

$$\begin{Bmatrix} \{D(\omega)\}_I \\ \{D(\omega)\}_J \\ \{D(\omega)\}_K \end{Bmatrix} = \begin{bmatrix} [H^d(\omega)]_{II} & [H^d(\omega)]_{IJ} \\ [H^d(\omega)]_{JI} & [H^d(\omega)]_{JJ} \\ [H^d(\omega)]_{KI} & [H^d(\omega)]_{KJ} \end{bmatrix} \begin{Bmatrix} \{F(\omega)\}_I \\ \{F(\omega)\}_J \end{Bmatrix} \qquad (4.13)$$

Imposing $\{D(\omega)\}_J = 0$, it follows that

$$[H^d(\omega)]_{JI}\{F(\omega)\}_I + [H^d(\omega)]_{JJ}\{F(\omega)\}_J = 0 \qquad (4.14)$$

Therefore,

$$\{F(\omega)\}_J = [T_f(\omega)]_{JI}\{F(\omega)\}_I \tag{4.15}$$

where

$$[T_f(\omega)]_{JI} = -[H^d(\omega)]_{JJ}^{-1}[H^d(\omega)]_{JI} \tag{4.16}$$

is the force transmissibility matrix.

This is the direct force identification method, i.e., one knows the applied forces and calculate the reactions at the supports, where the displacements are assumed as zero. The inverse problem is also possible, if one can measure the reaction forces and if their number is greater than or equal to the number of applied forces, one can calculate the pseudo-inverse of $[H(\omega)]_{JI}$:

$$\{F(\omega)\}_I = [T_f(\omega)]_{JI}^{+}\{F(\omega)\}_J \tag{4.17}$$

where

$$[T_f(\omega)]_{JI}^{+} = -[H^d(\omega)]_{JI}^{+}[H^d(\omega)]_{JJ} \tag{4.18}$$

In the inverse problem, one may not know how many applied forces exist and where they are applied. If that is the case, one must follow a different approach.

If the condition $\{D(\omega)\}_J = 0$ is relaxed, from Eqn. (4.13) it follows that:

$$\{D(\omega)\}_J = [H^d(\omega)]_{JI}\{F(\omega)\}_I + [H^d(\omega)]_{JJ}\{F(\omega)\}_J \tag{4.19}$$

$$\{F(\omega)\}_J = \left[T_f(\omega)\right]_{JI}\{F(\omega)\}_I + [H^d(\omega)]_{JJ}^{-1}\{D(\omega)\}_J \tag{4.20a}$$

and

$$\{F(\omega)\}_I = [T_f(\omega)]_{JI}^{+}\{F(\omega)\}_J + [H^d(\omega)]_{JI}^{+}\{D(\omega)\}_J \tag{4.20b}$$

4.2.2 Transmissibility of Forces in Terms of Dynamic Stiffness

As mentioned earlier, there is an alternative approach to obtain the force transmissibility matrix, using the dynamic stiffness matrices.

Assuming harmonic loading and the mentioned sets *I, J* and *K*, one can obtain (after grouping adequately the degrees of freedom of the problem) the following result:

$$\begin{bmatrix} [Z(\omega)]_{II} & [Z(\omega)]_{IK} & [Z(\omega)]_{IJ} \\ [Z(\omega)]_{KI} & [Z(\omega)]_{KK} & [Z(\omega)]_{KJ} \\ [Z(\omega)]_{JI} & [Z(\omega)]_{JK} & [Z(\omega)]_{JJ} \end{bmatrix} \begin{Bmatrix} \{D(\omega)\}_I \\ \{D(\omega)\}_K \\ \{D(\omega)\}_J \end{Bmatrix} = \begin{Bmatrix} \{F(\omega)\}_I \\ \{F(\omega)\}_K \\ \{F(\omega)\}_J \end{Bmatrix} \tag{4.21}$$

By joining the sets, *I* and *K* together in a new set *E* makes it easier to see that imposing $\{D(\omega)\}_J = 0$ one obtains the following relationships:

$$\begin{bmatrix} [Z(\omega)]_{EE} & [Z(\omega)]_{EJ} \\ [Z(\omega)]_{JE} & [Z(\omega)]_{JJ} \end{bmatrix} \begin{Bmatrix} \{D(\omega)\}_E \\ \{0\} \end{Bmatrix} = \begin{Bmatrix} \{F(\omega)\}_E \\ \{F(\omega)\}_J \end{Bmatrix} \tag{4.22}$$

from which it is clear that:

$$[Z(\omega)]_{EE}\{D(\omega)\}_E = \{F(\omega)\}_E \tag{4.23a}$$

$$[Z(\omega)]_{JE}\{D(\omega)\}_E = \{F(\omega)\}_J \tag{4.23b}$$

Eliminating $\{D(\omega)\}_E$ between Eqn. (4.23.a) and Eqn. (4.23.b), it turns out that

$$\{F(\omega)\}_J = [T_f(\omega)]_{JE}\{F(\omega)\}_E \tag{4.24}$$

where

$$[T(\omega)_f]_{JE} = [Z(\omega)]_{JE}[Z(\omega)]_{EE}^{-1} \tag{4.25}$$

The inverse problem corresponds to

$$\{F(\omega)\}_E = [T_f(\omega)]^+_{JE}\{F(\omega)\}_J \tag{4.26}$$

with

$$[T_f(\omega)]^+_{JE} = [Z(\omega)]_{EE}[Z(\omega)]^{-1}_{JE} \tag{4.27}$$

It is important to note that only some of the coordinates of the set *E* have applied forces. This means that in Eqn. (4.23) part a and b, some rows of $\{F(\omega)\}_E$ are zero and only the columns (in $[Z(\omega)]_{EE}$) whose coordinates have applied forces (set *I*) are needed for the transmissibility matrix. In other words, from the set *E* only the coordinates corresponding to the *I* set are used.

So as a conclusion from sections (4.2.1) and (4.2.2), that for the direct problem of transmissibility of forces there is no restrictions on the number of coordinates used in Eqn. (4.16) and Eqn. (4.18). For the inverse problem of transmissibility of forces, there are some restrictions that can make this option not very useful in practice, especially when using the dynamic stiffnesses. Since one needs to calculate the pseudo-inverse matrices in Eqn. (4.16) and Eqn. (4.18), it is not possible to perform the pseudoinverse of the transmissibility matrix if the number of applied forces is greater than the number of reactions. In this case, the condition to perform the pseudoinverse is $\#J \geq \#I$. So for these reasons the transmissibility of motion will be developed and used in this research for the inverse problem of force Identification.

4.3 Transmissibility in Terms of the Numerical Model

As stated previously, the transmissibility matrices may be obtained from a numerical model (which should be updated for the range of frequencies involved) or from results obtained experimentally. In this section, the transmissibility of motion is used as it is described in Sec. 4.1 and will be illustrated through different examples.

For the numerical model, one needs the knowledge of the structure within the discretization chosen, to create the receptance matrix$[H^d(\omega)]$, which is the inverse of the corresponding dynamic stiffness matrix $[Z(\omega)]$. Here, the numerical model is created using the Finite Element Method (FEM) with the help of ANSYS tool. As seen before, the dynamic stiffness matrix for a damped system is defined as:

$$[Z(\omega)] = ([K] - \omega^2[M] + i\omega[C]) \tag{4.28}$$

where $[C]$ represents the viscous damping matrix, often of the proportional type, i.e., $C=\alpha K+\beta M$, where α and β are constants to be evaluated experimentally. For undamped system the dynamic stiffness matrix can be written as:

$$[Z(\omega)] = [K] - \omega^2[M] \tag{4.29}$$

To build the dynamic stiffness matrix, a specific structural finite element is chosen according to the approximation considered. For example, in the case of a reasonably long and slender beam one can use the Euler-Bernoulli beam element (instead of a shell or solid structural element). Then, the global mass and stiffness matrices are assembled for the chosen discretization of the structure.

Although the receptance matrix $[H^d(\omega)]$ is the inverse of the corresponding dynamic stiffness matrix, one should avoid such direct numerical inversion (frequency by frequency). Instead, $[H^d(\omega)]$ is calculated from Eqn. (4.4), after a modal analysis of the free vibration problem. The maximum number of modes returned from a finite element model is equal model degrees of freedom, which can be a large number. Therefore, in many problems, numerical considerations make it impractical to retain all modes. Hence, a limited number (*m*) of modes are retained that are "enough" to approximate the receptance matrix. In this work, the decision on the number modes retained depends on the cumulative mass fraction captured by retained modes. For reasonable accuracy, an adequate number of (*m*) modes should be retained such that at least 90% of the cumulative mass fraction is captured by the retained modes. Then, using Eqn. (4.9) or Eqn. (4.16) one can calculate the needed transmissibility matrices.

4.4 Force Localization Based on the Transmissibility of Motion and Force Reconstruction

This section shows the force localization algorithm based on the transmissibility of motion and reconstruction using the measured responses and the updated numerical model. The force identification problem is a difficult problem, as one has a limited knowledge of the measured responses, due to structural complexity and lack of access to some locations for placements of sensors. In other words, there are difficulties due to the incompleteness of the model.

Due to this difficulty in estimating the load vector directly, the solution process is divided into two distinct phases as proposed by Lage *et al*. (2013):

1. The localization of the forces, i.e. the identification of the number (*N*) and locations (*P*) of the applied forces using the concept of transmissibility of motion.
2. Estimation of magnitudes of the loads identified in phase one.

For the first phase, a search for the number (*N*) and locations (*P*) of forces using the transmissibility of motion is performed. Essentially, this step consists of searching for the transmissibility matrix correspondent to the dynamics of the system and using the available measured data and the numerical model involved (Neves and Maia 2010). Once the corresponding transmissibility matrix is found, one has a solution for the number and locations of the forces applied to the structure.

The second phase consists of reconstructing the load vector with the results obtained in the first step. A more detailed description about this methodology is given in the following subsections.

4.4.1 Force Localization

At the first stage, the number (*N)* of the applied loads could be unknown along with their locations *(P)*. Therefore, the search process for the transmissibility matrix $[T(\omega)]_{JI}^{P}$ transforms the dynamic responses $\{D(\omega)\}_I$ into $\{D(\omega)\}_J$ examining all possibilities until the predicted response $\{D(\omega)\}_J$ matches the measured response $\{\widetilde{D}(\omega)\}_J$. Based on the assumption made regarding the number of applied loads, various combinations of the test nodes are checked. For the case where it is assumed that only one load applied *N*=1, the search process will start from the first node until the last node

(n) on the structure is traversed; the combinations of tested nodes will be: *{(1), ... n*}. For the case with two applied loads *N*=2, the combinations of tested nodes will be: *{(1,2), ... (1, n); (2,3), … (2, n); (3,4),…(3,n); to (n-1,n)*}. For the case with three applied loads *N*=3, the combinations of tested nodes will be: {(1,2,3),…,(1,2,n); …}. This approach can be extended to cover all possible combinations of load locations *P* and number of applied loads *N*.

The error in each combination is kept in a vector to identify the combination with the least associated error (in absolute value). Firstly, the algorithm scrolls through the possible combinations of position and number of forces. For each combination, the associated error between the calculated response vector $\{D(\omega)\}_J$ and the measured response vector $\{\tilde{D}(\omega)\}_J$ is calculated; this is carried out over a frequency range defined by the user. The error between the predicted and the measured dynamic response at each coordinate *k* can be defined as:

$$E_k = \sum_{\omega} \left(\log\left(abs\left(\tilde{D}_{J_k}(\omega) \right) \right) - \log(abs\left(D_{J_k}(\omega) \right)) \right)^2 \tag{4.30}$$

For each combination, the calculated error is kept in an entry of the error vector and analyzed later:

$$\{v\} = \{E_k\} \tag{4.31}$$

The accumulated error for a given combination of coordinates where *F* can be located is the norm of v . The calculations are repeated for successive combinations of number and position of forces. The combination of the force locations that gives the lowest error leads to the number and position of the forces applied to the structure. As already

mentioned, the maximum number of forces that can be found is equal to the dimension of the known dynamic response vector.

As one does not know in advance how many forces exist, one has to follow a trial and error procedure that consists basically in assuming an increasing number of forces and the corresponding number of measurements; if the right number of forces is *N*, one has a minimum error v for a certain set of coordinates. When one proceeds and assumes *N +1* forces and measurements, the error will be higher than v, telling the user that the right answer was effectively *N* forces at a certain set of coordinates.

It is clear that all the combinations of the *N +1* forces that contain the right combination of the *N* forces should exhibit a local minimum, though not the absolute one.

4.4.2 Force Reconstruction

In the second step, the reconstruction of the force amplitudes consists of solving an inverse problem using the measured dynamic responses $\{D(\omega)\}_I$.

$$\{F(\omega)\}_P = [H^d(\omega)]^+_{IP} \ \{D(\omega)\}_I \tag{4.32}$$

Note that for the given system to be invertible, the number of dynamic responses to be used (set *I*) must be higher or equal than the number of applied forces (set *P*). However, this is always verified, as in the first step of the solution process already forces a satisfaction of this requirement.

4.5 Examples

4.5.1 15-DOF Spring-Mass System with One Applied Load

To illustrate the load estimation using the concept of motion transmissibility discussed above, a fifteen degree of freedom system shown in Fig. 4.2 was analyzed with the following assumptions:

- The system is undamped;
- The first and the last mass are connected to fixed boundaries;
- Masses are assigned arbitrary values starting from 20 *kg* for *m*1 to 160 *kg* for *m*15 in 10 kg increments;
- Springs constants are assigned arbitrary values starting from 1×10^8 *N/m* for *k1* to 8×10^8 *N/m* for *k16* in increments of 0.5×10^8 *N/m;*
- One sinusoidal forcing function applied to mass *m*7; $f_7(t) = 500\sin(30\pi t) + 350\cos(20\pi t)$.

The task is to determine the location and the magnitude of applied force. It is divided into two phases as described in Sec. 4.4 where phase one aims to determine the location of this input load by looking for the transmissibility matrix in Eqn. (4.9) that transforms the dynamic responses $\{D(\omega)\}_I$ into $\{D(\omega)\}_J$ with minimum error as in Eqn. (4.30). So, for this attempt the *I* and *J* coordinates are chosen randomly as in Table 4.1. In the absence of any experimental data, the system responses at *I* and *J* coordinates were obtained by solving the differential equations of motion numerically. All numerical computations were performed in a MATLAB programming environment using the built-in

command (*ode45)* to get the system responses in time domain $\{D(t)\}$. Next using (*fft)* command the frequency responses $\{D(\omega)\}$ were obtained.

The frequency response functions $[H^d(\omega)]$ were obtained by using the modal system parameters, the modal matrix $[\phi]$ and ω_r after solving the eigenvalue problem for the system. Using modal analysis, it is found that the cumulative mass fraction (Irvine 2015) captured by the first five modes is 97% as shown in Table 4.2. Based on this observation, it was decided to retain five modes to reconstruct the receptance matrix $[H^d(\omega)]$. Following the procedure described in subsection 4.4.1 the accumulated error for a single load applied is shown in Fig. 4.3 and it displays the minimum error occurs at the combination number 7, means the applied load is on mass number 7.

After finding the location of the applied load, reconstruction of the load magnitude as in Eqn. (4.32) comes as the last phase. The applied and reconstructed forces are plotted in Fig. 4.4. According to the results shown in the Figs. 4.3 and 4.4, the following can be concluded:

1. The load location identification based on transmissibility of motion seems a good approach to estimate the location of a single load applied.
2. The load magnitude identification using randomly selected accelerometer locations is very poor and does not yield acceptable results.

Based on these conclusions, two points will be investigated. First checking the efficacy of the algorithm in case of multiple loads are applied, second improving the accuracy of the load estimation by studying the effect of the number and the locations of sensors used.

4.5.2 15-DOF Spring-Mass System with Two Applied Loads

The previous example is extended to the case when two applied loads are present. Two loads $f_5(t) = 500\sin(30\pi t) + 350\cos(20\pi t)$ and $f_{10}(t) = 250\sin(25\pi t) + 450\cos(15\pi t)$ are applied to masses m_5 and m_{10}, respectively. The first task is to determine the number and the locations of the applied loads using the localization method described earlier in Sec. 4.4.1, where the sensors locations in *I* coordinates are chosen to be uniformly distributed along the system. The *I* and *J* parameters are shown in Table 4.3.

It is seen that the proposed approach can correctly find the number of applied loads, i.e. two applied loads. As can be seen from Fig. 4.5, the accumulated errors have significantly low values for load combinations that correspond to two applied loads, which gives an accurate prediction for the number of loads applied. However, the locations of the two applied loads are not predicted accurately. The right combination of two applied loads at masses 5 and 10 is 70. Using five retained modes and a non-optimal placement of sensors, the minimum error is seen at combination number 60 which corresponds to load location on masses 4 and 10.

Another attempt was made to improve the prediction of load locations by increasing the number of retained modes from 5 modes to all 15 modes. As can be seen in Fig. 4.6, the minimum error occurs at combination number 79 which corresponds to the case when the loads are located at masses 6 and 10. It may be noted here that these minima have one load location correctly identified while the other one is near the actual location of node 5.

To examine the effect of sensor placement on prediction of load locations, several attempts were made for different sets of arbitrary locations for sensor positioning. The result for each set of sensor locations are shown in Table 4.4. Based on the results presented in Table 4.4, it can be seen that none of these attempts led to accurate load location prediction. An arbitrary selection of sensor locations is likely to get trapped at a local minimum of the error function and doesn't provide correct load locations. Since load identification is a two-phase sequential process, if the first phase doesn't yield accurate predictions for load locations, then the second phase is quite likely lead to inaccurate prediction for loads magnitudes.

An important conclusion that can be drawn from this example is that to improve the localization approach using the transmissibility of motion, it is important to pick the locations of the sensors (*l* coordinates) carefully.

4.6 Transmissibility of Motion Based on D-optimal Design

According to the study of Masroor and Zachary in (1991), they show that the location of sensor has significant effect on the accuracy of recovered load. The placement of sensor at a low sensitivity location may result in ill-conditioning. They defined a statistical parameter which directly relates the variance of load estimates and sensor locations. The minimization of this parameter leads to the minimization of variance of load estimates. Masroor and Zachary expected the user to select the sensor locations manually while estimating the loads. An arbitrary selection of sensor locations by the user

may not produce the right combination of sensors which produces least variance in load estimates, and thus they might not yield the optimal sensor locations.

As shown in the previous section, random selection of the sensor locations to localize the applied loads by using the transmissibility concept may lead to inaccurate prediction. For measurement of the acceleration response, there can be a large number of locations on the structure where the accelerometers can be mounted, and the precision with which the applied loads are estimated from measured acceleration response is strongly influenced by the locations selected for accelerometer placements. A solution approach, based on the construction of D-optimal designs, is presented to determine the number and optimum locations of accelerometers that will provide the most precise load identification estimates. The D-optimal criteria developed by Mitchell (1974), Galil (1980) and Johnson *et al.* (1983). D-optimal (Determinant-optimal) methods utilize sequential exchange as well as k-exchange algorithms to select optimum sensor locations. By using these algorithms for location selection, the best sensor locations are identified from all available locations.

4.6.1 D-optimal Design for Sensors Locations

To understand the logic behind the D-optimal design in determining the optimum locations of the sensors, it is worthwhile to mention the basic idea behind this approach is to minimize the determinant of $(A^TA)^{-1}$, or equivalently that maximize the determinant of the information matrix A^TA of the design. For our problem, the system matrix A corresponds to the modal matrix $[\phi]$.

In the problem of load localization and reconstruction using the concept of transmissibility of motion, where limited number of sensors in *l* coordinates are used, the

objective is to look for the best transmissibility that gives the minimum error. The system response can be transformed by using the following modal transformations:

$$\{\ddot{D}\ (t)\} = [\phi]\{\ddot{q}\ (t)\}$$

$$\{\dot{D}(t)\} = [\phi]\{\dot{q}(t)\} \tag{4.33}$$

$$\{D(t)\} = [\phi]\{q(t)\}$$

where $[\phi]$ is the modal matrix with the dimension equal to the number of total degrees of freedom of the structure. This modal matrix is considered to be the [A] matrix which will be used in the D-optimal design to look for the optimal sensor locations $\{\ddot{D}(t)\}_{opt.}$. In Eqn. (4.33), $\{q(t)\}$ are the Modal Participation Factors (MPF).

The least-squares estimate of $\{\ddot{q}\ (t)\}$ is given by:

$$\{\ddot{q}(t)\} = ([\phi]^T[\phi])^{-1}\ [\phi]^T\{\ddot{D}(t)\} \tag{4.34}$$

This criterion results in maximizing the differential Shannon information content of the parameter estimates and this usually constructed by algorithms that sequentially add and delete points from a potential design by using a candidate set of points spaced over the region of interest.

In fact, the acceleration vector is disposed to measurement errors. Based on the statistical study of Masroor and Zachary (1991), if the random errors in acceleration measurements are mutually independent and have the same standard deviation σ, then the variance-covariance matrix for the predicted load is given as:

$$var(\{F\}) = \sigma^2([\phi]^T[\phi])^{-1} \tag{4.35}$$

The matrix $([\phi]^T[\phi])^{-1}$ is known as the sensitivity of matrix $[\phi]$. The precision of load estimates depends on the variance in the acceleration measurements σ^2 and the conditioning of the sensitivity matrix. The accuracy of load estimates can be improved by improving the conditioning of matrix $([\phi]^T[\phi])^{-1}$. Two factors that affect the sensitivity matrix are, the number of sensors used and their locations on the structure. Therefore, choosing the optimum location and the suitable number of sensors can minimize the sensitivity of $[\phi]$; consequently, the variation in the load estimate will be minimized.

A solution procedure exists that can be used to provide the most precise estimates of the applied loads by the optimal selection of the locations and the number of accelerometers on the structure. This can be divided into three steps:

i) Generation of the candidate set.

ii) Determination of the number of accelerometers to be used.

iii) Determination of the D-optimal design.

The discussion for these steps is explained in detail in the following subsections.

4.6.2 Generation of the Candidate Set

Using the finite element method, the full structure can be meshed into numerous finite elements. The meshing should be done such that distance between a node where a sensor (accelerometers) placed, and its adjacent neighbors is not less than the physical size of the sensor. Initially all elements have equal potential to become an optimum location. Based on certain criteria, the designer needs to identify the possible locations where the accelerometer can be mounted. So all inaccessible locations are eliminated from the total because there are certain locations where it is impossible to mount

accelerometer and record measurements. The remaining sets of locations are called a candidate set for optimum sensor placement. The following section will detail the procedure to construct $[\phi]_{candidate}$ matrix.

The matrix $[\phi]_{optimum} \in R^{(N_I \, x \, m)}$ is such a subset of the candidate set $[\phi]_{candidate}$ matrix that provides the most precise estimates of the applied loads. The number of rows N_I of the matrix $[\phi]_{optimum}$ represents the number of accelerometers mounted on the structure and the number of columns m represents the number of modes retained. The element in each row of the matrix $[\phi]_{optimum}$ represents the response of an accelerometer at a particular location for each mode shape.

4.6.3 Determination of Number of Accelerometers

The accuracy of load estimation will improve by including more accelerometers. Adding more accelerometers offsets the cost effectiveness of the proposed procedure. Furthermore, practical and financial constraints place limitations on the number of accelerometers to be used. Since the algorithm uses left pseudo inverse to recover the load, the general condition is that the number of accelerometers on I coordinates (N_I) should be greater than or equal to the number of loads to be identified on P coordinates (N_P). If the maximum number of forces to be estimated is N_P, then the number of accelerometers N_I must satisfy the criterion $N_I \geq N_P$.

4.6.4 Determination of the D-optimal Design

To find optimum locations for a given number of accelerometers N_l, the candidate set is searched to determine N_l accelerometers locations that provide the least variance in the load estimates. Based on the required number of optimum accelerometers, an algorithm should select the optimum N_l accelerometers from $[\phi]_{candidate}$ which satisfy the condition stated above.

If the candidate points to be included in matrix $[\phi]_{candidate}$ such that the sensitivity of $[\phi]$ is minimized are determined by trial and error, the set so obtained may not be the optimum set and would lead to a higher variability in the estimated loads. Also, it would be too time consuming to take into account all the possible combinations of accelerometers placements to arrive at the set that would produce the best estimates of the forces.

Several statisticians have done research to improve the algorithm, which reduces the variance of a matrix $[\phi]$. (Kammer,1991; Atkinson and Donev,1992). The criterion of most relevance to the current application involves the maximization of $|[\phi]^T[\phi]|$ the determinant of $[\phi]^T[\phi]$. Design that maximizes $|[\phi]^T[\phi]|$ is called D-optimal design. The D-optimal designs guarantee low variance among parameters and low correlation between parameters. The major difficulty is the existence of local maxima, which can only be handled by an efficient algorithm.

In order to construct N_l-point D-optimal design, the N_l accelerometers locations that maximize $|[\phi]^T[\phi]|$ must be selected from the candidate set. To select the N_l-point

D-optimal design, algorithms based on the principles of optimal augmentation and reduction of an existing design can be implemented. With optimal augmentation, the candidate point with maximum prediction variance is added as a row to the matrix. Similarly, optimal reduction of the augmented design is achieved by eliminating the candidate point or row of the matrix having minimum prediction variance. This process of augmenting and deleting candidate points in an optimal fashion continues until no further improvement in the objective function can be made. Such procedures are called exchange algorithms; two such types of procedures are the sequential exchange algorithm (Galil and Keifer,1980) and the k-exchange algorithm (Johnson and Nachtsheim,1983).

The basic idea behind the sequential exchange algorithm is as follows. Given the candidate set, the number of accelerometer N_l and the number of modes retained m, the first step is to randomly select N_l distinct candidate points from the candidate set to initialize the (N_l × m) matrix $[\phi]$. Out of the remaining candidate set, a candidate point is then selected and the corresponding row is augmented to the matrix $[\phi]$ to form matrix $[\phi]_+$ such that $|[\phi]_+^T[\phi]_+|$ is maximum. Next, out of the N_l+1 rows in matrix $[\phi]_+$, a row is deleted to arrive at matrix$[\phi]_-$ such that $|[\phi]_-^T[\phi]_-|$ is maximum. This process of augmenting and deleting rows continues until there is no further improvement in the value of $|[\phi]^T[\phi]|$. The final D-optimal design $[\phi]_{optimum}$ is matrix $[\phi]$ and provides the information on the optimum accelerometers' locations. A flowchart depicting this algorithm is shown in Fig. 4.7.

As the candidate set gets bigger and bigger, it is very expensive to compute the determinant at each step. So by using $R = [\phi]^T[\phi]$ and then calculate the determinant $|R|$. An alternate method for calculating the determinant $|R_+| = |[\phi]_+^T[\phi]_+|$ from that of $|R|$ when a row d^T is added to the matrix $[\phi]$ is:

$$|R_+| = |R|(1[+]d^T R^{-1} d) \tag{4.36}$$

where [+] denotes addition and is replaced by subtraction in the case of deleting a row d^T from $[\phi]_+$. In order to be able to use Eqn. (4.36) R^{-1} can be maintained and updated as the row d^T is augmented to the matrix $[\phi]$ by:

$$|R_+|^{-1} = |R|^{-1}[-]\frac{(R^{-1}d)(R^{-1}d)^T}{(1[+]d^T R^{-1}d)} \tag{4.37}$$

where [-] denotes subtraction and is replaced by addition in the case of deleting a row d^T from $[\phi]_+$.

Once the optimum accelerometers locations are determined $[\phi]_{opt}$, accelerometers are mounted at those locations on the structure before the application of the unknown loads. The measured accelerations $\left\{\tilde{D}\ (\omega)\right\}_{I(opt.)}$, together with the optimum $[\phi]$ computed, are then used to estimate the unknown forces $\{f(\omega)\}$ in accordance with Eqn. (4.32).

The next example deals with numerical validation of the D-optimal algorithm presented above in the load identification problem using motion transmissibility. The

example also illustrates the effectiveness of using the optimal sensor locations to identify the loads applied to the structure.

4.6.5 15 DOF System Example Revisited-Load Identification with Optimal Sensor Locations

The numerical example dealing with 15 DOF spring-mass system described in Sec. 4.5 was revisited and load identification using the concept of transmissibility of motion in conjunction with the D-optimal design for optimum sensor location was applied. The inputs for the load recovery problem are tabulated in Table 4.5.

The result in Fig. 4.8 shows that by using the optimal locations for the accelerometers, the minimum accumulated error occurs at the right combination number (70) for the two applied loads at masses 5 and 10. This, in turn, leads to more accurate prediction for the loads magnitudes as shown in Figs. 4.9 and 4.10.

To simulate an experimental situation where the accelerations are measured experimentally, and measurement errors may be present, each element of response measurement in $\{\tilde{D}(\omega)\}_{I(opt.)}$ was corrupted with normally distributed random errors with zero mean and standard deviation of 10% of its value.

Using the algorithm described above, five optimum locations for accelerometers are found while *j* coordinates were chosen arbitrarily for same load locations. The data is given in Table (4.6).

The results in Fig. 4.11 show that by using the optimal locations for accelerometers and with errors present in response measurements, the minimum accumulated error occurs at the right combination number (70) for two applied loads at masses 5 and 10. It

may be noted that due to the presence of measurement errors in accelerometer readings, the absolute values of the accumulated errors have increased. As shown in Figs. 4.12 and 4.13, it can be seen that the applied loads are recovered accurately despite the presence of measurement errors.

Based on a close agreement between applied and predicted loads, the results of this example indicate that the proposed approach was in this case effective in not only determining load magnitudes but also unknown load locations. An example dealing with an application of proposed approach to a continuous system is presented next.

4.6.6 Load Identification for 3D Cantilever Beam

The numerical example discussed previously dealt with a discrete system. Next a continuous system is considered where two dynamic loads are applied to a 0.25 *m* long, 0.05 *m* wide and 0.005 *m* thick cantilevered steel beam. The material used is steel which has Young's modulus *Y*= 209 *GPa* and Poisson's ratio equal to 0.29. (See Fig. 4.14). Without loss of generality, the system is assumed to be undamped.

Using ANSYS, a finite element model of the beam was developed and meshed with SHELL181 elements. The beam has 36 nodes and each node has six degrees of freedom. Six of these nodes are completely constrained; so the structure has 30 unconstrained nodes with 180 degrees of freedom.

At the free end of the beam, a vertical load is applied on node 19 described as $f_{19}(t) = 500\sin(30\pi t) + 350\cos(20\pi t)$ with another vertical load applied on node 24 given as $f_{24}(t) = 200\cos(60\pi t)$.

As shown earlier for the discrete system, the solution approach will involve a prediction of the locations of the applied loads followed by a reconstruction of the load magnitudes by using the motion transmissibility and optimum locations for the sensors. A modal analysis was performed on the FE model of the beam to obtain the modal matrix for the structure. For this 180-dof example, the modal matrix is $[\phi]_{(180x180)}$. The mass $[M]_{(180x180)}$ and stiffness $[K]_{(180x180)}$ matrices were obtained using finite element method. ANSYS provides data for [M] and [K] matrices in the Harwell-Boeing file format. A program was written in MATALB to convert them into the matrix format suitable for current application.

As discussed earlier, a limited subset of modes is retained to reconstruct the applied loads. The retained modes should capture at least 90% of the cumulative mass fraction.

If only *m* modes are retained to reconstruct system response, the condensed modal matrix is an *mxm* matrix. If the direction of the applied loads is known a priori, then as a first step it may be adequate to construct the reduced modal matrix such that it has only the modes in the same direction as the applied loads. For this example, the reduced modal matrix will have thirty normal modes in the Y direction, $[\phi_Y]_{(30x30)}$. Therefore, the candidate modal matrix will be $[\phi_Y]_{(30x30)}$, and this will be the input for D-optimal program.

Following the D-optimal design algorithm described previously, the candidate set $[\phi_Y]_{(30x30)}$ is searched to determine its optimum subset $[\phi_Y]_{opt}$. After $[\phi_Y]_{opt}$ is found, the optimum accelerometer locations are determined. The accelerometers are mounted at the identified optimum locations and the acceleration $\{\ddot{D}(t)\}_{I(opt)}$ is measured, which can

be then be successively numerically integrated to obtain $\{\dot{D}(t)\}_{I(opt)}$ and $\{D(t)\}_{I(opt)}$. If using the finite element model in ANSYS, the displacement vector can be found directly from ANSYS at the optimal locations. From $\{D(t)\}_{I(opt)}$, one can use MATLAB program to get the responses in the frequency domain $\{D(\omega)\}_{I(opt)}$ which represent the displacement vector at optimal *I* coordinates $\{\tilde{D}(\omega)\}_{I(opt)}$ and will be used later in the force reconstruction step as shown in Eqn. (4.32). Table (4.7) shows the optimal *I* coordinates for the cantilevered beam.

To find the locations of the applied forces, both measured and predicted displacement vectors at *J* coordinates should be known to look for the minimum error as in Eqn. (4.30). For the measured responses at *J* coordinates $\{\tilde{D}(\omega)\}_J$, one can arbitrarily pick any locations. For the example considered here, *J* coordinates are assumed to be same *I* coordinates as shown in Table (4.7).

For the predicted response at *J* coordinates, all possibilities were explored until the calculated response matched the measured ones. This method was implemented in MATLAB. The algorithm scrolls through possible combinations of applied force locations. For each combination, it calculates the associated error between the calculated vector $\{D(\omega)\}_J$ and the measured responses vector $\{\tilde{D}(\omega)\}_J$; this is done over the range of frequencies defined by the user. For each combination, the calculated error is saved in an error vector and plotted as shown in Fig. 4.15. For this example, the total number of combinations explored for the case of two applied loads is 465. The applied load locations at nodes 19 and 24 correspond to combination number 364. It can be seen from Fig. 4.15

there is a minimum value at this combination number which corresponds to the load location being predicted correctly.

It is worth mentioning that in Fig. 4.15, there are three other minima which belong to the following combination numbers: (i) 276 which corresponds to the case when two loads are applied on nodes 14 and 15, (ii) combination number 284 which corresponds to loads on nodes 14 and 24, and (iii) combination number 298 and which corresponds to loads being applied on nodes 15 and 19. It can be seen from Fig. 4.14 that node 19 lies above node 14 while node 24 lies above node 15. Since both nodal pairs share the same applied load location, the algorithm is likely to pick one node from each of the two pairs.

During the next step, the load magnitudes were reconstructed using Eqn. (4.32) and transformed into time domain using Inverse Fourier Transform (IFT). To get an acceptable accuracy for reconstructed loads, it was decided to retain all 30 modes in the Y direction. The reconstructed loads are plotted along with applied loads as shown in Figs. 4.16 and 4.17. It can be seen from both figures that the load trends are recovered with reasonable accuracy.

As previously mentioned, to simulate a more realistic scenario where acceleration is measured experimentally, each element in $\{\tilde{D}(\omega)\}_{I(opt.)}$ was corrupted with normally distributed random errors with zero mean and standard deviation of 10% of its value. The applied and recovered loads, with errors in acceleration measurements, are plotted in Figs. 4.18 and 4.19. Once again, it can be seen that the proposed approach is able to recover the applied loads fairly accurately by retaining all 30 modes in the Y direction.

Practically, due to the limitations on the number of modes that can be retained, an improvement in the prediction of load magnitudes will be discussed in chapter 7 that utilizes a model order reduction technique. The objective of this technique is to reduce the number of degrees of freedom in a model without changing the system's dynamic characteristics significantly such that we can predict the applied load locations and magnitudes while improving the computational time required to solve the problem.

4.7 Conclusions and Summary

In this chapter, load identification (load location as well as magnitude) by using the concept of motion transmissibility has been examined for two different multi degree of freedom systems; a discrete system and a continuous system. Based on the results presented, it is shown that to improve the accuracy of the load location prediction problem, the placement of sensors at correct locations is important. Using optimum locations of accelerometers as determined by the D-optimal algorithm improves the identification for the unknown loads especially when multiple loads are applied and when the error function has multiple local minima. In addition, it has been shown numerically that even in the presence of simulated measurement errors, the proposed method yields promising results. However, two points need to be addressed:

1. It was seen that to obtain reasonably accurate load identification results, a large number of modes need to be retained during the load reconstruction process. Practically there are limitations on the number of modes whose MPF can be

estimated from sensor measurements. To overcome this limitation, the model order reduction techniques are proposed in Chapter 7.

2. The method proposed in this chapter uses acceleration measurements for load prediction. To improve the accuracy of load prediction, the next chapter investigates the feasibility of using strain gages and proposes a new approach based on the concept of strain transmissibility for force prediction.

Table 4.1 Input Data for Spring-Mass System with One Load Applied

I coordinates	[2,3,10,13]
J coordinates	[4,11]
P coordinate	[7]

Table 4.2 Modal Analysis for 15-DOF Spring-Mass System

Mode	**Frequency [Hz]**	**Effective Mass**	**Cumulative Mass Fraction**
1	61.8641	1085.03	0.803727
2	129.202	87.0485	0.868208
3	194.776	93.2697	0.937296
4	258.197	20.1218	0.952201
5	318.968	28.9669	0.973658

Table 4.3 Input Data for Load Identification with Uniformly Distributed Sensor Spring-Mass System

I coordinates	[3,6,9,12,15]
J coordinates	[4,13]
P coordinates	[5,10]

Table 4.4 Predicted Load Locations Using Arbitrary Locations for Sensor Placement for Spring-Mass System

Arbitrary selections of *I* and *J* coordinates	**Predicted load locations**
I = [2,4,9,11,14], *J* = [3,9]	(6,12)
I = [3,6,9,12,15], *J* = [3,9]	(5,11)
I = [3,4,6,8,12], *J* = [3,12]	(5,8)
I = [1,3,7,9,12], *J* = [3,12]	(6,8)
I = [2,6,8,12,14], *J* = [4,13]	(3,9)

Table 4.5 Input Data for Spring-Mass System

Optimal *I* coordinates	[4,6,8,11,15]
J coordinates	[3,9]
P coordinates	[5,10]

Table 4.6 Input Data for Spring-Mass System with Measurement Errors

Optimal *I* coordinates	[2,6,8,12,14]
J coordinates	[3,9]
P coordinates	[5,10]

Table 4.7 Input Data for Cantilevered Beam

Optimal *I* coordinates	[11,12,16,18]
J coordinates	[11,12,16,18]
P coordinate	[19,24]

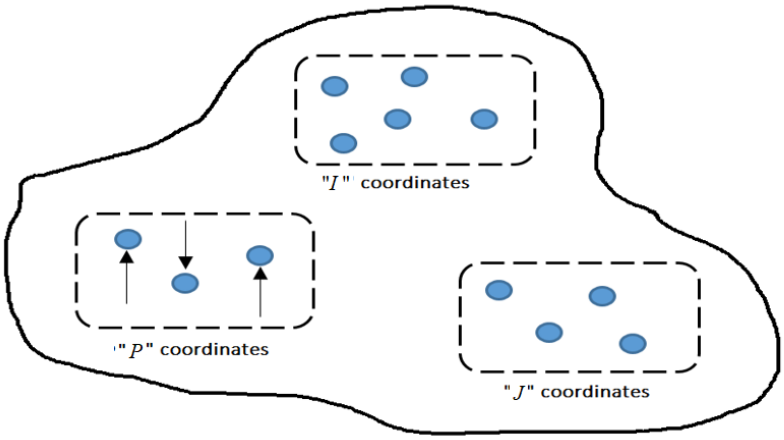

Figure 4.1 Elastic Body with the Three Sets of Coordinates *I*, *J* and *P*

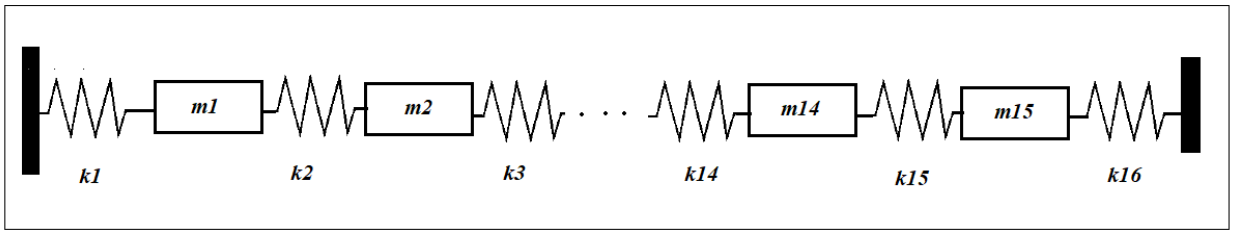

Figure 4.2 15-DOF Spring-Mass System

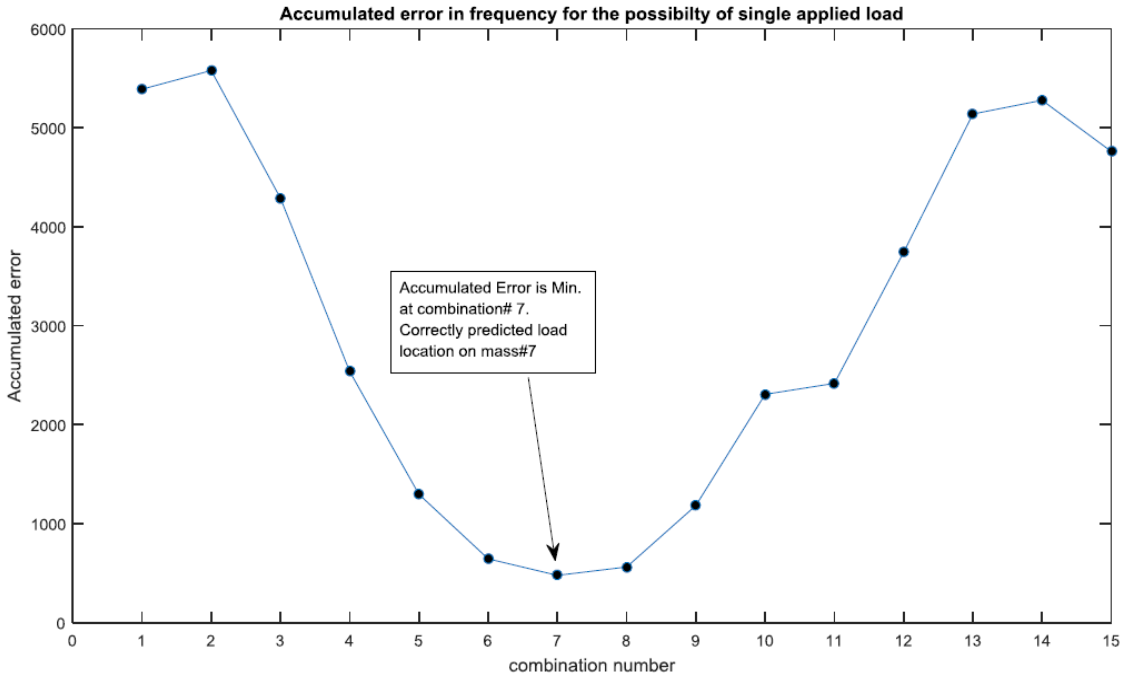

Figure 4.3 Accumulated Error for Single Load Application

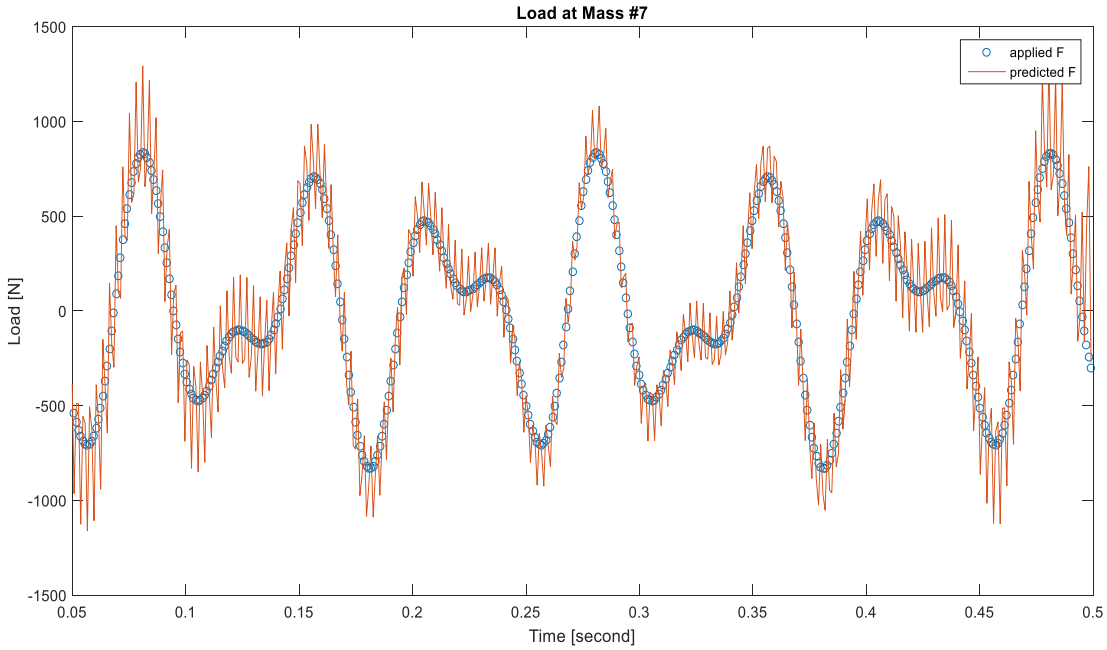

Figure 4.4 Applied and Recovered Load at Mass 7 with Random Sensors Locations

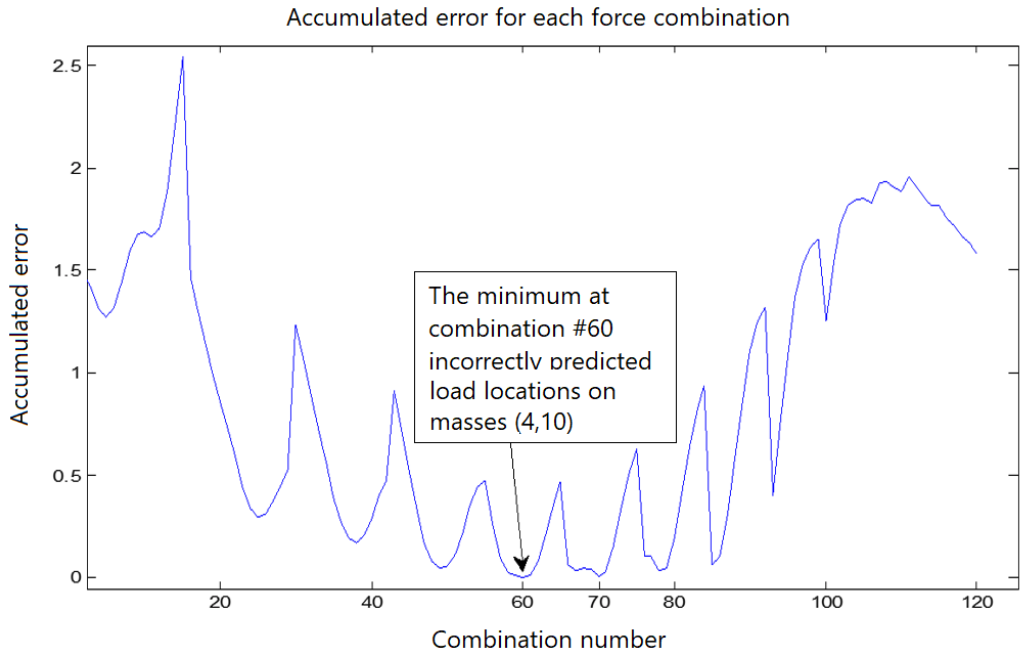

Figure 4.5 Accumulated Error in Case of Retaining 5 Modes and 5 Uniformly Distributed Sensors

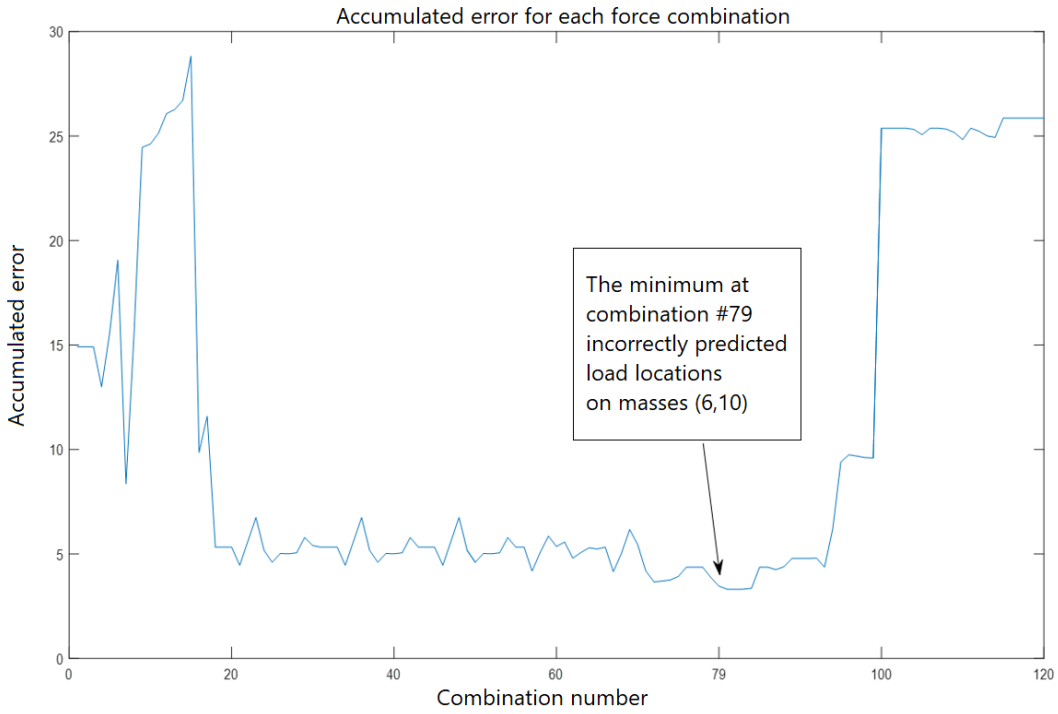

Figure 4.6 Accumulated Error in Case of Retaining 15 Modes and 5 Uniformly Distributed Sensors

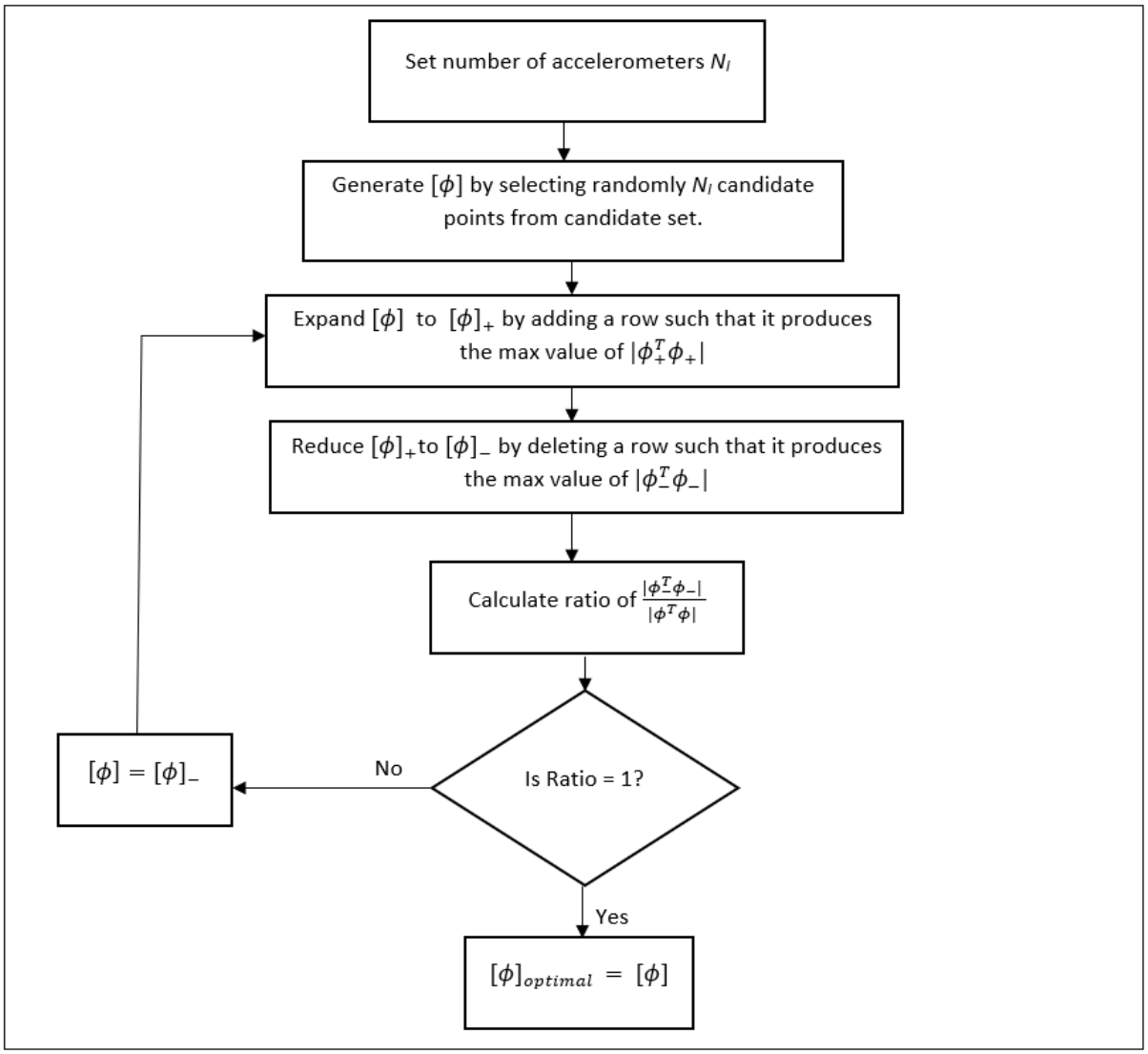

Figure 4.7 Flow Chart of The Sequential Exchange Algorithm

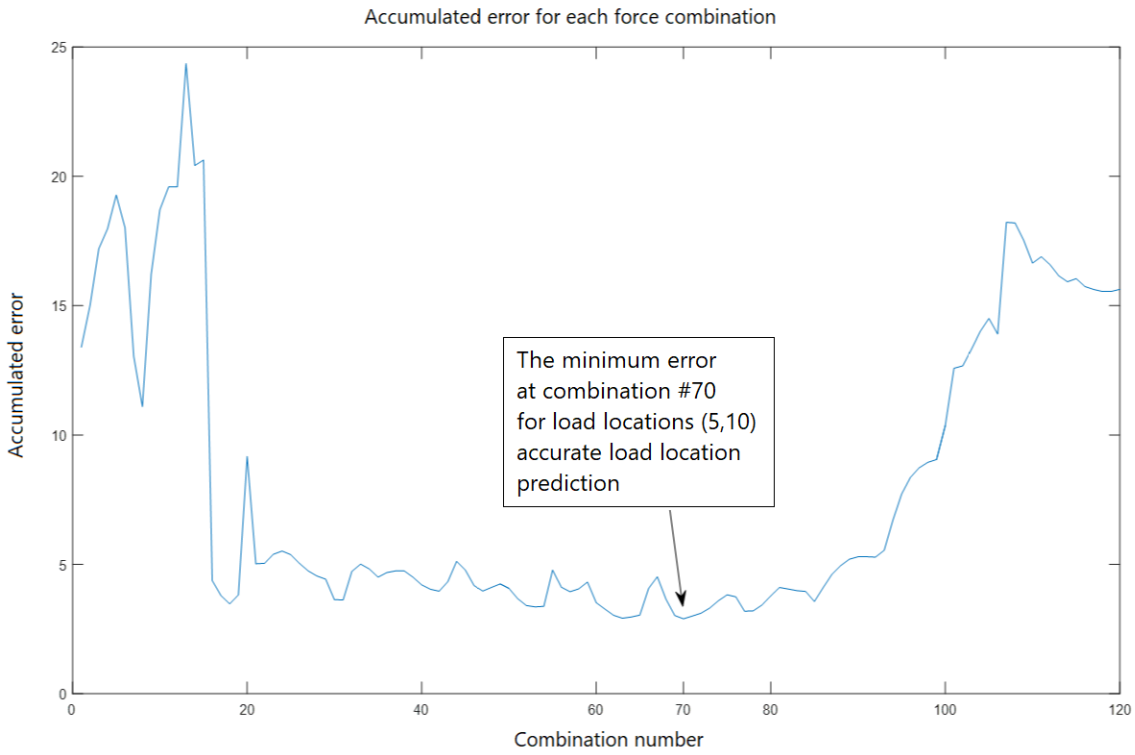

Figure 4.8 Accumulated Error in Case of Retaining 5 Modes and Using 5 Optimum Sensor Locations

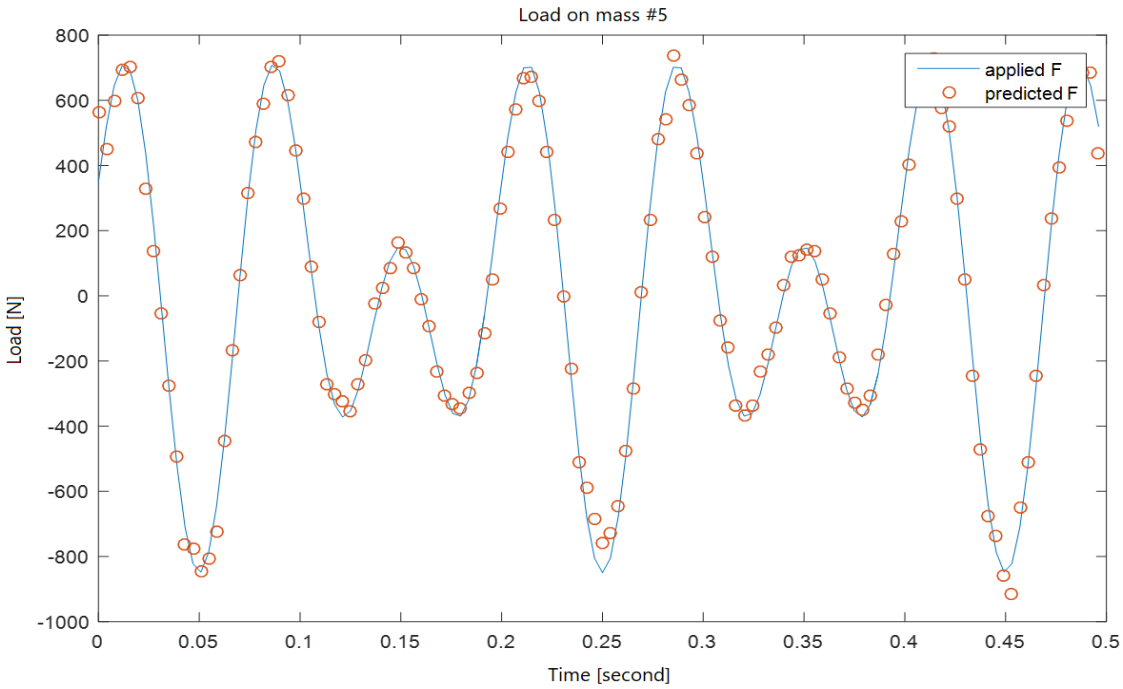

Figure 4.9 Applied and Reconstructed Load at Mass 5 Using 5 Optimum Sensor Locations with 5 Modes Retained

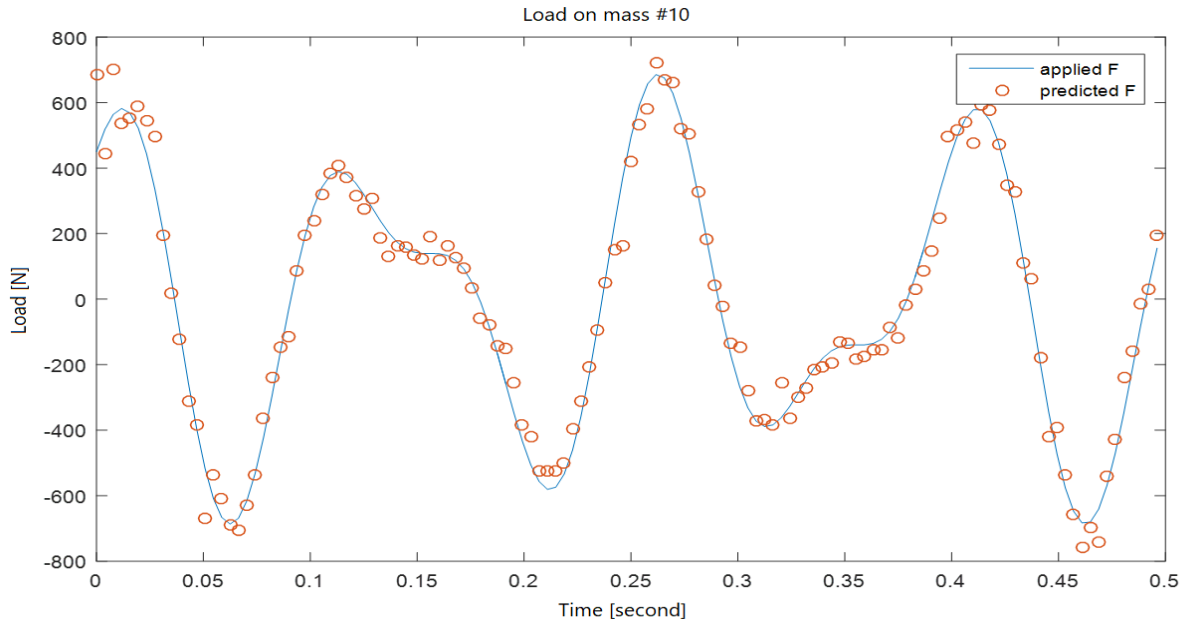

Figure 4.10 Applied and Reconstructed Load at Mass 10 Using 5 Optimum Sensor Locations with 5 Modes Retained

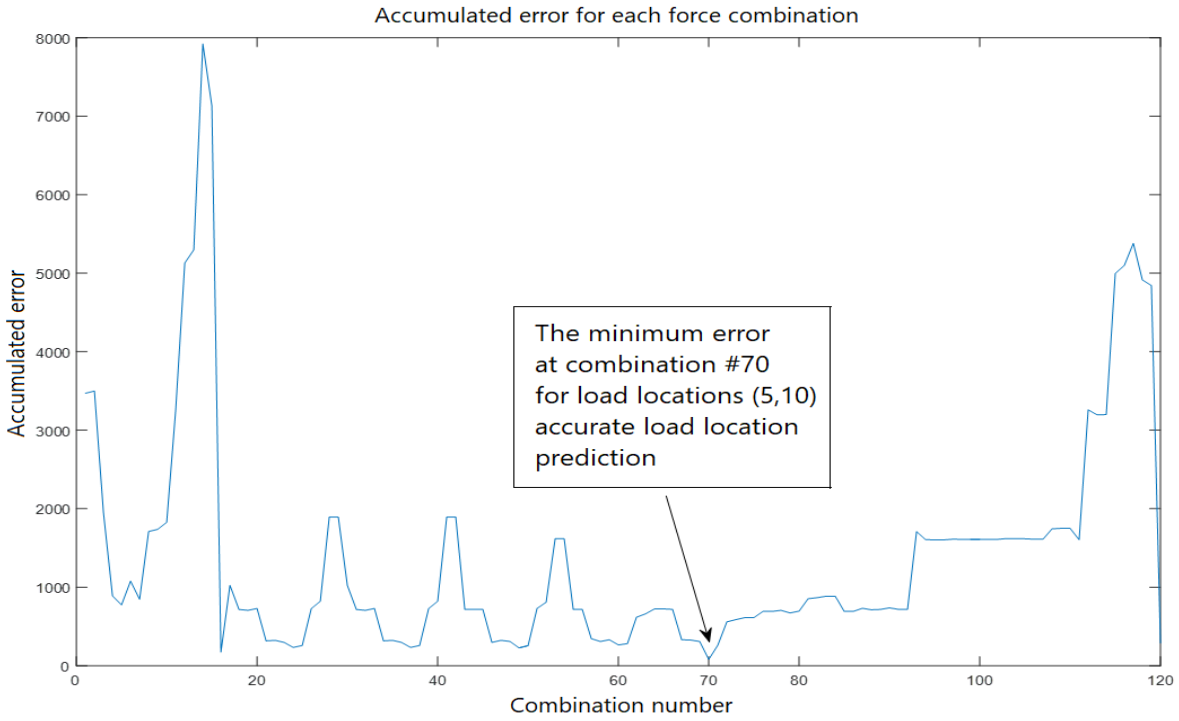

Figure 4.11 Accumulated Error with 5 Optimally Placed Sensors and Measurement Errors

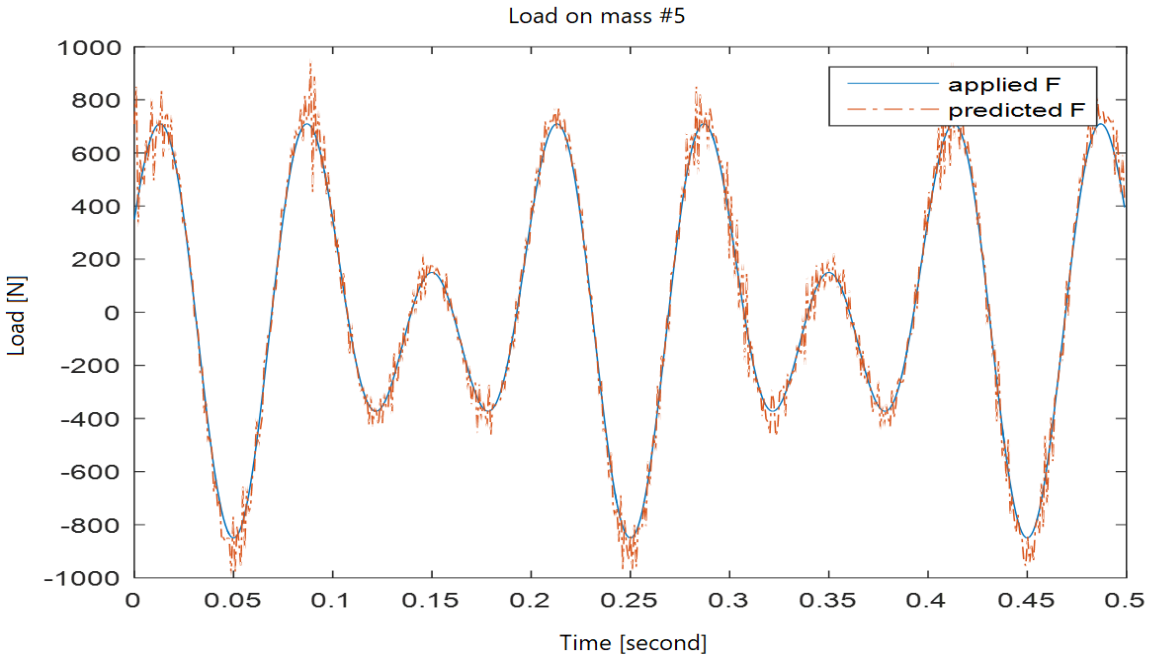

Figure 4.12 Applied and Reconstructed Load at Mass 5 with Measurement Errors

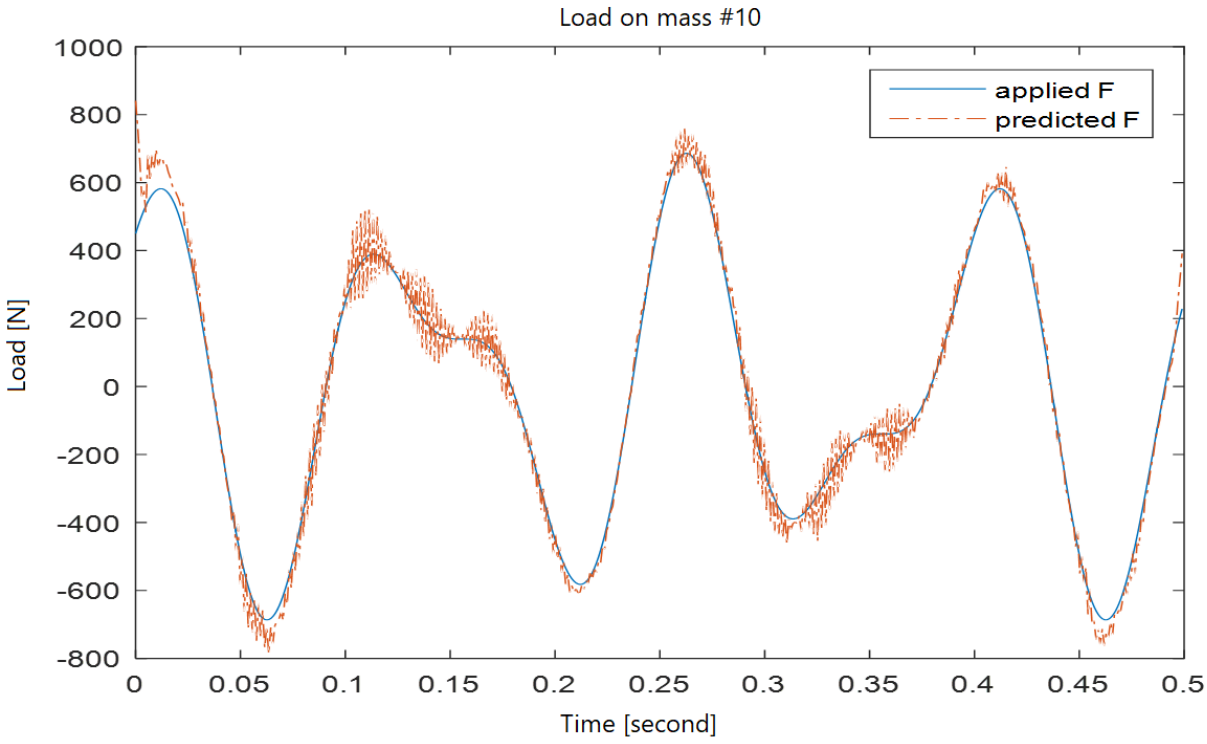

Figure 4.13 Applied and Reconstructed Load at Mass 10 with Measurement Errors

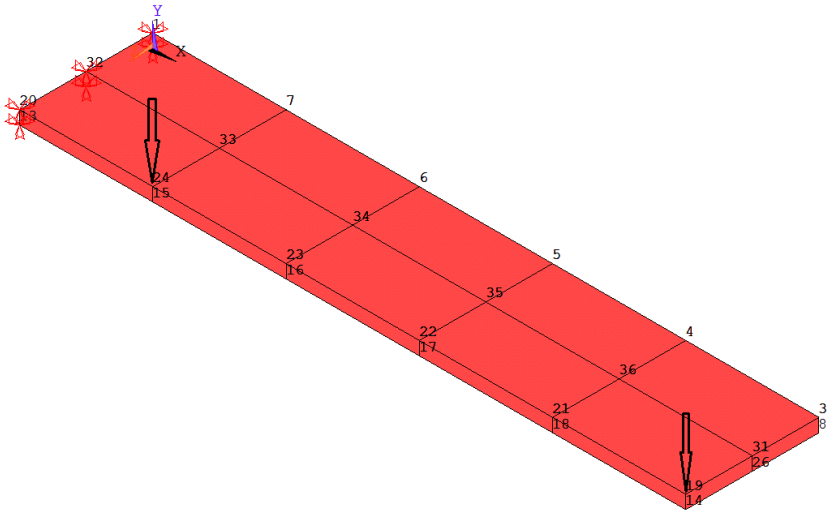

Figure 4.14 Finite Element Model of a 3D Cantilevered Beam

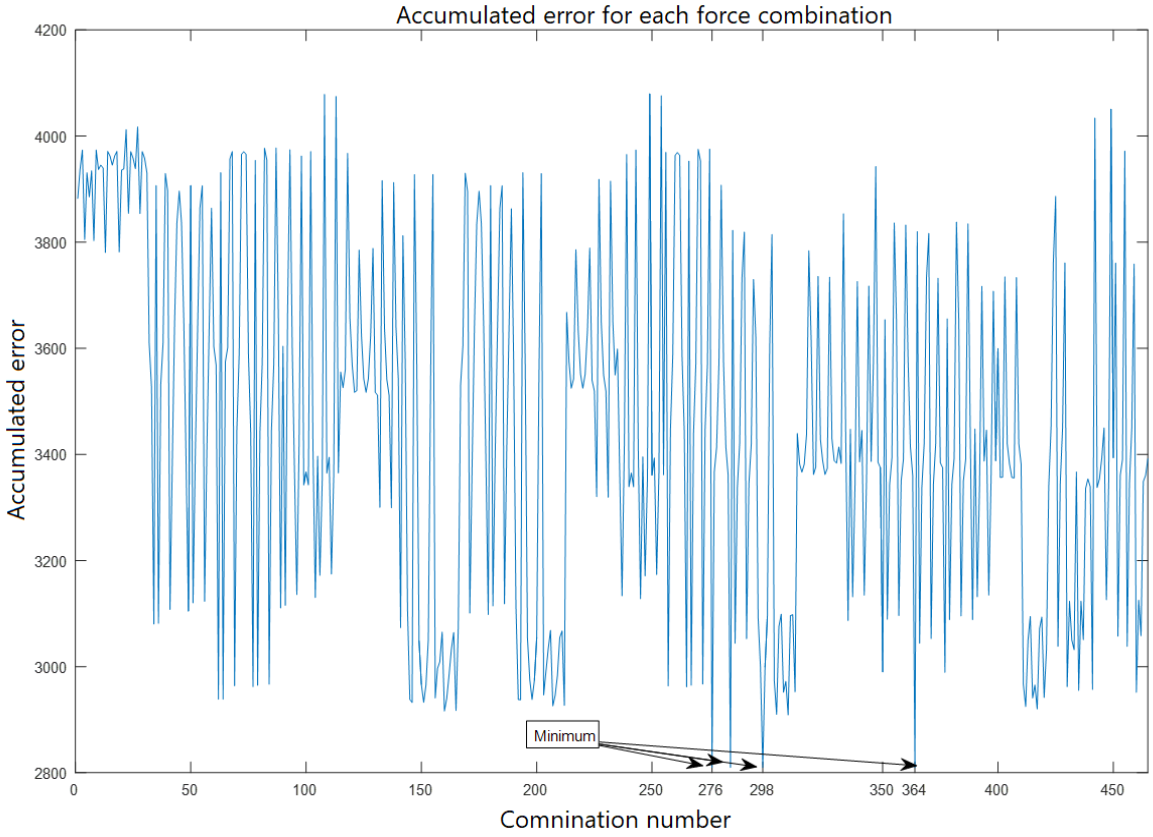

Figure 4.15 Accumulated Error in Frequency for 3D Cantilevered Beam

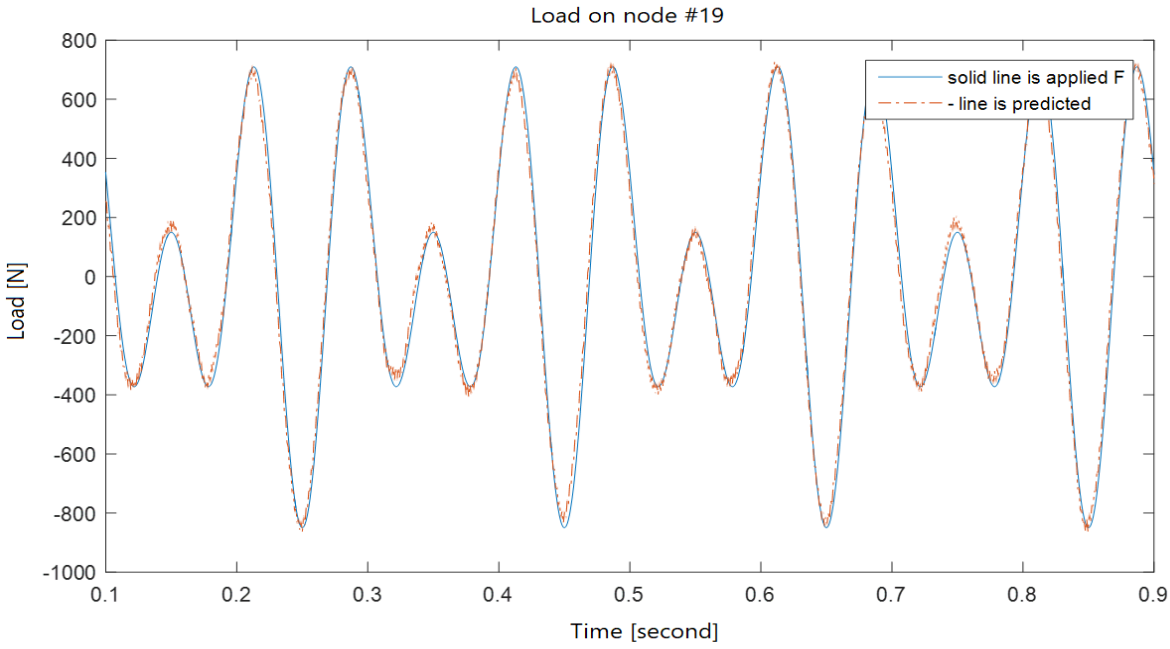

Figure 4.16 Applied and Reconstructed Load on Node 19 for 30 Retained Modes

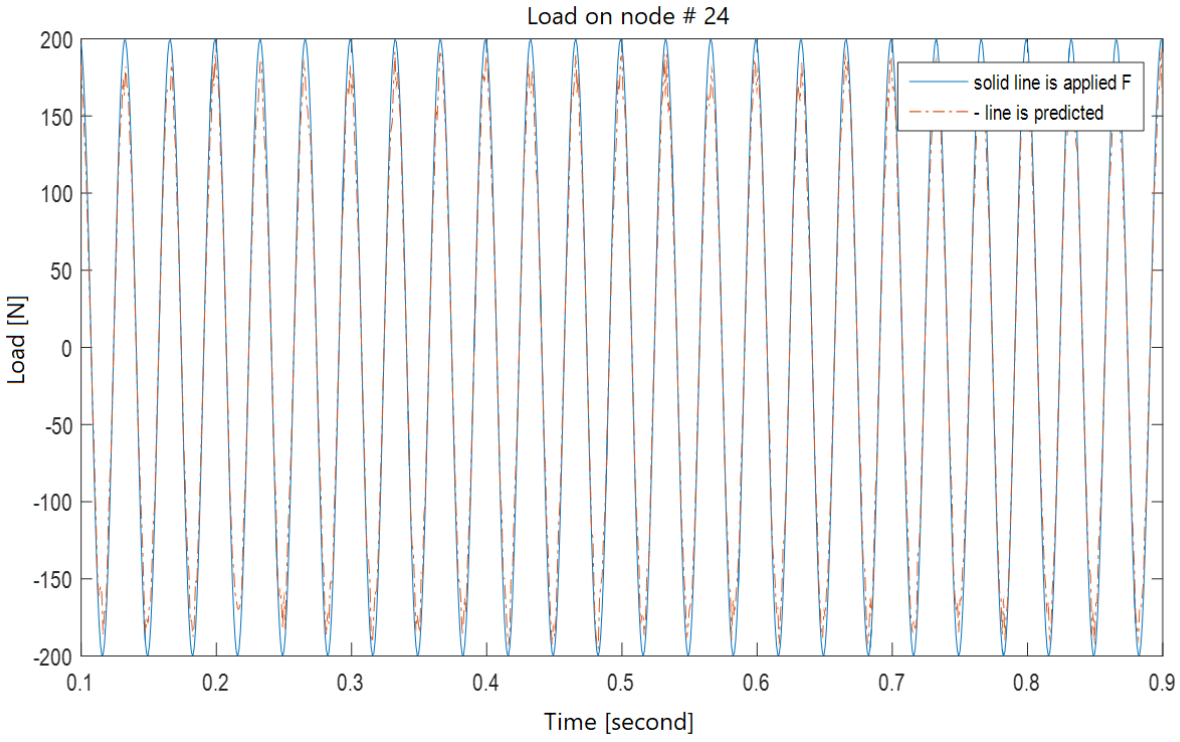

Figure 4.17 Applied and Reconstructed Load on Node 24 for 30 Retained Modes

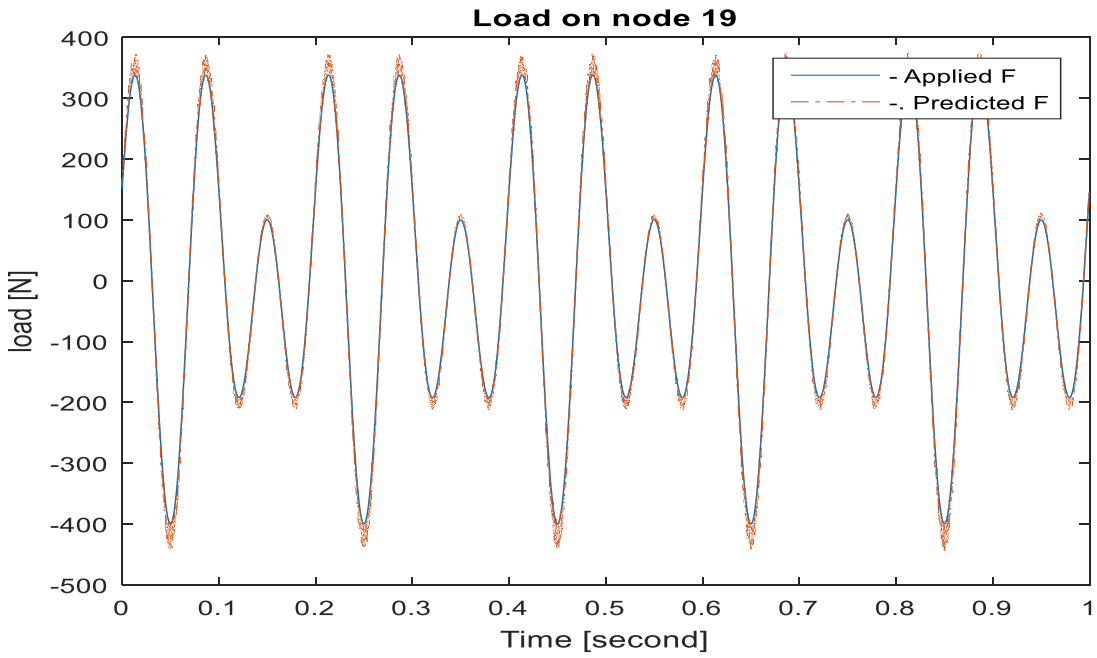

Figure 4.18 Applied and Reconstructed Load on Node 19 for 30 Retained Modes and with Measurement Errors

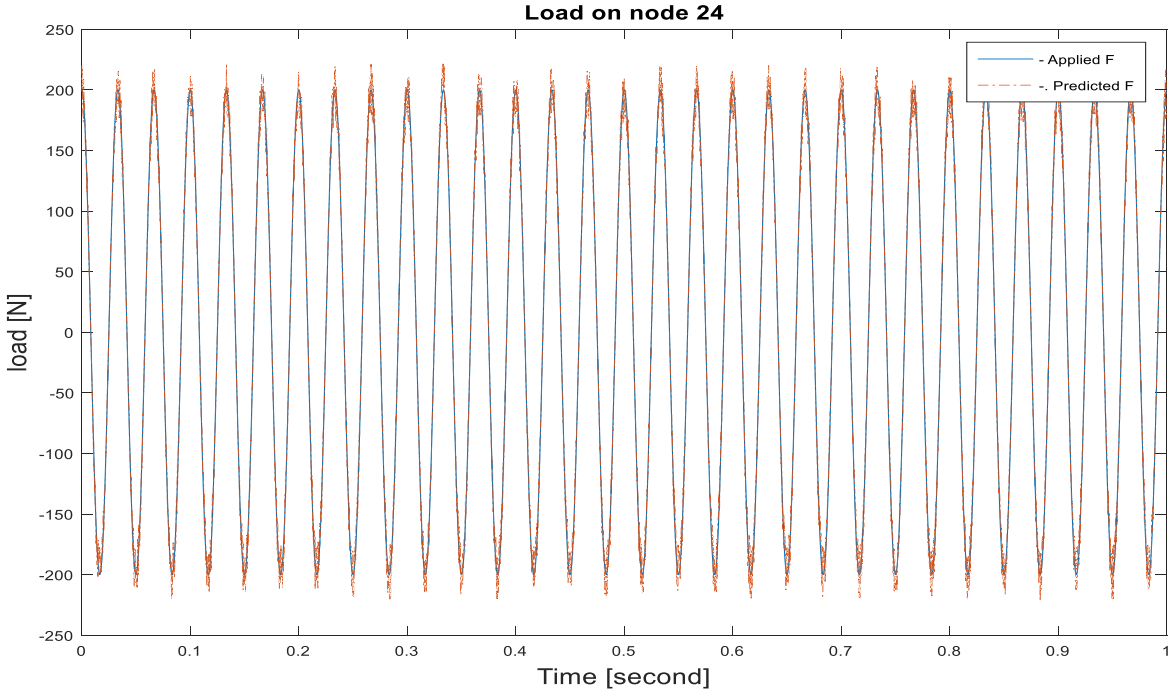

Figure 4.19 Applied and Reconstructed Load on Node 24 for 30 Retained Modes and with Measurement Errors

Chapter 5 - Load Identification Using Strain Transmissibility Concept and Optimum Sensor Placement

A detailed explanation of the load identification problem using motion transmissibility was presented in the previous chapter. The results from indirect force measurements as in Eqn. (4.5), are often highly sensitive to measurement noise and errors in structural modeling. An interesting observation was made by Hillary and Ewins (1984), who found that the measurements of strain may lead to more accurate results than measurements of acceleration for a beam-like structure. This is explained by the fact that for such structures, there are generally more vibrational eigen modes significantly contributing to the strain response than to the acceleration response. This sensitivity of the results to the number of participating structural modes has been investigated in detail by Fabunmi (1986), who suggested a scalar measure of the sensitivity based on this modal participation. Measures of the sensitivity have also been suggested by Starkey and Merrill (1989). In the work of Gupta (2013), it was also seen that strain-based load estimations lend themselves to better load estimates than acceleration-based approaches.

This chapter presents a frequency domain technique for predicting dynamic loads acting on a structure from a strain frequency response function (SFRF) measured at a finite number of optimally placed strain gages on the structure. The proposed technique uses a transmissibility concept to predict load locations and magnitudes. The structure basically acts as its own load transducer. The approach is based on the fact that the strain response of an elastic vibrating system can be expressed as a linear superposition of its

strain modes. Since the strain modes as well as the normal displacement modes are fundamental dynamic characteristics of a system, the dynamic loads exciting a structure are estimated by measuring induced strain fields.

As already discussed in the previous chapter, the accuracy of estimated loads depends on two factors:

1. The number and placement of sensors on the instrumented structure.
2. The number of retained displacement modes obtained from modal analysis.

Considering these two factors, a solution procedure based on strain modal analysis to obtain strain modes and the construction of a D-optimal design is applied to determine the optimum locations of strain gages that will provide the most precise load prediction for both location and magnitude. The concepts of a D-optimal design algorithm and candidate set have already been presented in the previous chapter. A novel approach is proposed in this chapter that makes use of a transmissibility concept resulting in significant improvement in accuracy in the dynamic load prediction. Validation of the proposed approach through numerical example problems is also presented, which illustrates the effectiveness and robustness of the technique.

5.1 Theoretical Background

According to the theory of modal analysis for vibrating elastic structures subject to dynamic loading, the structural displacement can be approximated by superposition of contributions from natural modes. The displacement can then be estimated by the obtained normal mode shapes and mode participation factors as:

$$u(t) = \sum_{i=1}^{m} \phi_i \, q_i(t) \tag{5.1}$$

In Eqn. (5.1), the displacement response in *x* direction is u, the i[th] (displacement) vibration mode is ϕ_i , the generalized modal coordinate is q_i whereas the time is denoted by t.

Corresponding to Eqn. (5.1), the strain field in the structure can be expressed as:

$$\varepsilon(t) = \sum_{i=1}^{m} \psi_i \, q_i(t) \tag{5.2}$$

where ψ_i is the strain mode. Assuming small displacements, the strains and displacements are related as:

$$\varepsilon_x = \frac{\partial u}{\partial x} \tag{5.3}$$

Consequently, the strain modes and normal modes are also related, and the strain mode function is obtained by differentiating the displacement mode function with respect to *x*:

$$\psi_i = \frac{\partial \phi_i}{\partial x} \tag{5.4}$$

Assuming a harmonic excitation input load *F*, the generalized modal coordinate q_i is expressed as:

$$q_i = \Delta_i^{-1} \phi_i \, F \tag{5.5}$$

where Δ can be defined for a damped system and undamped system as in Eqns. (5.5a) and (5.5b) below

$$\Delta_i = (-\omega^2 m_i + j\omega c_i + k_i) \quad (5.5a)$$

$$\Delta_i = (-\omega^2 m_i + k_i) \quad (5.5b)$$

Here m_i, c_i and k_i are the i^{th} modal mass, modal damping and modal stiffness, and ω is the excitation frequency. By substituting Eqn. (5.5) into Eqn. (5.2), a relationship between the input force and the strain output can be obtained:

$$\varepsilon_i(\omega) = \sum_{i=1}^{m} \psi_i \, \Delta_i^{-1} \phi_i F(\omega) \quad (5.6)$$

When written in matrix form, the expression above is called the strain frequency response function (SFRF) and is represented by:

$$[H^{\varepsilon}(\omega)] = \sum_{i=1}^{m} \Delta_i^{-1} \{\psi_i\}\{\phi_i\} = [\psi]\,[\Delta]^{-1}[\phi]^T \quad (5.7)$$

where $[\psi]$ denotes the modal strain matrix containing the strain modes. $[\phi]$denotes the modal matrix containing the displacement normal modes.

Expanding the matrix form yields:

$$\begin{bmatrix} H_{11}^{\varepsilon}(\omega) & H_{12}^{\varepsilon}(\omega) & \cdots & H_{1N_i}^{\varepsilon}(\omega) \\ H_{21}^{\varepsilon}(\omega) & H_{22}^{\varepsilon}(\omega) & \cdots & H_{2N_i}^{\varepsilon}(\omega) \\ \vdots & \vdots & \vdots & \vdots \\ H_{N_o 1}^{\varepsilon}(\omega) & H_{N_o 2}^{\varepsilon}(\omega) & \cdots & H_{N_o N_i}^{\varepsilon}(\omega) \end{bmatrix} = \sum_{i=1}^{m} \Delta_i^{-1} \cdot \begin{bmatrix} \psi_{1i}\phi_{1i} & \psi_{1i}\phi_{2i} & \cdots & \psi_{1i}\phi_{N_i i} \\ \psi_{2i}\phi_{1i} & \psi_{2i}\phi_{2i} & \cdots & \psi_{2i}\phi_{N_i i} \\ \vdots & \vdots & \vdots & \vdots \\ \psi_{N_o i}\phi_{1i} & \psi_{N_o i}\phi_{2i} & \cdots & \psi_{N_o i}\phi_{N_i i} \end{bmatrix} \quad (5.8)$$

where the number of strain gauge measurements is represented by N_o and the number of excitation points is represented by N_i.

From Eqn. (5.8) it is seen that each row of the SFRF matrix contains information related to the displacement modes (ϕ), and each column in the SFRF matrix contains information related to the strain modes (ψ). Basically, the strain mode shapes can be

obtained by fixing an excitation point and measuring the strain responses. Meanwhile, the displacement mode shapes can be obtained by moving the excitation point and using the strain gage as a fixed reference sensor.

Therefore, SFRF may be applied in two ways, to predict structural stresses due to various loading conditions, as well as to predict the load applied using the output response of the strain gages. A system modeled using SFRF has its input-output relationship as given in Eqn. (5.9):

$$\begin{Bmatrix} \varepsilon_1(\omega) \\ \varepsilon_2(\omega) \\ \vdots \\ \varepsilon_{N_o}(\omega) \end{Bmatrix} = \begin{bmatrix} H_{11}^{\varepsilon}(\omega) & H_{12}^{\varepsilon}(\omega) & \cdots & H_{1N_i}^{\varepsilon}(\omega) \\ H_{21}^{\varepsilon}(\omega) & H_{22}^{\varepsilon}(\omega) & \cdots & H_{2N_i}^{\varepsilon}(\omega) \\ \vdots & \vdots & \vdots & \vdots \\ H_{N_o 1}^{\varepsilon}(\omega) & H_{N_o 2}^{\varepsilon}(\omega) & \cdots & H_{N_o N_i}^{\varepsilon}(\omega) \end{bmatrix} \begin{Bmatrix} F_1(\omega) \\ F_2(\omega) \\ \vdots \\ F_{N_i}(\omega) \end{Bmatrix} \tag{5.9}$$

where $F_{N_i}(\omega)$ is the Fourier spectrum of the excitation force at point N_i, $\varepsilon_{N_o}(\omega)$ is the Fourier spectrum of the response at point N_o , $H_{N_o N_i}^{\varepsilon}(\omega)$ is the SFRF with input point N_i and response point N_o . Rewriting Eqn. (5.9) gives:

$$\{\varepsilon(\omega)\} = [H^{\varepsilon}(\omega)]\{F(\omega)\} \tag{5.10}$$

If the number of excitation points N_i and the number of response points N_o are the same (N_i = N_o), force spectra are identified by pre-multiplying the inverse of the frequency response function matrix H^{ε} with the strain vector as follows:

$$\{F(\omega)\} = [H^{\varepsilon}(\omega)]^{-1}\{\varepsilon(\omega)\} \tag{5.11}$$

On the other hand, to improve the identification accuracy of the force spectra, it is common that the number of response points is usually more than the number of excitation points (N_i < N_o). In this case, the excitation force is identified using the least squares method. This condition is desirable to increase the accuracy of identification. The excitation force is identified as follows:

$$\{F(\omega)\} = [H^{\varepsilon}(\omega)]^{+}\{\varepsilon(\omega)\} \tag{5.12}$$

where $H^{\varepsilon}(\omega)^{+}$ is pseudo-inverse matrix given by:

$$(H^{\varepsilon}(\omega)^{+} = (H^{\varepsilon}(\omega)^{H}H^{\varepsilon}(\omega))^{-1}H^{\varepsilon}(\omega)^{H}) \tag{5.13}$$

The superscript ^{H} indicates the conjugate transpose. The excitation force is estimated by using Eqn. (5.11) or (5.12).

5.2 Strain Transmissibility for MDOF system

To develop the strain transmissibility for MDOF system, one can take advantage of the similarity between Eqn. (4.5) and Eqn. (5.11) so the procedure described earlier in Sec. 4.1 can be used.

Based on harmonically applied forces at coordinates *P*, one may establish that strains at coordinates *J* and *I* are related to the applied forces at coordinates *P* by the following relationships:

$$\{\varepsilon(\omega)\}_J = [H^{\varepsilon}(\omega)]_{JP}\{F(\omega)\}_P \tag{5.14}$$

$$\{\varepsilon(\omega)\}_I = [H^{\varepsilon}(\omega)]_{IP}\{F(\omega)\}_P \tag{5.15}$$

From Eqn. (5.15) using $\{F(\omega)\}_P = [H^{\varepsilon}(\omega)]^{+}_{IP}\{\varepsilon(\omega)\}_I$ and substituting in Eqn. (5.14) yields:

$$\{\varepsilon(\omega)\}_J = [H^{\varepsilon}(\omega)]_{JP}[H^{\varepsilon}(\omega)]^{+}_{IP}\{\varepsilon(\omega)\}_I = [T_{\varepsilon}(\omega)]^{P}_{JI}\{\varepsilon(\omega)\}_I \tag{5.16}$$

where $[H^{\varepsilon}(\omega)]^{+}_{IP}$ denotes the pseudo-inverse of the SFRF matrix and the strain transmissibility matrix that relates both sets of strains is defined as:

$$[T_{\varepsilon}(\omega)]_{JI}^{P} = [H^{\varepsilon}(\omega)]_{JP}[H^{\varepsilon}(\omega)]_{IP}^{+} \quad (5.17)$$

Here $[H^{\varepsilon}(\omega)]_{IP}^{+}$ is the pseudo-inverse of the sub-matrix $[H^{\varepsilon}(\omega)]_{IP}$ and can be obtained experimentally or analytically. The only required condition for the pseudo inverse to exist in Eqn. (5.17) is that the number of strain data measurements on *I* coordinates should be greater than or equal to the number of applied point loads on *P* coordinates i.e., $N_I \geq N_P$.

An important property of the strain transmissibility matrix to be used here is that it does not depend on the magnitude of the involved forces and only requires the knowledge of a set of coordinates that include all the coordinates where the forces are applied. One important aspect of this definition is that submatrices $[H^{\varepsilon}(\omega)]_{JP}$ and $[H^{\varepsilon}(\omega)]_{IP}$ may be obtained experimentally or analytically.

5.3 Force Localization Based on Strain Transmissibility and Force Reconstruction

This section shows the force localization algorithm based on the strain transmissibility and reconstruction using the measured strains and the updated numerical model. As discussed earlier in Sec. 4.4 from the previous chapter, the force identification problem is divided into two distinct steps. The localization of the forces, i.e., the identification of the number and location of the applied forces using the strain transmissibility concept, followed by estimation of magnitudes of the loads at those predicted locations.

Based on the measured strain data, a search for the number and location of forces is performed using strain transmissibility. Basically, this step consists of searching for the strain transmissibility matrix that corresponds to the dynamics of the system and using the available measured strain data and the numerical model involved. Once the corresponding strain transmissibility matrix is found, one has a solution for the number and location of the forces applied to the structure.

The second phase consists of reconstructing the load vector with the results obtained in the first phase. A more detailed description about this methodology is given in the following sections.

5.3.1 Force Localization

At the first stage, to apply the method suggested in the previous section, one finds the strain transmissibility matrix that transforms the dynamic strains $\{\varepsilon(\omega)\}_I$ into $\{\varepsilon(\omega)\}_J$. As one does not know the location of the applied forces, all the possibilities should be covered until the calculated strains $\{\varepsilon(\omega)\}_J$ match the measured ones $\{\tilde{\varepsilon}(\omega)\}_J$ over a range of frequencies. Then calculation of vector $\{\varepsilon(\omega)\}_J$ is done by using Eqn. (5.16)

The maximum number of forces must be less than or equal to the dimension of the known dynamic strain vector $\{\varepsilon(\omega)\}_I$.

The successive combinations of the tested nodes are obtained as described in Sec. 4.4.1. The error in each combination is kept in a vector to identify the combination with the least associated error (in absolute value). Firstly, the algorithm scrolls through the possible combinations of position and number of forces. For each combination, the associated error between the calculated vector $\{\varepsilon(\omega)\}_J$ and the measured strain vector

$\{\tilde{\varepsilon}(\omega)\}_J$ is calculated; this is carried out over a frequency range defined by the user. The error between the predicted and the measured dynamic strain at each coordinate *k* can be defined as:

$$S_k = \sum_{\omega} \left(\log\left(abs\left(\tilde{\varepsilon}_{J_k}(\omega) \right) \right) - \log\left(abs\left(\varepsilon_{J_k}(\omega) \right) \right) \right)^2 \tag{5.18}$$

For each combination, the calculated error is kept in an entry of the error vector and analyzed later. The accumulated error for a given combination of coordinates where ***F*** can be located is the norm of e:

$$\{e\} = \{S_k\} \tag{5.19}$$

The calculations are repeated for successive combinations of the number and the position of forces. The combination of the force locations that gives the lowest error leads to the number and position of the forces applied to the structure. As already mentioned, the maximum number of forces that can be found is equal to the dimension of the known dynamic strain vector.

5.3.2 Force Reconstruction

In a second phase, the reconstruction of the force amplitudes consists of solving an inverse problem using the measured dynamic strains $\{\varepsilon(\omega)\}_I$ as in Eqn. (5.20).

$$\{F(\omega)\}_P = [H^{\varepsilon}(\omega)]^{+}_{IP} \ \{\varepsilon(\omega)\}_I \tag{5.20}$$

Note that for the given system to be invertible, the number of dynamic strains to be used (set *I*) must be higher than or equal to the number of applied forces (set *P*).

However, this is always verified, as the first step of the solution process already forces a satisfaction of this requirement.

5.4 Strain Transmissibility and D-optimal design

As shown in Sec. 4.5.2 in the previous chapter, using the non-optimal locations of sensors (set *I*) does not provide correct load locations since the error function is likely to get trapped at a local minimum. In this section, an approach based upon the D-optimal design and the strain transmissibility concept is proposed to help select the optimum locations of the strain gages such that precise load estimates are obtained.

It is well known that strain data in $\{\varepsilon(\omega)\}_I$ is prone to measurement errors and the inverse problem identified by Eqn. (5.20) tends to be ill-conditioned. The precision with which $\{F(\omega)\}_P$ is estimated from a measured strain response depends on the number, the locations of strain gages on the structure, and the number of retained modes. For a given number of strain gages *g*, and a given number of retained modes *m*, following the D-optimal design algorithm described at length in Sec. 4.6.4, the candidate set from the strain modal matrix $[\psi]_{cand.}$ is searched to determine its optimum subset $[\psi]_{opt.}$. Then the strain frequency response functions (SFRF) at optimum locations $I_{opt.}$ for all possible load locations for a given range of frequencies can be calculated to get $[H^{\varepsilon}(\omega)]_{opt}$. Based on these optimum locations, the strain data will be measured to get $\{\varepsilon(\omega)\}_{I(opt)}$.

Following the procedure described in subsection 4.4.1 the accumulated errors for all possible applied loads are calculated as given in Eqn. (5.18) and saved in a vector

error to be analyzed later such that the minimum error will give the combination number that corresponds to the right load locations.

As a result, from the first phase, applying the second phase to estimate load magnitudes can be done using Eqn. (5.21):

$$\{F(\omega)\}_P = [H^{\varepsilon}(\omega)]^{+}_{IP(opt)} \ \{\varepsilon(\omega)\}_{I(opt)} \tag{5.21}$$

Two examples dealing with numerical validation of the proposed approach are presented to illustrate the effectiveness of using the optimal strain gages' locations to identify the loads applied to the structure. In addition, the effect of the number of modes retained on the accuracy of the recovered load is also presented.

5.5 Examples

Two numerical examples are presented next to identify the loads applied to a structure using the concept of strain transmissibility. Optimum locations of strain gages are determined using the D-optimal algorithm programmed in MATLAB. The first example deals with the prediction of a point load acting on a motorcycle horn bracket whereas the second example addresses the prediction of two loads applied to a simply supported beam. The influence of the number of retained modes on the quality of the load estimates is also demonstrated. The finite element (FE) models of the test components were created using the ANSYS-APDL software.

5.5.1 Motorcycle Horn Bracket

This example deals with the prediction of a point load acting on a motorcycle horn bracket. A finite element model of the bracket was developed in ANSYS using SHELL181

elements. Without loss of generality, the system is assumed to be undamped. The finite element model including boundary conditions and the applied load is shown in Fig. 5.1. All degrees of freedom at the two holes were restrained. The model consists of 198 shell elements and has 233 unconstrained nodes with 6 degrees of freedom per node. The total number of degrees of freedom was 1398. A single point force on Y direction was applied to node number 142 and is given as:

$$F(t) = 5000\sin(60t) + 8000\sin(40t)$$

In this example, assuming the number of applied loads is known in advance, two cases were implemented. The first case is using the strain transmissibility for the load location and the magnitude prediction assuming the load direction is known in advance. The second case is using the strain transmissibility for the load location and the magnitude prediction when the load direction is assumed to be unknown.

Case 1: Point-load prediction using strain transmissibility and optimum strain gages locations for a known load direction

In the first phase, the search process to predict the load direction and the location on the structure depends on the degree of freedom for each node ; knowing the number and the direction of the applied load ahead of time will shorten the search process and save the computational time, so as a first step; it may be suitable to construct the reduced strain modal matrix such that it has only the strain modes in the same direction as the applied load. For this example, the reduced strain-modal matrix will have 233 strain

normal modes in the Y direction. Therefore, the candidate strain-modal matrix $[\psi_Y]_{cand.}$ will be $[\psi_Y]_{233x233}$, and this will be the input for the D-optimal program.

Using the D-optimal algorithm to find the optimum locations for ten strain gages (*g=10*), and for a given number of retained Y strain modes *m* that capture at least 90% of the cumulative mass fraction, the candidate set from the strain modal matrix $[\psi_Y]_{cand.}$ is searched to determine its optimum subset $[\psi_Y]_{opt.}$. After $[\psi_Y]_{opt.}$ is found, the optimum strain gages locations are determined (I_{opt}). Then the strain frequency response functions at optimum locations for all possible load locations for a given range of frequencies are calculated using a MATLAB program to get $[H_Y^{\varepsilon}(\omega)]_{opt}$. Based on these optimum locations, the strain data are measured to get $\{\varepsilon_Y(t)\}_{I(opt)}$. For the measured strains at *J* coordinates $\{\varepsilon_Y(t)\}_J$, one can arbitrarily pick any locations. In the example considered here, *J* coordinates are assumed to be the same *I* coordinates. (See Table 5.1).

The strain vector can be found directly from the finite element model in ANSYS at the optimal *I* coordinates $\{\varepsilon_Y(t)\}_{I(opt)}$ and at *J* coordinates $\{\varepsilon_Y(t)\}_J$. From $\{\varepsilon_Y(t)\}_{I(opt)}$ and $\{\varepsilon_Y(t)\}_J$, a MATLAB program is used to get the strain data in a frequency domain $\{\varepsilon_Y(\omega)\}_{I(opt)}$ and $\{\varepsilon_Y(\omega)\}_J$ using (fft) command. Then the procedure described in subsection 4.4.1 is implemented to calculate the accumulated errors for all possible applied load locations as given in Eqn. (5.18) and plotted as shown in Fig. 5.2. For this case where the load direction is known a priori, the total number of combinations explored for one applied load is 233. The applied load location at node 142 corresponds to combination number 142. It can be seen from Fig. 5.2 that there is a minimum value at this combination number that corresponds to the load location being predicted correctly.

Next, the second phase is implemented to reconstruct the load magnitude for a chosen number of retained modes (*m*=25 modes); those retained modes should capture at least 90% of the cumulative mass fraction. Using Eqn. (5.21) and transforming into a time domain using an Inverse Fourier Transform (IFT), the reconstructed load is plotted along with the applied load as shown in Fig.5.3. It can be seen from the figure that the load trends are covered with reasonable accuracy.

Case 2: Point-load prediction using strain transmissibility and optimum strain gages locations for an un-known load direction

There are some applications where the directions of loads under consideration are unknown. In this case, to use the strain transmissibility for load prediction, the same procedure will be followed except that the number of combinations to be tested will be increased. In this example where there are 233 unconstrained nodes, each node has three possible directions for the applied load (X, Y, and Z) directions, so the total number of combinations is 699. Therefore, the candidate strain-modal matrix $[\psi]_{cand.}$will be $[\psi_{XYZ}]_{699\text{x}699}$, and this will be the input for the D-optimal program.

Applying the D-optimal algorithm to find the optimum locations for ten strain gages (*g=10*), and for a given number of retained strain modes *m*, the candidate set from the strain modal matrix $[\psi]_{cand.}$is searched to determine its optimum subset $[\psi]_{opt.}$. After $[\psi]_{opt.}$is found, the optimum strain gages locations are determined (I_{opt}). Then the strain frequency response functions at optimum locations for all possible load locations for a given range of frequencies are calculated to get $[H^{\varepsilon}_{XYZ}(\omega)]_{opt}$, based on these optimum locations (I_{opt}) and choosing *J* coordinates for this example as *I* coordinates. (see Table

5.2). The strain data $\{\varepsilon_{XYZ}(t)\}_{I(opt)}$ and $\{\varepsilon_{XYZ}(t)\}_J$ could be measured experimentally or found directly from the finite element model in ANSYS. Later, all strain data $\{\varepsilon_{XYZ}(t)\}_{I(opt)}$ and $\{\varepsilon_{XYZ}(t)\}_J$ are transformed to a frequency domain through a MATLAB program using (fft) command to get $\{\varepsilon_{XYZ}(\omega)\}_{I(opt)}$ and $\{\varepsilon_{XYZ}(\omega)\}_J$.

Following the procedure described in subsection 4.4.1 the accumulated errors for all possible applied load locations are calculated as given in Eqn. (5.18) and plotted as shown in Fig. 5.4. For this case where the load direction is unknown, the total number of combinations explored for one applied load is 699. The applied load location at node 142 on Y direction corresponds to combination number 425. It can be seen from Fig. 5.4 there is a minimum value at this combination number that corresponds to the load location and direction being predicted correctly.

It is worth mentioning that in Fig.5.4, there are other two minima that belong to the following combination numbers, 410, which corresponds to the load on the Y direction for node 137 and, 440, which corresponds to the load on the Y direction for node 147. Both nodes are very close from the exact applied load location. (See Fig. 5.1).

In phase two, the load magnitude on the predicted load location is constructed using Eqn. (5.21) for a chosen number *m* of retained modes and transformed into a time domain using (IFT). To study the effect of the number of the retained modes *m* on the accuracy of the prediction process, two options were explored, one with 15 retained modes (*m*=15), and the second one with 25 retained modes (*m*=25). The reconstructed loads are plotted along with the applied load as shown in Figs. 5.5 and 5.6. It can be seen from the figures that the load trends are covered with reasonable accuracy and increasing the number of retained modes increases the prediction accuracy.

5.5.2 3D Cantilevered Beam

The numerical example discussed previously dealt with a single load prediction. Next a cantilevered beam is considered where two dynamic loads in different directions are applied to the cantilevered steel beam described in Sec. 4.6.5 (see Fig. 5.7). One of the loads is applied in the Z direction on node 3 and described as $f_3(t) = 500\sin(3\pi t)$, and the other applied load is a vertical load in the Y direction on node 22 and given as $f_{22}(t) = 500\cos(3\pi t)$.

As shown in the previous example, the load identification process will involve two phases. The first phase is to estimate the number, the locations, and the directions of the applied loads. The second phase is to reconstruct the loads' magnitudes by using the strain transmissibility and optimum locations for the strain gages. As discussed earlier, a limited subset of modes is retained to reconstruct the applied loads. The strain modal matrix of the FE model of the beam can be obtained from the strain modal analysis using ANSYS.

Considering the modes in the Y and Z directions only, the reduced strain modal matrix will have 60 strain normal modes. Therefore, the candidate strain-modal matrix $[\psi]_{cand.}$ will be $[\psi_{YZ}]_{60\text{x}60}$, which will be the input for the D-optimal program.

Using the D-optimal algorithm to find the optimum locations for five strain gages (*g=5*), and for a given number of retained strain modes *m* the candidate set from the strain modal matrix $[\psi]_{cand.}$ is searched to determine its optimum subset $[\psi]_{opt.}$. After $[\psi]_{opt.}$ is found, the optimum strain gages locations are determined (I_{opt}). Then the strain frequency response functions at optimum locations for all possible load locations for a

given range of frequencies are calculated to get $[H_{YZ}^{\varepsilon}(\omega)]_{opt}$. Based on these optimum locations and choosing *J* coordinates to be as *I* coordinates for this example (see Table 5.3), the strain vector is obtained for $\{\varepsilon_{YZ}(t)\}_{I(opt)}$ and $\{\varepsilon_{YZ}(t)\}_J$ from the finite element model in ANSYS, then transformed to $\{\varepsilon_{YZ}(\omega)\}_{I(opt)}$ and $\{\varepsilon_{YZ}(\omega)\}_J$ by using a MATLAB program.

Next, the accumulated errors for all possible applied load locations and directions are calculated as given in Eqn. (5.18) and plotted as shown in Fig. 5.8. For this example, there are 30 unconstrained nodes, so the number of combinations with the assumption of one load applied in the Y or Z direction is 60 combinations. While the number of combinations with the assumption of two loads applied in the Y and/or Z direction is 1769 combinations, so the total number of combinations to cover these two assumptions is 1829 combinations. The combination number that corresponds to the case of two applied loads on node 3 in the Z direction and on node 22 in the Y direction is 152. It can be seen from Fig. 5.8 that there is a minimum value at this combination number that corresponds to the load's locations and directions being predicted correctly. Other local minima can be seen in Fig. 5.8, these are the following:

i.) At combination number 144 that corresponds to the case of two loads applied on (3Z,17Y).

ii.) At combination number 669 that corresponds to the case of two applied loads on (8Z,17Y).

iii.) At combination number 679 that corresponds to the case of two loads applied on (8Z,22Y).

From Fig.5.7 it is shown that node 3 lies on top of node 8 and node 22 lies on top of node 17, which explains why there are minimum errors are observed at these combination numbers.

One more point can be clarified from Fig. 5.8 regarding the errors' values for combination numbers ranging from 1 to 60 that belong to the assumption of a single load applied. The errors values in that range have significant large magnitudes compared with the errors' magnitudes for combination numbers that belong to the case of two loads applied, which assure that this structure is subjected to two loads.

Next, the load magnitude reconstruction phase is implemented by using Eqn. (5.21) and transforming into a time domain using Inverse Fourier Transform (IFT). The reconstructed loads are plotted along with applied loads as shown in Figs. 5.9 and 5.10 It can be seen from the figures that the load trends are covered with reasonable accuracy. It may be noted that these figures correspond to the case when no error was assumed to be present in strain measurements. Therefore, to simulate a more realistic scenario where strains are measured experimentally, each element in $\{\varepsilon_{YZ}(t)\}$ was corrupted with normally distributed random errors with zero mean and standard deviation of 10% of its value. The applied and recovered loads, with errors in strain measurements, are plotted in Figs. 5.11 and 5.12. Once again, it can be seen that the proposed approach is able to recover the applied loads fairly accurately. It is worth mentioning that due to the difference in the magnitudes of moments of inertia about y- and z-axes, the strains induced due to loads about y- and z-directions are quite different in magnitudes. Since the strain induced to load in the y-direction is significantly larger than the strain induced by a load in the z-

direction, the load estimates in z-direction are more susceptible to errors compared to imposed loads in y-direction.

5.6 Conclusions and Summary

In this chapter, load identification (load location, direction and magnitude) by using the concept of strain transmissibility has been proposed and examined for two different multi degree of freedom continuous systems. Based on the results presented, using optimum locations of strain gages as determined by the D-optimal algorithm improves the identification for the unknown loads especially when multiple loads are applied and when the error function has multiple local minima. In addition, it was seen that increasing the number of retained modes to reconstruct the response improves the accuracy of load identification results. Practically there are limitations on the number of modes whose MPF can be estimated from strain gages measurements. This issue on model condensation will be conducted in chapter 7 to overcome this limitation and so that the accuracy of load identification results can be improved further.

Using strain gages as system responses has been verified numerically for its effectiveness in solving the load identification problem based on the strain transmissibility even in the presence of simulated measurement errors, the proposed method yields promising results. In the interest of studying the effect of using different types of sensors in the accuracy of load prediction; a computational comparison for load magnitudes' identification using accelerometers and strain gages will be presented in the coming chapter.

Table 5.1 Input Data for Motorcycle Horn Bracket with Known Load Direction

Optimal *I* coordinates	[14,30,75,83,106,168,191,193,228,239]
J coordinates	[14,30,75,83,106,168,191,193,228,239]
P coordinate	[142]

Table 5.2 Input Data for Motorcycle Horn Bracket with Unknown Load Direction

Optimal *I* coordinates	[14,75,83,106,159,191,193,200,228,238]
J coordinates	[14,75,83,106,159,191,193,200,228,238]
P coordinate	[142]

Table 5.3 Input Data for 3D Cantilevered Beam with Two Loads Applied in Different Directions

Optimal *I* coordinates	[11,14,16,19,24]
J coordinates	[11,14,16,19,24]
P coordinate	[3Z,22Y]

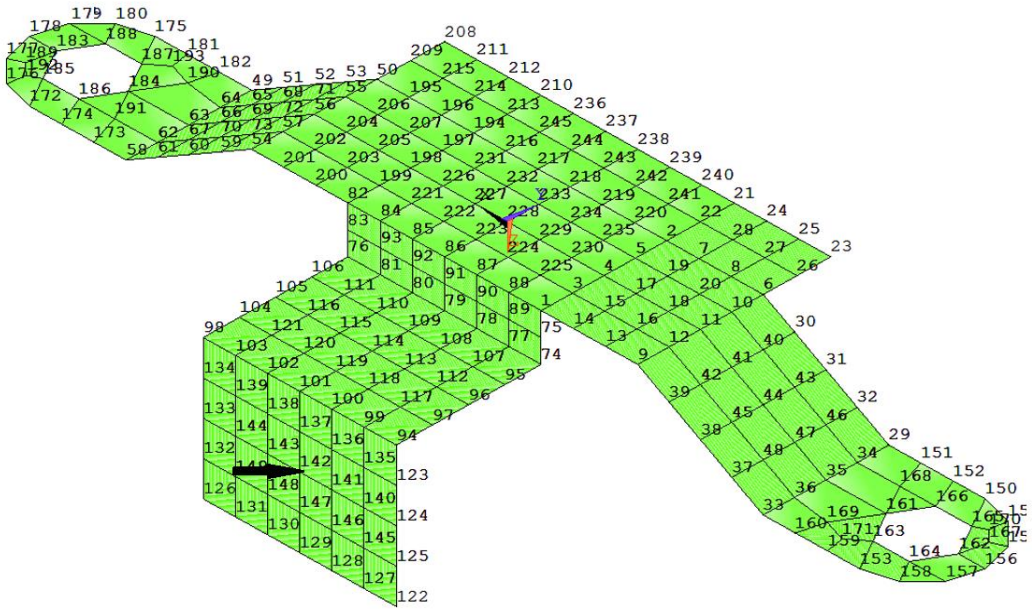

Figure 5.1 Finite Element Model for Motorcycle Horn Bracket

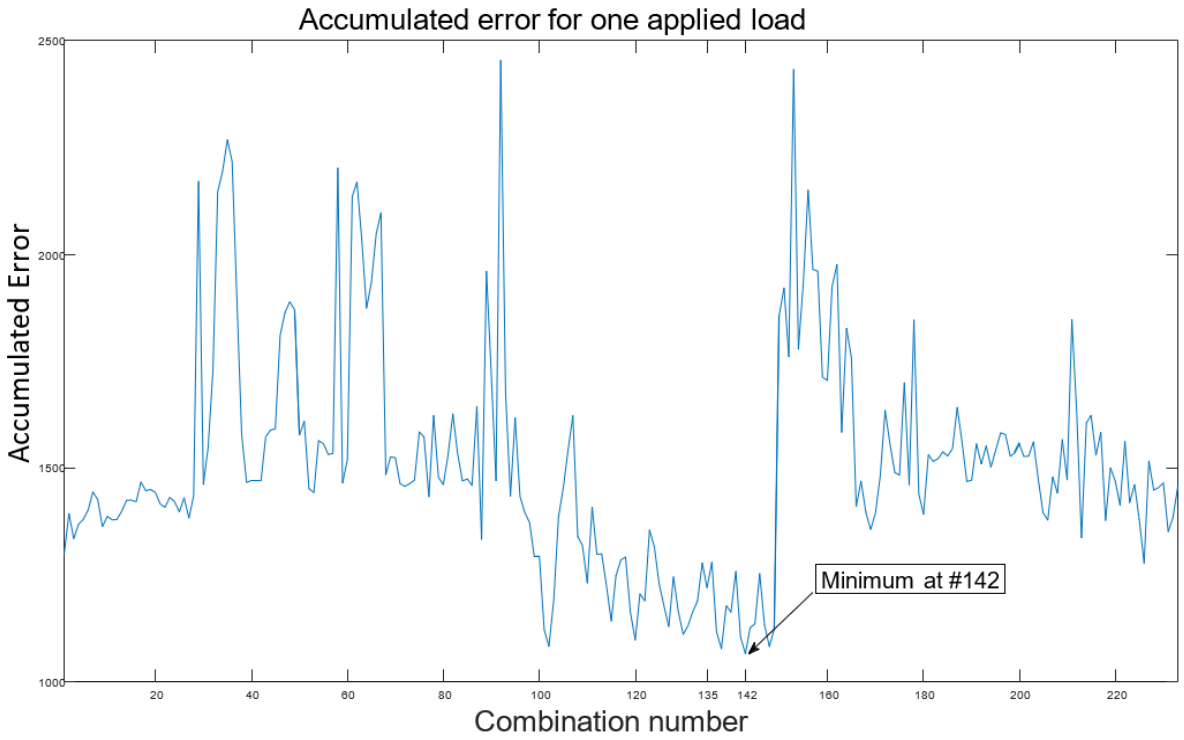

Figure 5.2 Accumulated Error for Motorcycle Horn Bracket Example Case 1

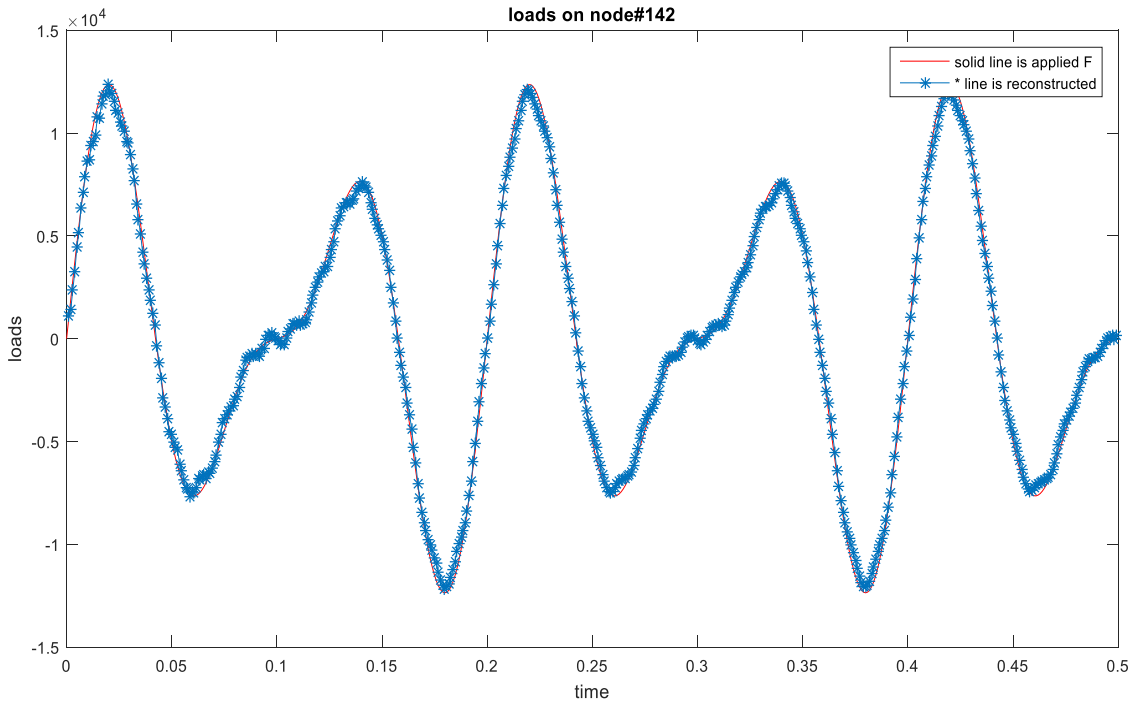

Figure 5.3 Applied and Predicted Loads Using Strain Transmissibility with 25 Retained Modes and 10 Strain Gages

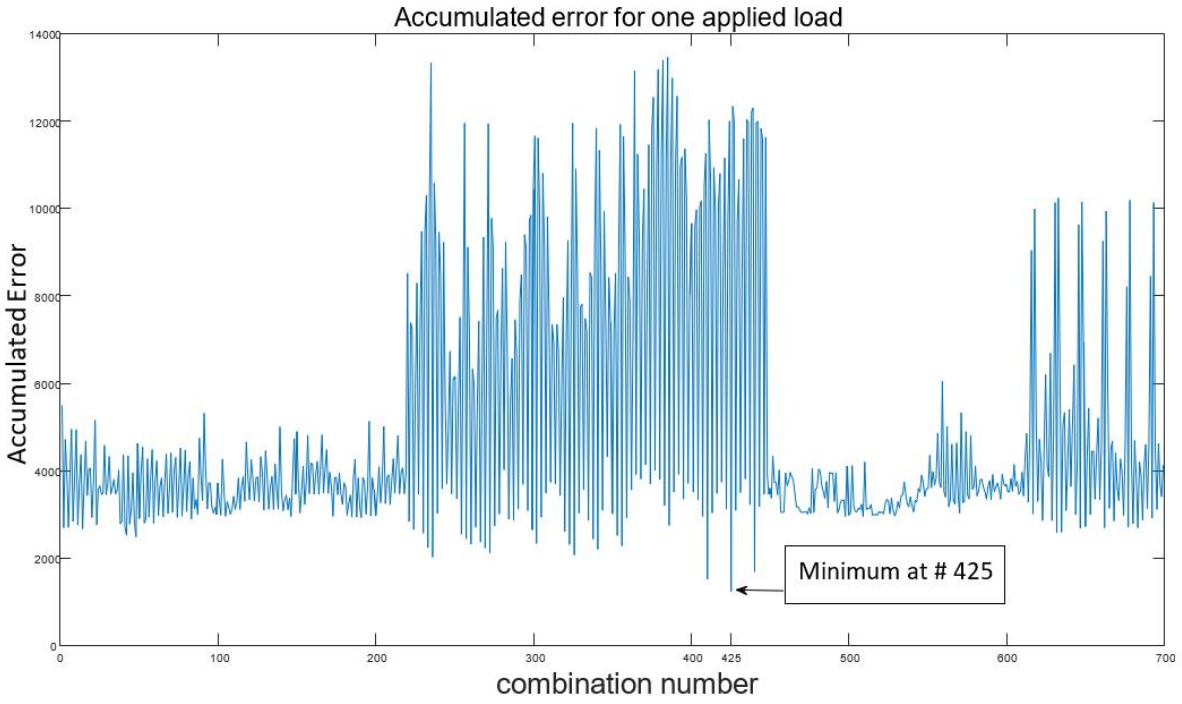

Figure 5.4 Accumulated Error for Motorcycle Horn Bracket Example Case 2

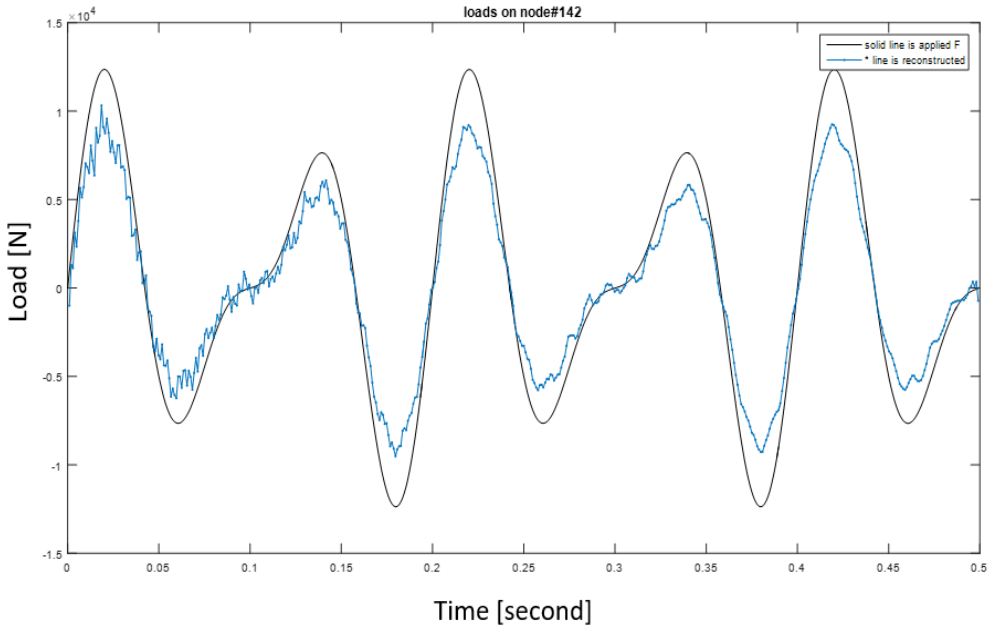

Figure 5.5 Applied and Predicted Loads Using Strain Transmissibility with 15 Retained Modes and 10 Strain Gages

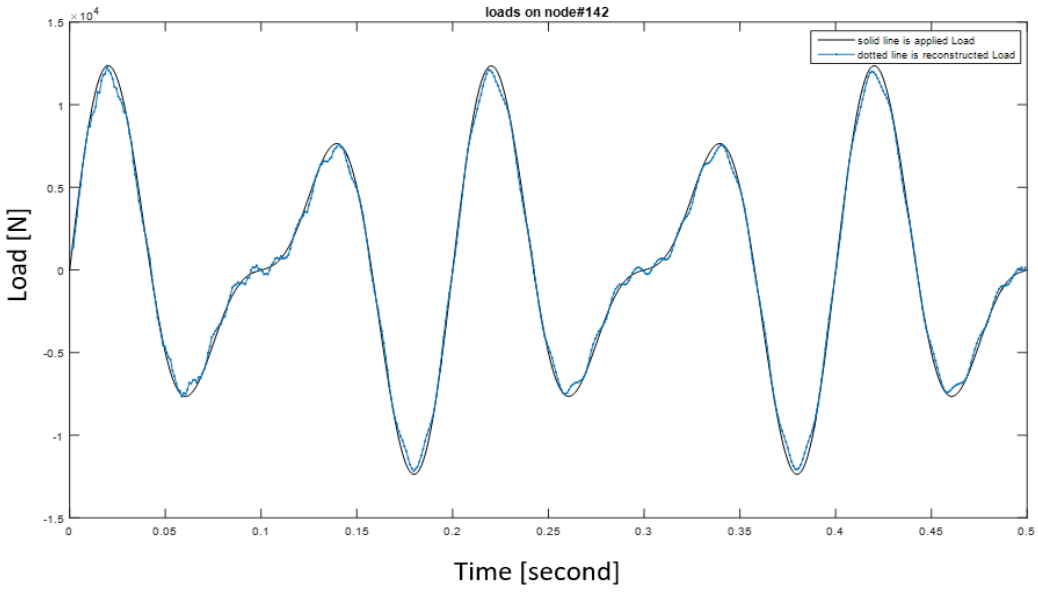

Figure 5.6 Applied and Predicted Loads Using Strain Transmissibility with 25 Retained Modes and 10 Strain Gages

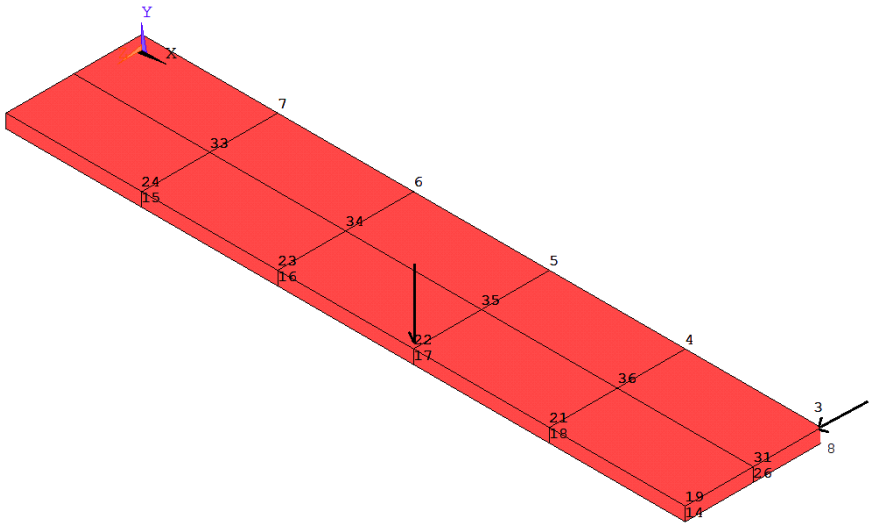

Figure 5.7 Finite Element Model of a 3D Cantilevered Beam with Two Loads Applied in Different Directions

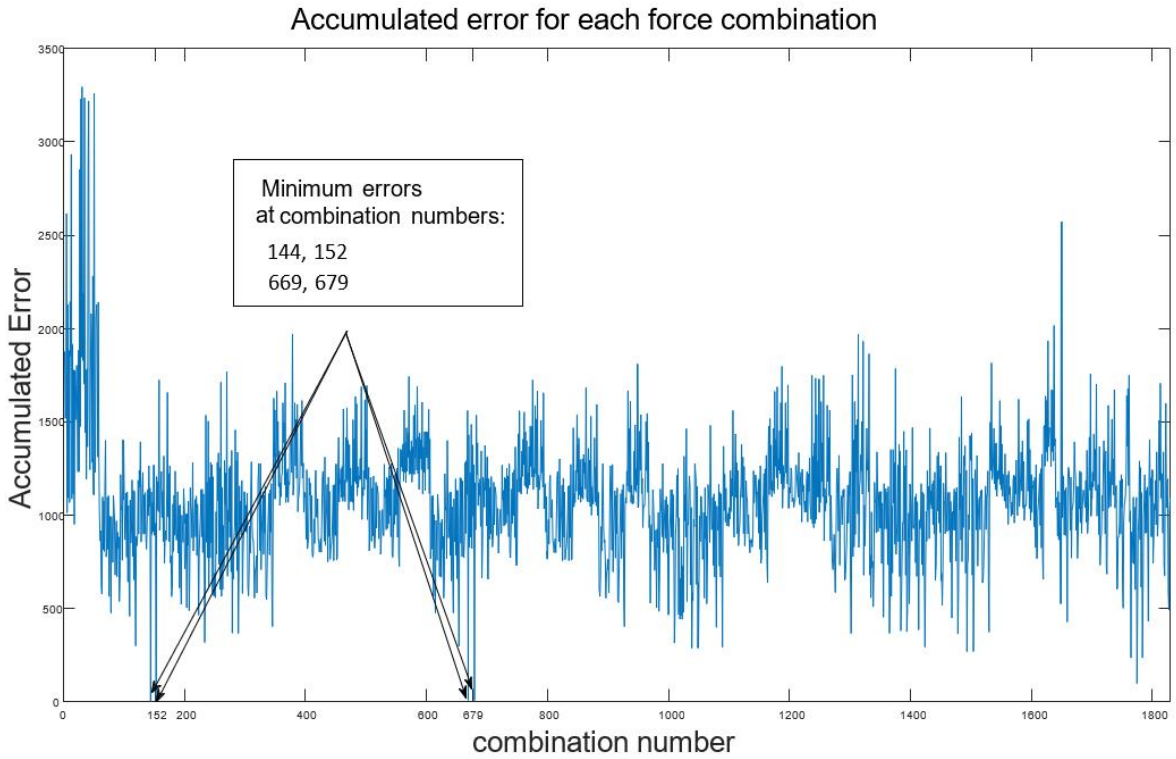

Figure 5.8 Accumulated Error for The Cantilever Beam with Two Loads

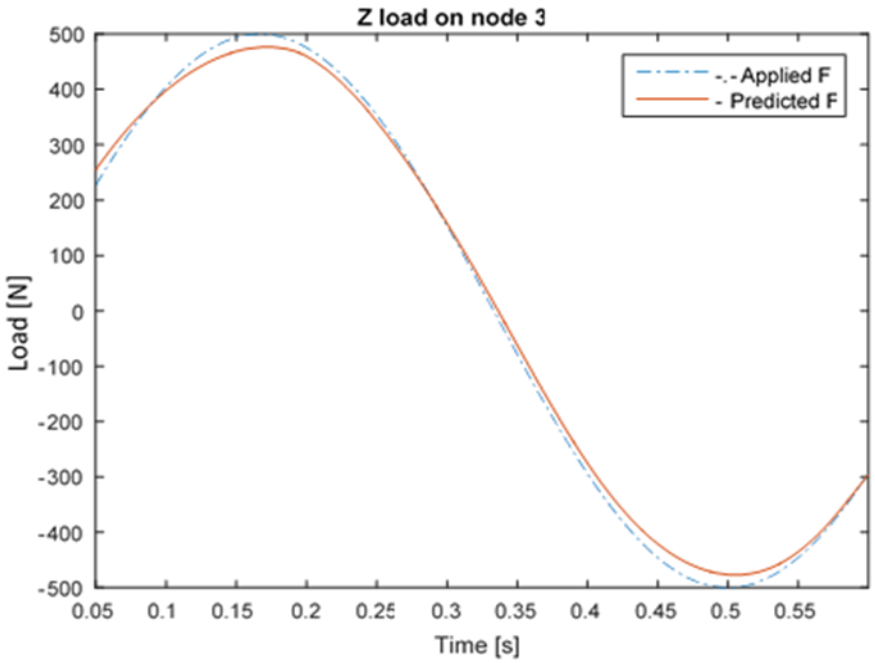

Figure 5.9 Applied and Reconstructed Load on Node 3 in Z Direction

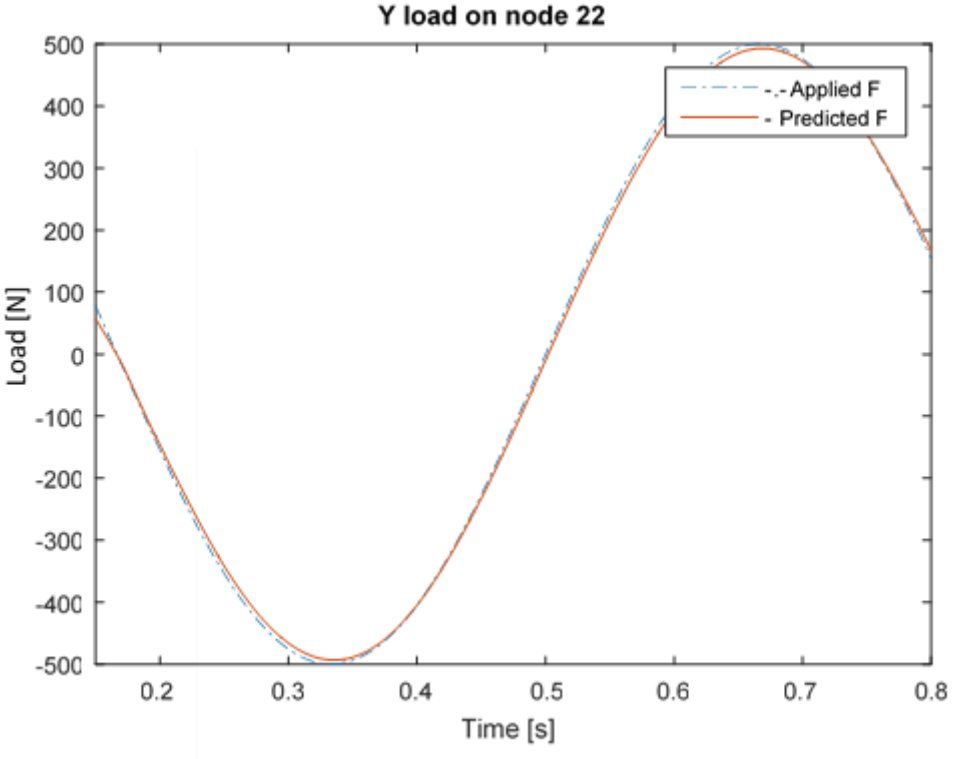

Figure 5.10 Applied and Reconstructed Load on Node 22 in Y Direction

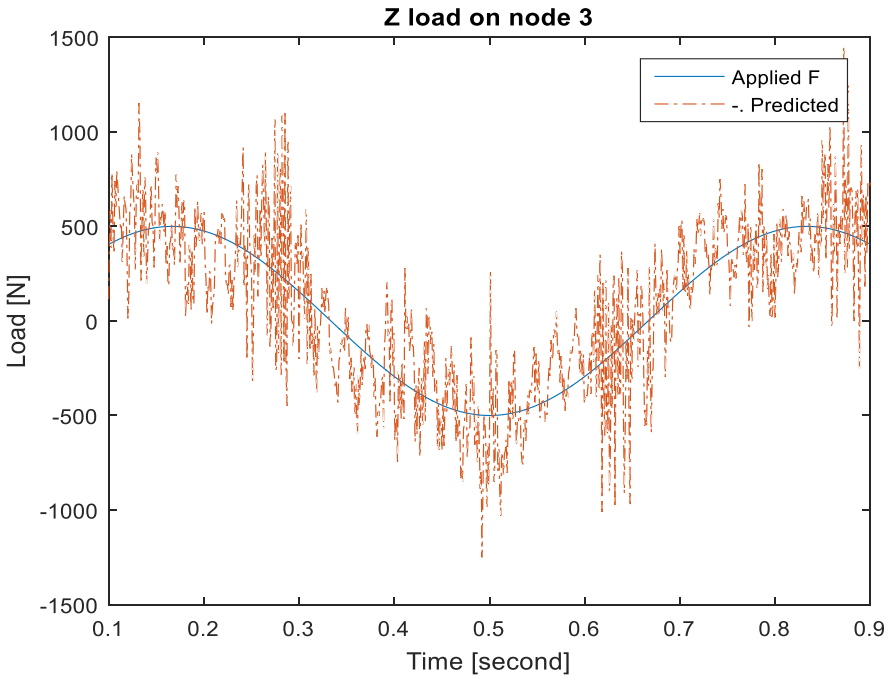

Figure 5.11 Applied and Reconstructed Load on Node 3 in Z Direction with Strain Errors

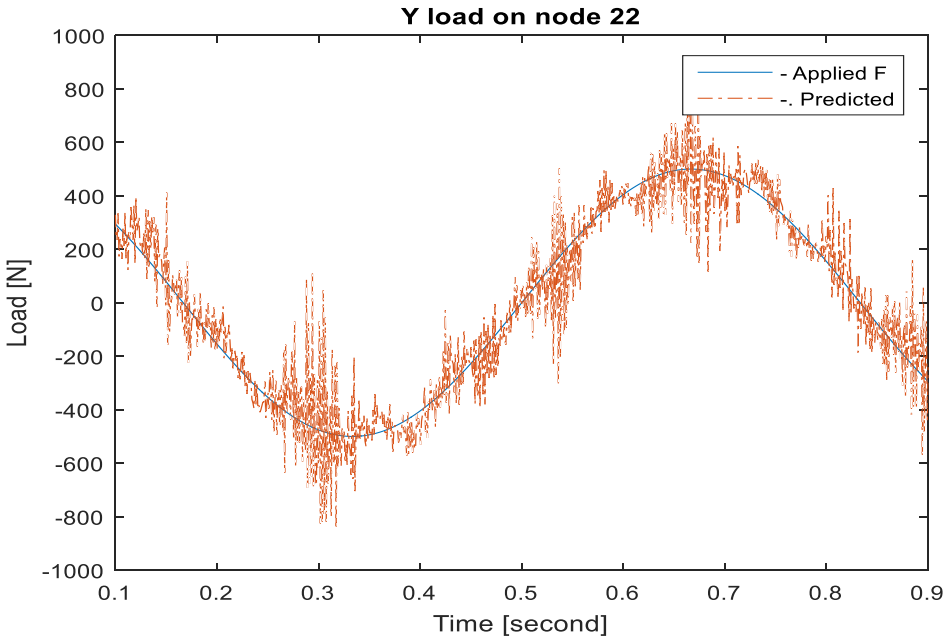

Figure 5.12 Applied and Reconstructed Load on Node 22 in Y Direction with Strain Errors

Chapter 6 - Frequency Response Based Indirect Load Identification Using Optimum Placement of Strain Gages and Accelerometers

The previous chapters presented load identification using motion and strain transmissibility; both approaches are based on the concept of FRF. The process of indirect load identification in the frequency domain, using the FRF, yields a linear relationship between the measured response and the excitation load. However, the FRF matrix is nearly singular and ill-conditioned. A review of approaches proposed to address the problem ill-conditioning in frequency domain has been recently presented by Hui *et al.* (2017).

One of the main features that affects the accuracy of the load prediction is the type of sensor used for output response measurements. As mentioned earlier, Hillary and Ewins (1984) investigated the effect of sensor type on the accuracy of load prediction. They concluded that the strain-based model gave more accurate results than the acceleration-based model because the strain responses are more influenced by higher modes at low frequencies; therefore, they capture the effect of higher modes better than the acceleration responses. Han and Wicks (1990) also studied the application of displacement and strain measurements. As a conclusion from both studies, it is apparent that selection of an appropriate type of sensor can improve the condition of the frequency response function matrix, thereby leading to better force predictions.

Yang *et al*. (2014) compared a use of two types of sensors, strain gages and accelerometers. They showed experimentally that using strain gages for load

identification improves the condition of the solution thereby resulting in a more robust solution. Another study done by Manzato *et al*. (2014) compared strain based modal analysis with modal analysis using accelerometers and presented the possibility of combining strain and acceleration signals to derive a common model.

This chapter presents a comparative study for indirect identification of dynamic loads acting on a structure through different types of measurement of structural response at a finite number of optimally selected locations. Two different types of sensors are investigated to measure the structural response. These include a use of accelerometers that leads to the identification of the displacement mode shapes as explained in Chapter 4. The second measurement approach involves a use of strain gages as done in Chapter 5 since strain measurements are directly related to imposed loads. A use of mixed strain-acceleration measurements is also presented in this chapter. Optimum sensor locations are determined herein using the D-optimal design algorithm that provides most precise load estimates. The similarities and differences between acceleration-based load identification and strain-based load identification are discussed through numerical examples. The effect of the number of retained modes on the accuracy of load recovered is also investigated.

From chapters 4 and 5, the two approaches based on response (displacement and strain) transmissibility give accurate load location prediction when using optimum locations of sensors. The comparison between the two approaches will be done utilizing the assumption if load location is known a priori such that the magnitude prediction will be tested for different number of modes retained.

6.1 Theoretical Development

Consider the inverse problems defined in Eqn. (4.5) and Eqn. (5.12) and expand them in matrix format so the excitation force is identified as follows:

$$\begin{Bmatrix} F_1(\omega) \\ F_2(\omega) \\ \vdots \\ F_{N_i}(\omega) \end{Bmatrix} = \begin{bmatrix} H^d_{11}(\omega) & H^d_{12}(\omega) & \cdots & H^d_{1N_i}(\omega) \\ H^d_{21}(\omega) & H^d_{22}(\omega) & \cdots & H^d_{2N_i}(\omega) \\ \vdots & \vdots & \vdots & \vdots \\ H^d_{N_o 1}(\omega) & H^d_{N_o 2}(\omega) & \cdots & H^d_{N_o N_i}(\omega) \end{bmatrix}^{+} \begin{Bmatrix} d_1(\omega) \\ d_2(\omega) \\ \vdots \\ d_{N_o}(\omega) \end{Bmatrix} \tag{6.1}$$

$$\begin{Bmatrix} F_1(\omega) \\ F_2(\omega) \\ \vdots \\ F_{N_i}(\omega) \end{Bmatrix} = \begin{bmatrix} H^{\varepsilon}_{11}(\omega) & H^{\varepsilon}_{12}(\omega) & \cdots & H^{\varepsilon}_{1N_i}(\omega) \\ H^{\varepsilon}_{21}(\omega) & H^{\varepsilon}_{22}(\omega) & \cdots & H^{\varepsilon}_{2N_i}(\omega) \\ \vdots & \vdots & \vdots & \vdots \\ H^{\varepsilon}_{N_o 1}(\omega) & H^{\varepsilon}_{N_o 2}(\omega) & \cdots & H^{\varepsilon}_{N_o N_i}(\omega) \end{bmatrix}^{+} \begin{Bmatrix} \varepsilon_1(\omega) \\ \varepsilon_2(\omega) \\ \vdots \\ \varepsilon_{N_o}(\omega) \end{Bmatrix} \tag{6.2}$$

where $[H^d_{N_o N_i}(\omega)]$ is the displacement frequency response function DFRF with input point N_i and response point N_o, and $[H^{\varepsilon}_{N_o N_i}(\omega)]$ is the strain frequency response function SFRF with input point N_i and response point N_o. Both of the DFRF and SFRF can be found by using the displacement mode shape matrix $[\phi]$ and strain mode shape matrix $[\psi]$ as shown in Eqn. (4.4) and Eqn. (5.7) respectively.

It is conjectured that combining strain gage and accelerometer measurements can lead to many benefits. It is known the strain modes can provide valuable information that otherwise is not obtainable by exclusively using accelerometers. But in some complex structures, interpreting the strain modes can be very hard. Therefore, using both strain gage and accelerometer measurements, one can combine the ease of interpretation that comes from displacement mode shapes, to the additional strain information provided by the strain modes.

The combined strain and displacement frequency response function (SDFRF) has the same format but is composed of the displacement and strain parts and can also be viewed in matrix form as:

$$\begin{Bmatrix} F_1(\omega) \\ F_2(\omega) \\ \vdots \\ F_N(\omega) \\ \vdots \\ F_{N_i}(\omega) \end{Bmatrix} = \begin{bmatrix} H_{11}^{\varepsilon}(\omega) & H_{12}^{\varepsilon}(\omega) & \cdots & H_{1N_i}^{\varepsilon}(\omega) \\ H_{21}^{\varepsilon}(\omega) & H_{22}^{\varepsilon}(\omega) & \cdots & H_{2N_i}^{\varepsilon}(\omega) \\ \vdots & \vdots & \vdots & \vdots \\ H_{N1}^{d}(\omega) & H_{N2}^{d}(\omega) & \cdots & H_{NN_i}^{d}(\omega) \\ \vdots & \vdots & \vdots & \vdots \\ H_{N_o 1}^{d}(\omega) & H_{N_o 2}^{d}(\omega) & \cdots & H_{N_o N_i}^{d}(\omega) \end{bmatrix}^{+} \begin{Bmatrix} \varepsilon_1(\omega) \\ \varepsilon_2(\omega) \\ \vdots \\ d_N(\omega) \\ \vdots \\ d_{N_o}(\omega) \end{Bmatrix} \tag{6.3}$$

Rewriting Eqn. (6.3):

$$\{F(\omega)\} = [H^{\varepsilon d}(\omega)]^{+} \{\varepsilon d(\omega)\} \tag{6.4}$$

where $[H^{\varepsilon d}(\omega)]$ is the SDFRF and $\{\varepsilon d(\omega)\}$ is the strain response and the displacement response measurements vector.

6.2 D-optimal Design for Sensors Placement in FRF

The previous section presents the inverse problem whether using displacement measurement or strain measurements as in Eqn. (6.1) and Eqn. (6.2) or using the mixed measurements as in Eqn. (6.3). As shown earlier, to improve the accuracy of the load location prediction problem, the placement of sensors at correct locations is important. Implementing the D-optimal algorithm explained earlier to get the optimum locations of sensors and re- writing Eqn. (6.1), Eqn. (6.2) and Eqn. (6.3) give:

$$\{F(\omega)\} = [H^{d}(\omega)]_{opt}^{+} \{d(\omega)\}_{opt} \tag{6.5}$$

$$\{F(\omega)\} = [H^{\varepsilon}(\omega)]^{+}_{opt}\ \{\varepsilon(\omega)\}_{opt} \tag{6.6}$$

$$\{F(\omega)\} = [H^{\varepsilon d}(\omega)]^{+}_{opt}\ \{\varepsilon d(\omega)\}_{opt} \tag{6.7}$$

6.3 Numerical Examples

Two numerical examples are presented next to identify the loads applied to a structure using the concepts of DFRF, SFRF, as well as the SDFRF. Optimum locations of sensors are determined using the D-optimal algorithm programmed in MATLAB. A comprehensive flow chart of the solution procedure is given in Fig. 6.1 that describes the steps followed to identify the loads applied to a structure. The first example deals with estimation of point load applied to a simply supported beam whereas the second example addresses the estimation of load acting on a motorcycle horn bracket. The influence of the number of retained modes on the quality of load estimates is also demonstrated. The finite element (FE) models of the test components were created using the ANSYS-APDL software.

6.3.1 Cantilevered Beam

A cantilevered steel beam with same physical properties mentioned in Sec. 4.6.6 is used and modeled using Solid45 element in ANSYS (See Fig.6.2). Without loss of generality, the system is assumed to be undamped. All degrees of freedom at the left end of the beam were constrained. The model consists of 200 free nodes with three degrees of freedom per node, i.e., the total number of degrees of freedom in the FE model is 600.

The FE meshing should be done such that the distance between a node where a sensor placed, and its adjacent neighbors is not less than the physical size of the sensor.

The system mass and stiffness matrices were generated using data provided by ANSYS in the Harwell-Boeing format. A harmonic point load was applied at the free end of the beam on node number 149 and is given as:

$$F(t) = 500\sin(30\pi t) + 350\cos(20\pi t)$$

6.3.2 Numerical Results-Cantilevered Beam

Three cases, based on a use of DFRF, SFRF, and SDFRF were chosen to illustrate load identification using optimal locations for strain gages and accelerometers. The influence of number of retained modes on the quality of load estimate is examined by looking at the root mean square (RMS) error between the applied load and the predicted load. The RMS error is calculated as:

$$RMS = \sqrt{\frac{\sum_{t=1}^{N}(F_t - \tilde{F}_t)^2}{N}} \tag{6.8}$$

where F_t is the magnitude of the applied load at time= t and $\tilde{F}_t$ is the magnitude of the predicted load.

Case I: Load identification using SFRF and optimum strain gage locations

Using the D-optimal algorithm and Eqn. (6.6), the optimum locations for seven strain gages are identified to be node numbers [7,22,24,45,60,80,184]. The load prediction model is tested for varying number of modes retained in dynamic analysis.

Numerical results from use of strain frequency response function are given in Table 6.1. The applied and the recovered loads for ten and twenty retained modes are plotted in Figs. 6.3 and 6.4. Based on the results obtained (Fig. 6.4), it is seen that the applied load can be identified using the SFRF and the optimal locations for the strain gages. Further, it can be concluded that the accuracy of the proposed approach is improved by increasing the number of the modes retained in Eqn. (6.6).

A sensitivity analysis was performed by varying the number of sensors as well retained modes. The results are presented in Table 6.2. Based on the results presented in Table 6.2, it can be seen that (i) as the number of sensors used increases and/or (ii) as the number of retained modes increases, the RMS error reduces.

Case II: Load identification using DFRF and optimum accelerometer locations

Using the D-optimal algorithm and Eq. (6.5), the following nodes numbers [29,44,48,52,64,69,102] are identified as the optimum locations for seven accelerometers. The influence of number of retained modes on the accuracy of load estimates is examined. Results from use of displacement frequency response function are also given in Table 6.1. The applied and recovered loads are plotted in Figs. 6.5 and 6.6. Based on the results obtained, it is seen that while the trends in the load applied are captured accurately using DFRF, the magnitude estimates are still off. As with the SFRF based approach, it is seen that the accuracy of the load estimates is improved by increasing the number of the modes retained in Eqn. (6.5).

Comparing the results obtained using accelerometers with the previous case where strain gages are used, it is seen that the load identification using SFRF yields better results than those obtained using DFRF. One of the underlying reasons is that the

condition number value of SFRF matrix (Eq. 6.6) is smaller than the condition number value of the DFRF matrix (Eq. 6.5).

Case III: Load identification using SDFRF and optimum strain gage and accelerometer locations

Next, the D-optimal algorithm is used in conjunction with Eq. (6.7) to find the optimal locations for seven sensors that consist of five strain gages and two accelerometers. Nodes [9,22,30,45,83] are identified as optimum locations for the five strain gages whereas nodes [19,182] are identified as optimum accelerometer locations. As before, two results cases are presented to examine the influence of number of retained modes on the quality of results. Numerical results from combined use of strain and displacement frequency response functions are presented in Table 6.1. The applied and recovered loads are plotted in Fig. 6.7 and 6.8.

Based on the results obtained, the load applied can be identified using the SDFRF and the optimal locations for both strain gages and accelerometers. Comparing the results for Case (iii) with the previous two cases, it is seen that the load identification using SDFRF has a better accuracy than using SFRF or DFRF for all three cases with 10, 15 and 20 retained modes. For the cases with 10, 15 and 20 retained modes presented in Table 6.1, when the RMS error values between SFRF and SDFRF approaches are compared, the results show that the average RMS error is reduced by 8% when using the SDFRF. Likewise, when comparing the RMS error values using SDFRF and DFRF approaches, the average RMS error is reduced by 40% when using SDFRF.

An additional check on the recovery procedure using SDFRF is done by using non-optimal locations for the strain gages and the accelerometers. Results for RMS error

values are shown in Table 6.3. The applied and the recovered loads are plotted in Figs.6. 9 and 6.10. Based on the results and comparing them with the previous cases, it is clear that using non-optimal locations for sensors degrades the accuracy of the load identification.

While is the loading used in this example has a zero mean, it was also seen that when a DC component is present in the applied load leading to a non-zero mean, the observed trends discussed above as well as the accuracy of load estimates does not change.

6.3.3 Motorcycle Horn Bracket

The next example deals with determination of a point load acting on a motorcycle horn bracket. The same model described in Sec. 5.5.1 is used (See Fig. (5.1)) with a single point force being applied to node number 142 and is given as:

$$F(t) = 5000\sin(60t) + 8000\sin(40t)$$

Using the D-optimum design algorithm, the optimum locations for the strain gages and the accelerometers were determined for different number of retained modes in the dynamic model. The results obtained using SFRF, DFRF and SDFRF approaches are presented next.

6.3.4 Numerical Results-Horn Bracket

Case I: Load identification using SFRF and optimum strain gage locations

Using Eqn. (6.6) and the D-optimal algorithm to find optimum locations for ten strain gages, the algorithm yielded the following nodes numbers [14,75,83,106,159,191,193,200,228,238] for sensor placement. The load prediction model is tested for varying number of modes retained in dynamic analysis. Numerical results from use of strain frequency response function are shown in Table 6.4. The applied and the recovered loads for fifteen and twenty-five retained modes are plotted in Figs. 6.11 and 6.12. Based on the results obtained (Fig. 6.12), it is seen that the applied load can be identified using the SFRF and the optimal locations for the strain gages. Once again it is seen that the accuracy of the proposed approach is improved by increasing the number of the modes retained in Eqn. (6.6).

Case II: Load identification using DFRF and optimum accelerometer locations

Using Eqn. (6.5) and the D-optimal algorithm to find optimum locations for sensors, the following nodes numbers [6,23,26,50,76,104,118,122,200,208] are identified as the optimum locations for ten accelerometers. The influence of number of retained modes on the accuracy of load estimates is examined. The results are also given in Table 6.4 and plotted in Figs. 6.13 and 6.14. Based on the results obtained, it is seen that while the trends in the load applied are captured accurately using DFRF, the magnitude estimates are still off. Comparing the DFRF results with those obtained using SFRF, it is seen that SFRF approach yields better results with a 60% reduction in the RMS error.

Case III: Load identification using SDFRF and optimal strain gage and accelerometer locations

Next, the D-optimal algorithm is used in conjunction with Eq. (6.7) to find the optimal locations for ten sensors that consist of seven strain gages and three accelerometers. Nodes [30,75,83,159,168,199,239] are identified as optimum locations for the seven strain gages whereas nodes [132,209,211] are identified as optimum accelerometer locations. As before, two results cases are presented to examine the influence of number of retained modes on the quality of results. Numerical results from combined use of strain and displacement frequency response functions are presented in Table 6.4. The applied and recovered loads are plotted in Fig. 6.15 and 6.16.

For the case with 15, 18 and 25 retained modes presented in Table 6.4, when the RMS error values between SFRF and SDFRF approaches are compared, the results show that the average RMS error is reduced by 62% when using the SDFRF. Likewise, when comparing the RMS error values using SDFRF and DFRF approaches, the average RMS error is reduced by 86% when using SDFRF.

6.4 Conclusions and Summary

In this chapter, it was shown that strain modal analysis, in combination with displacement modal analysis, can be used to develop modal models and a strain to displacement transformation. A computational technique in the frequency domain is then presented that allows for indirect measurement of dynamic loads acting on a structure. This allows the structure to act as its own transducer as long as the deformations remain

within elastic range and the principle of linear superposition holds. The results of two numerical examples using SFRF, DFRF and SDFRF in conjunction with optimum sensor placement constitute a powerful set of tools for load identification applications. The results show that if only one type of sensor is used, strain gages, in general, give better results than accelerometers alone, hence, their use as sensors for load identification is attractive. It was seen that the condition number of a SFRF matrix is several order magnitudes lower than condition number of DFRF matrix. Therefore, the SFRF matrix poses a less ill-conditioned inverse operation for the loading cases than would be the case for the DFRF matrix. Strain modal analysis thus provides an improved force estimated ability compared for displacement modal analysis.

Furthermore, the chapter also investigated load identification based on response measurements using both strain gages and accelerometers. It is seen that the combined SDFRF approach yields results that are good as if not better than those obtained using pure SFRF or DFRF approaches. This method has a better identification accuracy than using SFRF or DFRF even while retaining a limited number of modes.

Results of a limited investigation on the number of retained modes and number of sensors used on accuracy of recovered loads are also presented. Acceptable load estimates may only be obtained by retaining a high number of modes in the analysis, which is not often possible in real world problems. To overcome this restriction, a different approach, which utilizes model order reduction, is proposed next chapter. The approach, which when applied to the load identification procedure, results in significant improvements in load estimation.

Table 6.1 RMS Error Values for Different Number of Retained Modes

Modes retained	Error Case (i)	Error Case (ii)	Error Case (iii)
10	172.85	231.77	154.60
15	161.26	222.89	151.11
20	48.41	101.2	45.23

Table 6.2 RMS Error with Varying Number of Sensors and Retained Modes

# of strain gages	10 modes retained	15 modes retained	20 modes retained
5	261.12	249.77	190.01
7	172.82	161.26	48.41
10	156.35	114.09	35.87

Table 6.3 RMS Error Values with Non-Optimal Sensor Locations Using SDFRF

Modes retained	RMS
10	256.31
20	161.71

Table 6.4 RMS Error Values for Different Number of Retained Modes - *Horn Bracket*

Modes retained	Error Case (i)	Error Case (ii)	Error Case (iii)
15	128.52	387.75	53.028
18	123.65	321.53	43.397
25	111.10	281.18	40.59

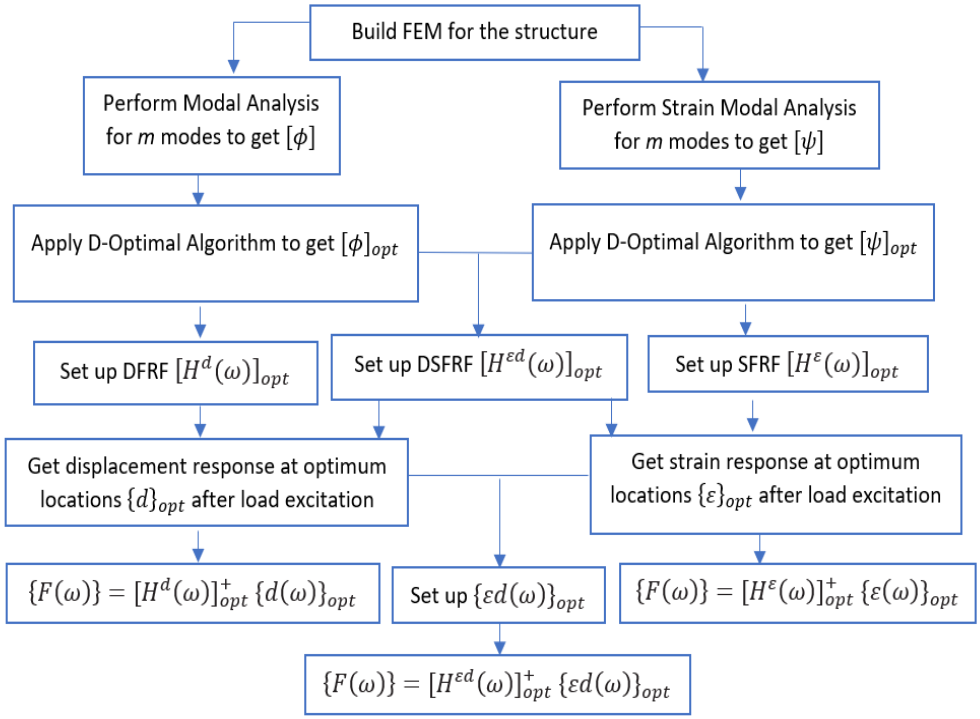

Figure 6.1 Complete Description of Indirect Load Identification in Frequency Domain

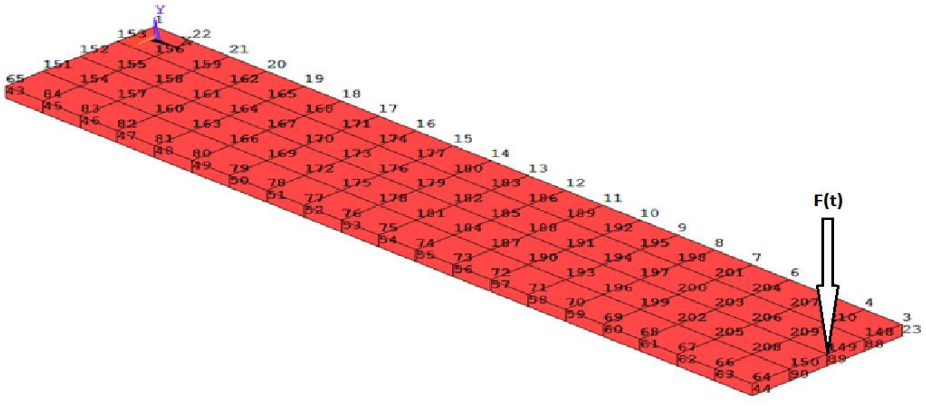

Figure 6.2 Finite Element Model of a Cantilevered Beam

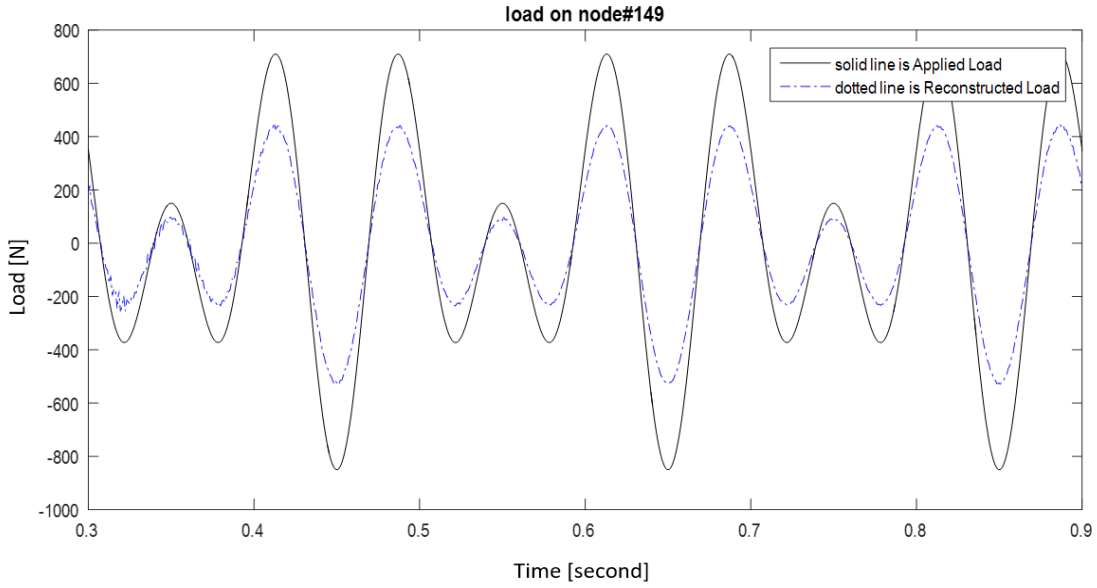

Figure 6. 3 Difference Between Applied Load and Predicted Load Using SFRF 10 Retained Modes and 7 Strain Gages

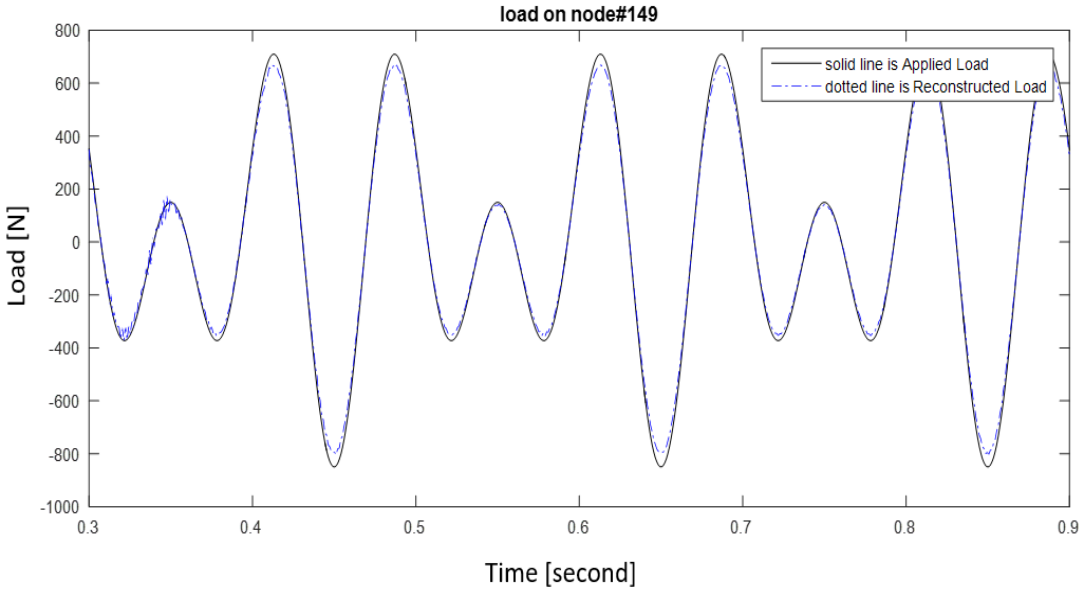

Figure 6.4 Difference Between Applied Load and Predicted Load Using SFRF 20 Retained Modes and 7 Strain Gages

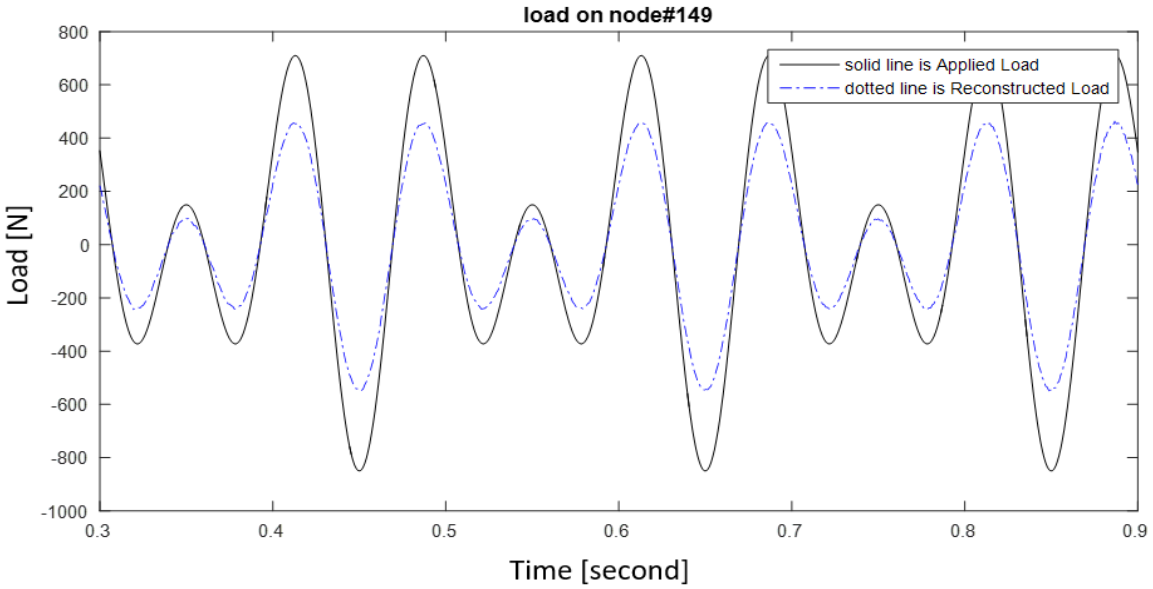

Figure 6.5 Difference Between Applied Load and Predicted Load Using DFRF-10 Retained Modes and 7 Accelerometers

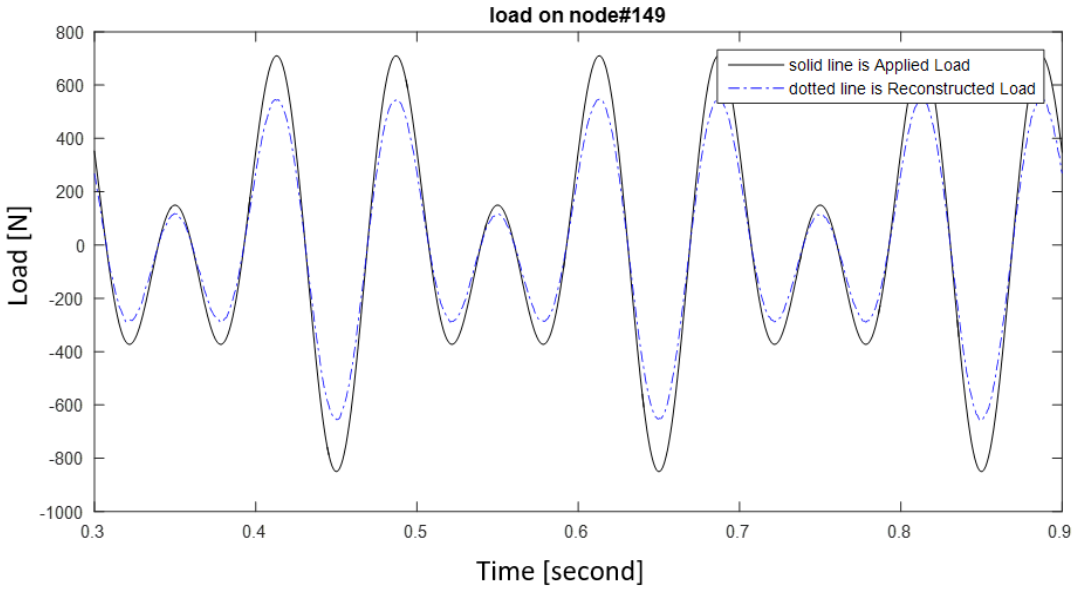

Figure 6.6 Difference Between Applied Load and Predicted Load Using DFRF-20 Retained Modes and 7 Accelerometers

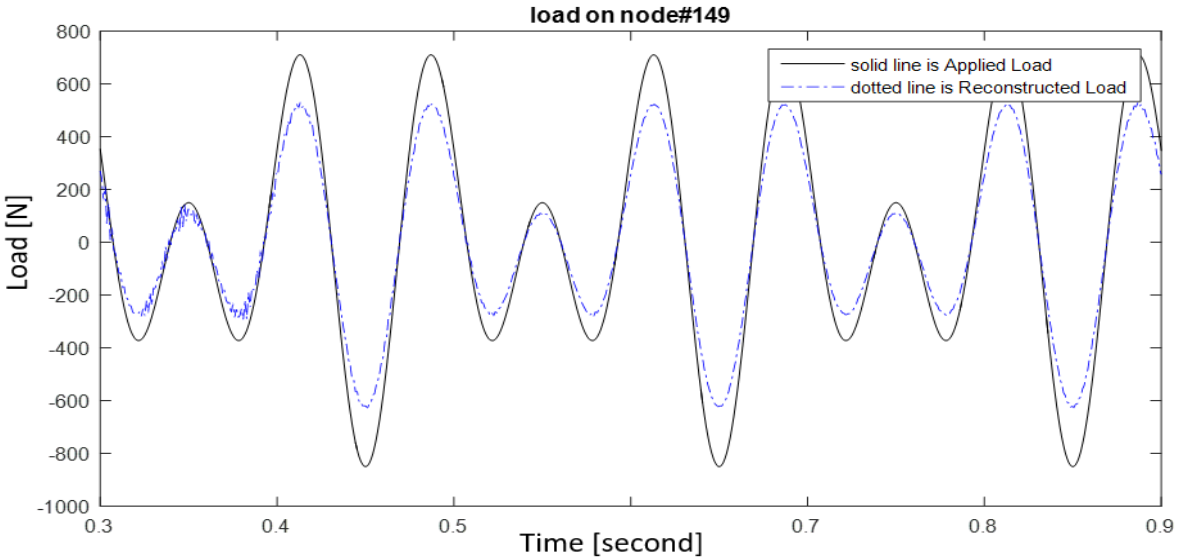

Figure 6.7 Difference Between Applied Load and Predicted Load Using SDFRF-10 Retained Modes with 5 Strain Gages and 2 Accelerometers

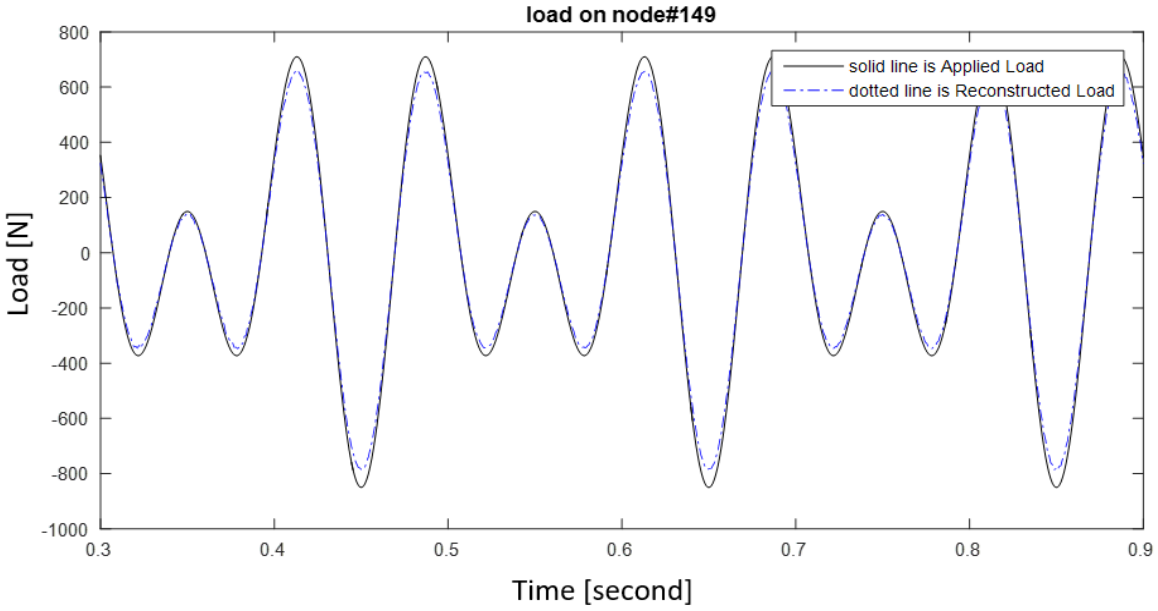

Figure 6.8 Difference Between Applied Load and Predicted Load Using SDFRF-20 Retained Modes with 5 Strain Gages and 2 Accelerometers

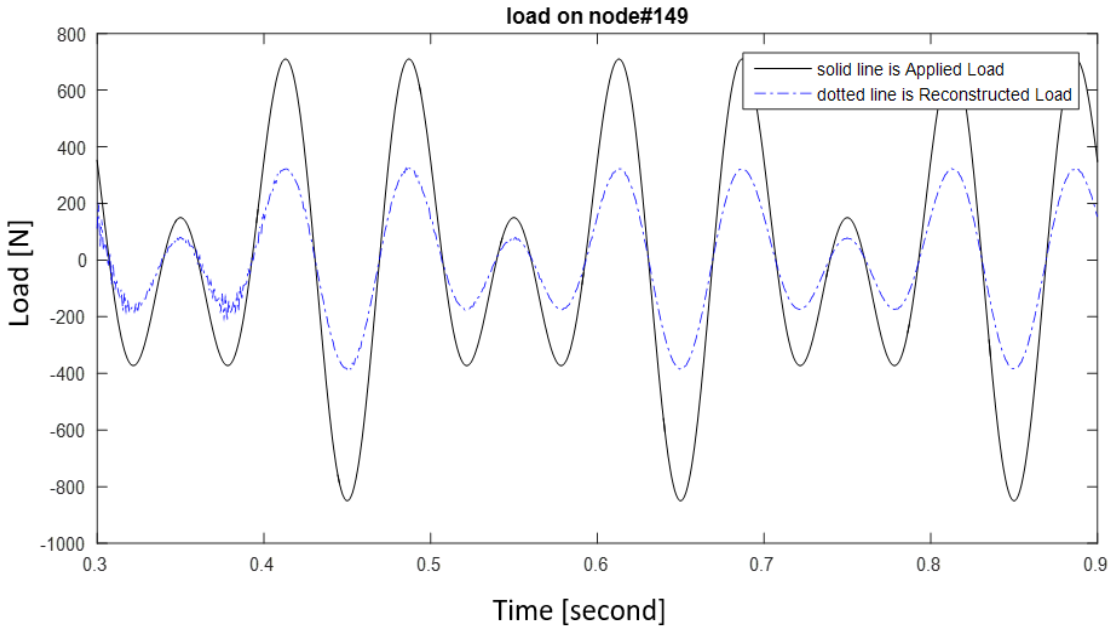

Figure 6.9 Difference Between Applied Load and Predicted Load Using SDFRF-10 Retained Modes with Non-Optimally Placed Sensors

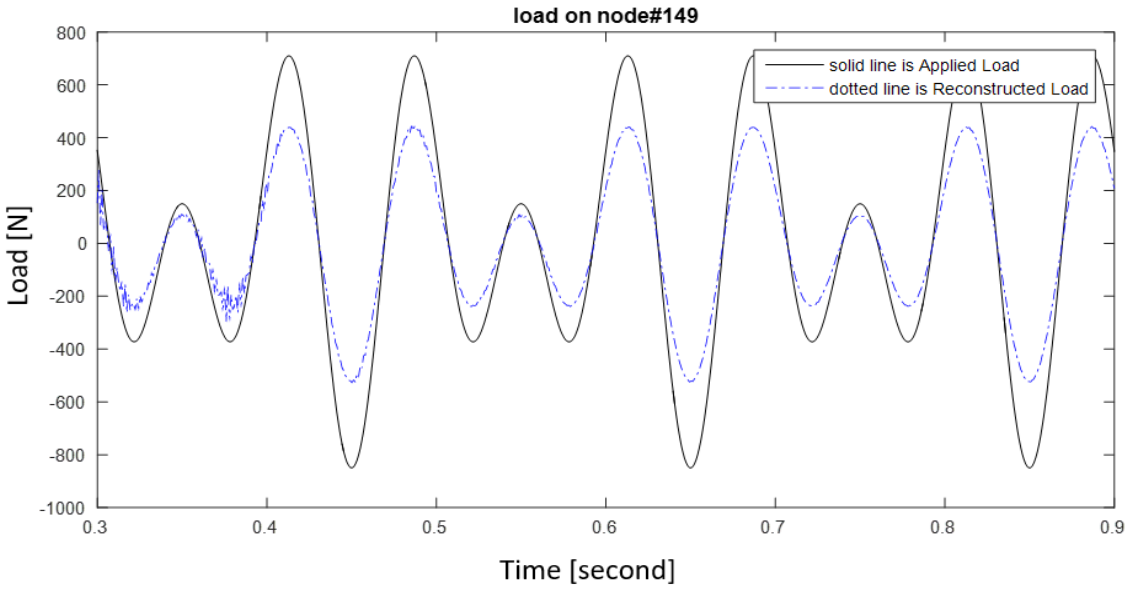

Figure 6.10 Difference Between Applied Load and Predicted Load Using SDFRF-20 Retained Modes with Non-Optimally Placed Sensors

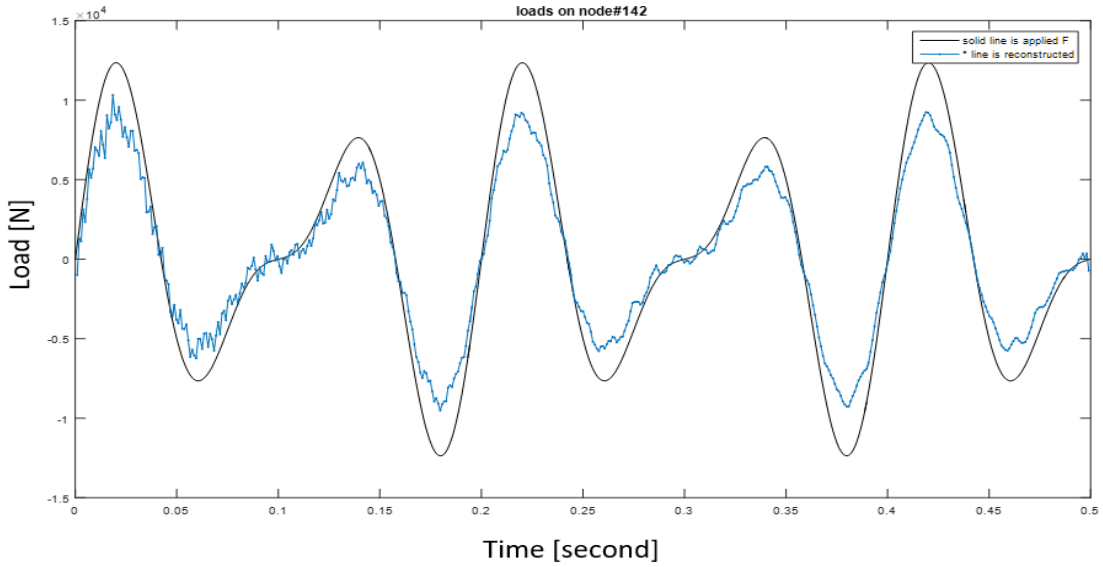

Figure 6.11 Difference Between Applied Load and Predicted Load Using SFRF-15 Retained Modes and 10 Strain Gages

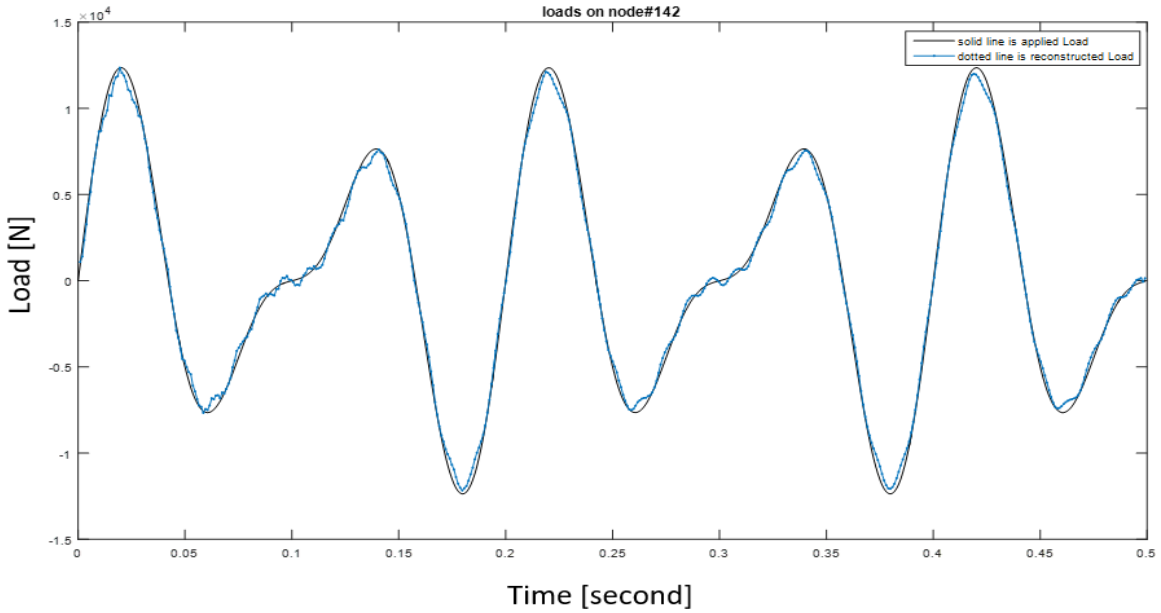

Figure 6.12 Difference Between Applied Load and Predicted Load Using SFRF-25 Retained Modes and 10 Strain Gages

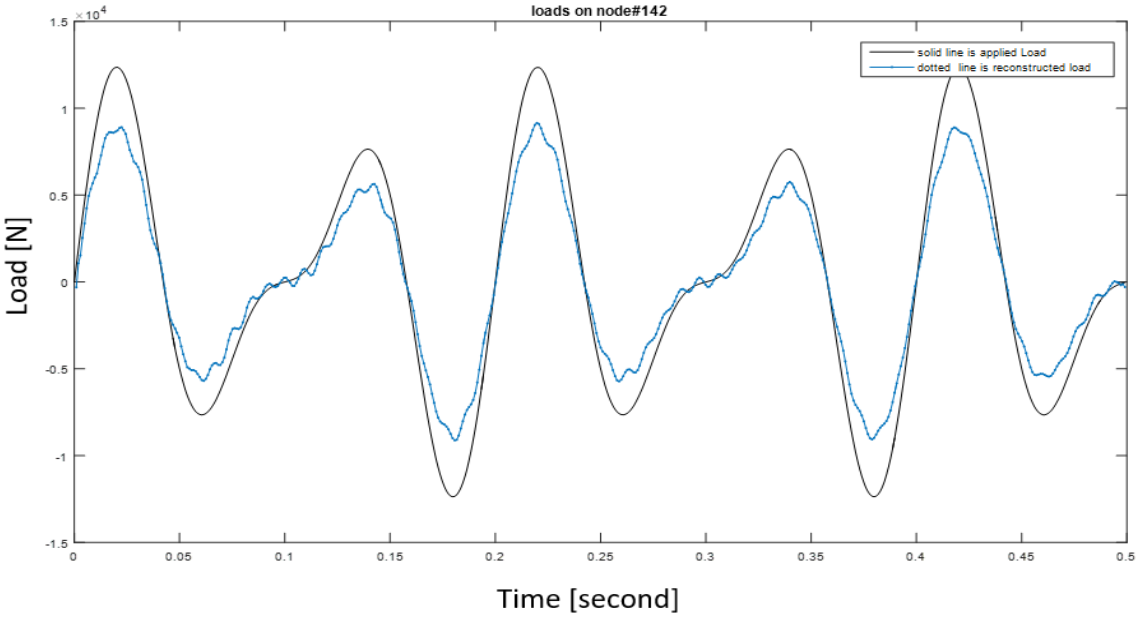

Figure 6.13 Difference Between Applied Load and Predicted Load Using DFRF-15 Retained Modes and 10 Accelerometers

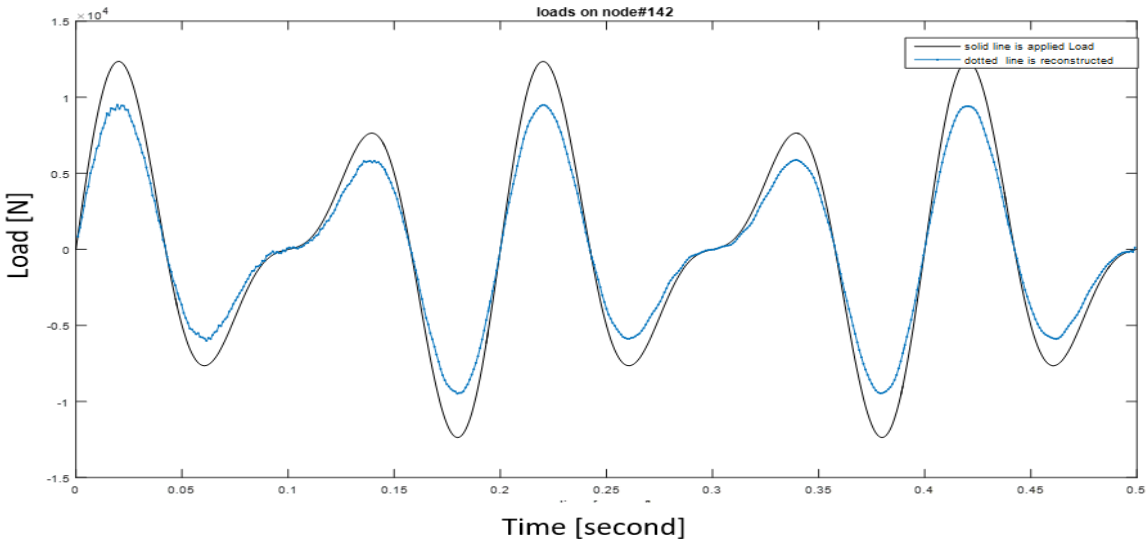

Figure 6.14 Difference Between Applied Load and Predicted Load Using DFRF-25 Retained Modes and 10 Accelerometers

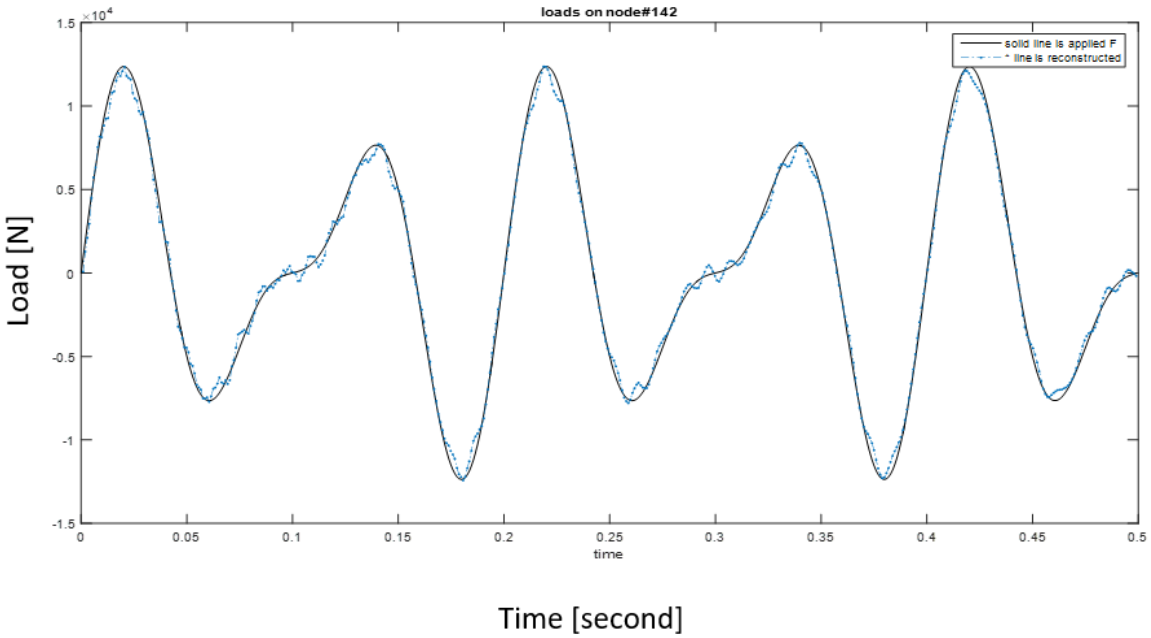

Figure 6.15 Difference Between Applied Load and Predicted Load Using SDFRF-15 Retained Modes with 7 Strain Gages and 3 Accelerometers

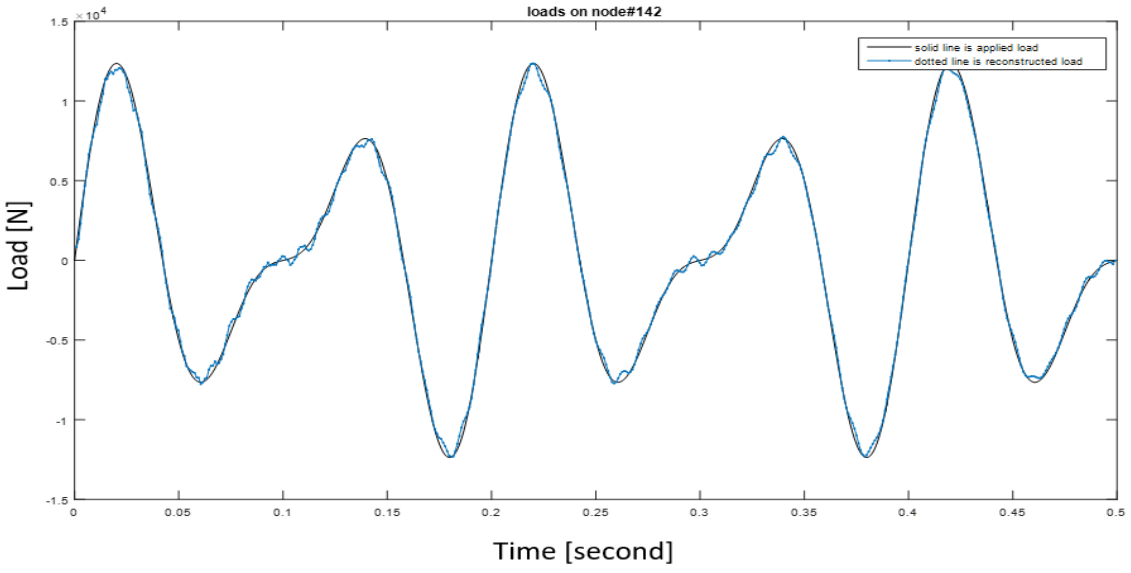

Figure 6.16 Difference Between Applied Load and Predicted Load Using SDFRF-25 Retained Modes with 7 Strain Gages and 3 Accelerometers

Chapter 7 - Load Identification Based on Response Transmissibility and Model Reduction

This chapter proposes a development of the response (motion and strain) transmissibility using model reduction. Examples considered in previous chapters show that the quality of results obtained depends on how accurately the mathematical model represents the real physical system. As the structural complexity grows, so does the number of degrees of freedom in the structure. As a result, the number of modes, as well as the time required, to solve the free vibration problem grows. The objective is to able to approximate the structural response while using a limited number of modes; this also has an influence on the accuracy of the frequency response function that is obtained from the finite element model. As a result of these reasons the Model Order Reduction (MOR) techniques are commonly used to reduce the full finite element model (Paz, 1985). In addition, the choice of the sensor locations to be determined has a major influence on the quality of results. The issue of sensor locations will be handled using the D-optimal methods discussed earlier.

As mentioned earlier, there is a need to simplify dynamical models that may contain many equations and/or variables. Such simplification is needed to perform simulations within an acceptable amount of time and storage capacity, but with a reliable outcome. Model order reduction tries to capture the essential features of the structure. This means that the most basic properties of the original model must also be present in

the smaller approximation. As the model is reduced more and more, there is a loss of accuracy and the process of reduction is stopped. At that point, all necessary properties of the original model must be captured in the reduced model with sufficient precision.

There are many MOR techniques (Qu, 2004), such as static condensation/reduction (Guyan, 1965), dynamic condensation, and Component Mode Synthesis (CMS). The basic idea of these techniques involves dividing the coordinates as master and slave DOF. In this chapter, dynamic condensation techniques will be investigated to improve usage of the transmissibility of response for load identification.

The overall objective is to reduce the number of degrees of freedom in a model without changing the system's dynamic characteristics significantly such that we can predict the applied load locations and magnitudes while improving the computational time required to solve the problem. Throughout this chapter, it is assumed that structures under investigations are linear in nature.

7.1 Component Mode Synthesis

Hurty (1965) developed a dynamic condensation method called the component mode synthesis (CMS). This method has significant condensation advantages and can be used for modeling and simulation of large and complex structures. The main idea of CMS is to divide the large system into *N* subsystems that can be analyzed separately and then combining them together by an assembly algorithm. Based on that idea, many CMS

techniques were developed such as the free interface CMS and the fixed interface CMS. The latter one is considered one of the most accurate and widely used CMS methods, known as Craig-Bampton model reduction method. This method uses the sub-structuring of the complete structure into small sub-structures. Using the finite element method or other discretization means, the DOF of the system can be divided into two groups, boundary degrees of freedom *b* and internal degrees of freedom *i,* (Craig and Bampton 1968).

Boundary degrees of freedom are those that are shared with other substructures and the internal degree of freedom are those belonging only to the related substructure. In the Craig-Bampton method, the normal modes of the component models will be used, along with the constrained modes.

The CMS methods can be classified into two different approaches in terms of the representation of system response:

1. Time-domain based approach;
2. Frequency-domain based approach.

In the time-domain based approach, each substructure is described by mass [M], stiffness [K], and damping [C] matrices while in the frequency-based approach, each substructure is described in terms of FRF's of the uncoupled sub-structures. In this chapter, the frequency-based Craig-Bampton reduction method will be used to predict the magnitudes of the load applied on structure under investigation.

7.2 Frequency-Based Craig-Bampton Reduction Method

The objective of the frequency-based Craig-Bampton condensation method is to predict the magnitudes of loads applied on a structure that is discretized using FEM based on free-interface FRF of the uncoupled components.

7.2.1 Fundamental Formulation

Assuming *r*-DOF undamped linear structure discretized using FEM, Eqn. (4.1) can be written as:

$$\{D(\omega)\}_{rx1} = [H^d(\omega)]_{rxr}\{F(\omega)\}_{rx1} \tag{7.1.a}$$

$$\{D(\omega)\}_{rx1} = [([K]_{rxr} - \omega^2[M])_{rxr}]^{-1}\{F(\omega)\}_{rx1} \tag{7.1.b}$$

In order to accomplish model reduction using sub-structuring, the degrees of freedom of each substructure can be divided into internal degrees of freedom *i* and boundary degrees of freedom *b* as mentioned earlier. Re-writing Eqn. (7.1.b) using partitioning matrices as:

$$\begin{Bmatrix} \{D(\omega)\}_b \\ \cdots \\ \{D(\omega)\}_i \end{Bmatrix} = \left(\begin{bmatrix} [K]_{bb} & \vdots & [K]_{bi} \\ \cdots & \vdots & \cdots \\ [K]_{ib} & \vdots & [K]_{ii} \end{bmatrix} - \omega^2 \begin{bmatrix} [M]_{bb} & \vdots & [M]_{bi} \\ \cdots & \vdots & \cdots \\ [M]_{ib} & \vdots & [M]_{ii} \end{bmatrix} \right)^{-1} \begin{Bmatrix} \{f(\omega)\}_b \\ \cdots \\ \{f(\omega)\}_i \end{Bmatrix} \tag{7.2}$$

where $\{D(\omega)\}_b$ is the displacement vector corresponding to the boundary degrees of freedom and $\{D(\omega)\}_i$ is the displacement vector corresponding to the internal degrees of freedom.

In this dynamic reduction method, two different types of modes are considered:

1. Normal modes or constrained normal modes of a substructure; these modes can be defined by motion of interior coordinates, relative with all boundaries fixed $\{D(\omega)\}_b = \{0\}$ and no force acts on the substructure $\{f(\omega)\}_b = \{0\}$.
2. Static modes of substructure can be defined as the static deformation of a substructure when a unit displacement is applied to each boundary degree of freedom while the remaining boundary degrees of freedom are restrained and all internal degrees of freedom of the sub-structure are free.

The sum of normal modes and static modes is the displacement of the internal degrees of freedom as in Eqn. (7.3):

$$\{D(\omega)\}_i = \{D(\omega)\}_i^n + \{D(\omega)\}_i^s \tag{7.3}$$

where static modes $\{D(\omega)\}_i^s$ can be obtained from Eqn. (7.2), assuming zero inertia effects and $\{f(\omega)\}_i = \{0\}$, as in Eqn. (7.4):

$$\{D(\omega)\}_i^s = -[K]_{ii}^{-1}[K]_{ib}\{D(\omega)\}_b \tag{7.4}$$

Solving the eigenvalue problem of Eqn. (7.5) provides the constrained modal matrix $[\phi]_c$ which is used to calculate the constrained normal modes $\{D(\omega)\}_i^n$ as in Eqn. (7.6).

$$-[\lambda^2][M]_{ii} + [K]_{ii} = \{0\} \tag{7.5}$$

$$\{D(\omega)\}_i^n = [\phi]_c\{q(\omega)\}_{\mathcal{R}} \tag{7.6}$$

where $[\lambda^2]$ is the diagonal matrix of eigen-values, $\mathcal{R}$ is the number of constrained Craig-Bampton (CB) normal modes and usually very less compared with the internal degrees of freedom, and $\{q(\omega)\}_{\mathcal{R}}$ is the column vector of the reduced CB normal modes. The complete displacement vector $\{D(\omega)\}$ can be expressed as:

$$\begin{aligned}\{D(\omega)\} = \begin{Bmatrix}\{D(\omega)\}_b \\ \{D(\omega)\}_i\end{Bmatrix} &= \begin{Bmatrix}\{D(\omega)\}_b \\ -[K]_{ii}^{-1}[K]_{ib}\{D(\omega)\}_b + [\phi]_c\{q(\omega)\}_{\mathcal{R}}\end{Bmatrix} \\ &= [\gamma]_{CB}\begin{Bmatrix}\{D(\omega)\}_b \\ \{q(\omega)\}_{\mathcal{R}}\end{Bmatrix}\end{aligned} \tag{7.7}$$

where $[\gamma]_{CB}$ represents the transformation matrix that transforms the full model DOF to the CB reduced model and can be given for the N^{th} substructure as:

$$[\gamma]_{CB} = \begin{bmatrix}[I] & [0] \\ -[K]_{ii}^{-1}[K]_{ib} & [\phi]_c\end{bmatrix} \tag{7.8}$$

Using the transformation matrix $[\gamma]_{CB}$ along with the full system matrices; the reduced system matrices $[M]_{CB}$, $[K]_{CB}$, and $[C]_{CB}$ can be expressed as:

$$\begin{aligned}[M]_{CB} &= [\gamma]_{CB}^T[M][\gamma]_{CB} \\ [K]_{CB} &= [\gamma]_{CB}^T[K][\gamma]_{CB} \\ [C]_{CB} &= [\gamma]_{CB}^T[C][\gamma]_{CB}\end{aligned} \tag{7.9}$$

Transforming the equation of motion of the full model for undamped system (Eqn. (7.1.b)) to the reduced model using the CB reduction gives:

$$\begin{Bmatrix}\{D(\omega)\}_b\\ \{D(\omega)\}_i\end{Bmatrix} = [\gamma]_{CB}\begin{Bmatrix}\{D(\omega)\}_b\\ \{q(\omega)\}_{\mathcal{R}}\end{Bmatrix} = [([K]_{CB} - \omega^2[M])_{CB}]^{-1}\begin{Bmatrix}\{f(\omega)\}_b\\ \{f(\omega)\}_{\mathcal{R}}\end{Bmatrix} \tag{7.10}$$

Here $[([K]_{CB} - \omega^2[M])_{CB}]^{-1}$ is defined as the reduced receptance matrix $[H^d(\omega)]_{CB}$ or the CB reduced DFRF. Re-writing Eqn. (7.10):

$$\begin{Bmatrix}\{D(\omega)\}_b\\ \{D(\omega)\}_i\end{Bmatrix} = [\gamma]_{CB}\begin{Bmatrix}\{D(\omega)\}_b\\ \{q(\omega)\}_{\mathcal{R}}\end{Bmatrix} = [H^d(\omega)]_{CB}\begin{Bmatrix}\{f(\omega)\}_b\\ \{f(\omega)\}_{\mathcal{R}}\end{Bmatrix} \tag{7.11}$$

The inverse problem can be defined by rewriting Eqn. (7.11) as the following:

$$\begin{Bmatrix}\{f(\omega)\}_b\\ \{f(\omega)\}_{\mathcal{R}}\end{Bmatrix} = [H^d(\omega)]^{+}_{CB}\,[\gamma]_{CB}\begin{Bmatrix}\{D(\omega)\}_b\\ \{q(\omega)\}_{\mathcal{R}}\end{Bmatrix} \tag{7.12}$$

where $[H^d(\omega)]^{+}_{CB}$ is pseudo-inverse matrix given by

$$[H(\omega)^d]^{+}_{CB} = ([H^d(\omega)]^{H}_{CB}\,[H^d(\omega)]_{CB})^{-1}[H(\omega)^d]^{H}_{CB} \tag{7.13}$$

Because of the similarities between strain modal and displacement modal analysis discussed in chapters 5 and 6, the same dynamic condensation method can be used when using strain modal analysis and strain measurements. Eqn. (7.14) shows the CB reduced system model using SFRF.

$$\begin{Bmatrix}\{\varepsilon(\omega)\}_b\\ \{\varepsilon(\omega)\}_i\end{Bmatrix} = [T]_{CB}\begin{Bmatrix}\{\varepsilon(\omega)\}_b\\ \{q(\omega)\}_{\mathcal{R}}\end{Bmatrix} = [H^{\varepsilon}(\omega)]_{CB}\begin{Bmatrix}\{f(\omega)\}_b\\ \{f(\omega)\}_{\mathcal{R}}\end{Bmatrix} \tag{7.14}$$

The load identification model can be defined by re-writing Eqn. (7.14) as:

$$\begin{Bmatrix}\{f(\omega)\}_b\\ \{f(\omega)\}_{\mathcal{R}}\end{Bmatrix} = [H^{\varepsilon}(\omega)]^{+}_{CB}[T]_{CB}\begin{Bmatrix}\{\varepsilon(\omega)\}_b\\ \{q(\omega)\}_{\mathcal{R}}\end{Bmatrix} \tag{7.15}$$

where $[H(\omega)^{\varepsilon}]^{+}_{CB}$ is the pseudo-inverse matrix of the CB reduced SFRF $[H^{\varepsilon}(\omega)]_{CB}$and defined as:

$$\begin{bmatrix}[H^{\varepsilon}]_{bb} & \vdots & [H^{\varepsilon}]_{bi}\\ \cdots & \vdots & \cdots\\ [H^{\varepsilon}]_{ib} & \vdots & [H^{\varepsilon}]_{ii}\end{bmatrix} = \begin{bmatrix}[\psi]_{bb} & \vdots & [\psi]_{bi}\\ \cdots & \vdots & \cdots\\ [\psi]_{ib} & \vdots & [\psi]_{ii}\end{bmatrix}\begin{bmatrix}[\Delta]_{bb} & \vdots & [\Delta]_{bi}\\ \cdots & \vdots & \cdots\\ [\Delta]_{ib} & \vdots & [\Delta]_{ii}\end{bmatrix}^{-1}\begin{bmatrix}[\phi]_{bb} & \vdots & [\phi]_{bi}\\ \cdots & \vdots & \cdots\\ [\phi]_{ib} & \vdots & [\phi]_{ii}\end{bmatrix}^{T} \tag{7.16}$$

Based on displacement modal and strain modal analysis, the CB reduced SFRF $[H^{\varepsilon}(\omega)]_{CB}$ can be calculated as in Eqn. (7.17):

$$[H^{\varepsilon}(\omega)]_{CB} = [\psi]_{CB}[\Delta]^{-1}_{CB}[\phi]^{T}_{CB} \tag{7.17}$$

where $[\phi]_{CB}$, $[\Delta]_{CB}$ can be obtained from the condensed system matrices; $[M]_{CB}$ and $[K]_{CB}$, while $[\psi]_{CB}$ is given as:

$$[\psi]_{CB} = [T]^{T}_{CB}[\psi][T]_{CB} \tag{7.18}$$

where $[T]_{CB}$ represents the transformation matrix and can be given for the *N*th substructure as:

$$[T]_{CB} = \begin{bmatrix} [I] & [0] \\ -[\psi]_{ii}^{-1}[\psi]_{ib} & [\psi]_{ii} \end{bmatrix} \tag{7.19}$$

The inverse problem defined in Eqns. (7.12) and (7.15) represents the case of the CB reduced model where the number of condensed DOFs is purposely made equal (or nearly equal) to the number of MPFs available for the full model. In such a case, the number of modes is equal to the number of DOFs of the reduced model, all of whose MPFs are previously estimated. In other words, more dynamic information is condensed into fewer numbers of modes of the reduced model than the information contained in the same number of modes of the full model. Therefore, Eqns. (7.12) and (7.15) are dynamically more complete and are expected to produce better load estimates than Eqn. (6.1) and (6.2) for the same number of available/retained modes.

7.2.2 D-Optimal Design in Frequency-based Craig-Bampton Reduced Model for Load Estimation

As described earlier, D-optimal design is used to determine optimum locations for given numbers of sensors and modes retained to get $\{D(\omega)\}_{opt}$, and $[\phi]_{opt}$ in the case of using acceleration measurements and $\{\varepsilon(\omega)\}_{opt}$ and $[\psi]_{opt}$ in the case of using strain measurements. Regarding the type of sensors used, the optimum mode participation factor for retained modes can be calculated as:

$$\{q(\omega)\}_{opt} = ([\phi]_{opt}^T[\phi]_{opt})^{-1}[\phi]_{opt}^T\{D(\omega)\}_{opt} \quad (7.20)$$

$$\{q(\omega)\}_{opt} = ([\psi]_{opt}^T[\psi]_{opt})^{-1}[\psi]_{opt}^T\{\varepsilon(\omega)\}_{opt} \quad (7.21)$$

The full displacement vector $\begin{Bmatrix}\{D(\omega)\}_b \\ \{D(\omega)\}_i\end{Bmatrix}$ and the strain vector $\begin{Bmatrix}\{\varepsilon(\omega)\}_b \\ \{\varepsilon(\omega)\}_i\end{Bmatrix}$ can be identified and transformed to the CB reduced vectors using the Eqn. (7.7) and (7.14) respectively, as well as the CB reduced DFRF matrix $[H^d(\omega)]_{CB}$ as in Eqn. (7.10) and the CB reduced SFRF matrix as in Eqn. (7.17). It is to be noted that the DOFs corresponding to the load application locations must be a subset of the boundary DOFs. Based on that condition, the CB reduced model can be implemented after determining the location of the applied load, i.e., after implementing the first phase of the response transmissibility algorithm.

7.2.3 Example: Frequency-based Craig-Bampton Reduced Model- Motorcycle Horn Bracket

From the example discussed in subsection 6.3.3 and shown in Fig. 5.1, it was concluded that the load estimation accuracy depends on the number of modes retained. Acceptable load estimates may only be obtained by retaining a high number of modes in the analysis, which is not often possible in real world problems. To overcome this restriction, this example was revisited and load identification procedure using the CB reduction method in conjunction with the D-optimal algorithm was applied. For comparison purposes, two cases were solved. The first one is based on the acceleration

measurements whereas the second one is based on strain measurements. Again, all DOFs, except the DOF where the load was applied, were selected to be the locations where sensors can potentially be mounted, i.e., the DOF corresponding to the applied load did not form a part of the candidate set. When subjected to the D-optimal design algorithm, the optimal sensors locations were found for each case and tabulated with additional inputs for the load recovery problem in Tables 7.1 and 7.2. Using Eqns. (7.20) and (7.21) the modal participation factor of the retained modes can be calculated from the response measurements at the optimum locations.

The system response for the full model $\{D(\omega)\}$ or $\{\varepsilon(\omega)\}$ can be identified and transformed to match the CB reduced system matrices by using Eqns. (7.7) and (7.14) respectively. The applied load was finally recovered by using Eqns. (7.12) and (7.15). The applied and recovered loads are plotted in Figs. 7.1 and 7.2. It can be seen that both cases have excellent agreements in the applied and recovered loads when the CB model reduction is implemented to the load recovery procedure. Next, to simulate a more realistic scenario where accelerations and strains are measured experimentally, each element in $\{D(t)\}$ and $\{\varepsilon(t)\}$ was corrupted with normally distributed random errors with zero mean and standard deviation of 10% of its value. The applied and recovered loads, with errors in acceleration and strain measurements, are plotted in Figs. 7.3 and 7.4. Once again, it can be seen that the proposed approach is able to recover the applied loads fairly accurately.

The influence of the sensor type on the quality of load estimate is examined by calculating the RMS error values between the applied and the predicted loads for both cases. For the first case, the RMS error value is 18.26 while it is reduced to 14.55 for the second case. Comparing the RMS error values obtained, it can be concluded that using the strain measurements yields better results than using the acceleration measurements by about 20% for this example.

Finally, comparing these results with results obtained for load prediction without model reduction for the Horn Bracket (Table 6.4), it can be seen that, the load's magnitude prediction without model reduction needed 10 sensors and 25 retained modes to have RMS error values 281.18 and 111.1 using accelerometers and strain gages respectively. However, for the same load prediction problem but using MOR technique, only 7 sensors and 5 retained modes are needed to have the RMS error values being reduced to 18.26 and 14.55 using the acceleration and strain measurement respectively. So, with a smaller number of sensors used and a smaller number of modes retained, the accuracy of load prediction is improved significantly for this example.

7.3 Response Transmissibility for Load Identification Improved by D-Optimal Design and Frequency-Based Craig-Bampton Reduced Model

This section presents a complete algorithm to determine the unknown load location and magnitude based on response transmissibility. The algorithm is divided into two

phases; the first phase concerns the load location determination based on the use of the response transmissibility concept and the optimum location of sensors. The second phase is to reconstruct the applied load magnitudes using the reduced CB model defined in Eqn. (7.12) or (7.15) based on the type of sensors being used. A comprehensive flow chart for load identification using the response transmissibility concept and CB reduction is shown in Fig. 7.5.

Presented next is a numerical example demonstrating the efficacy of the proposed approach on a problem where it is shown that the applied load is recovered accurately.

Example: Load Identification for 3D cantilevered Beam

The numerical example of a 3D cantilevered beam described in Sec. 4.6.5 is considered to demonstrate the solution procedure for load identification. The initial step starts with building an FE model of the structure under consideration, since the first phase concerns the determination of the load location by using the response transmissibility concept. The algorithm searches all possible locations. One important factor affectings the complexity of the search algorithm is the number of nodes of the FE model; therefore, a finer mesh makes the search algorithm longer. It is suggested that a coarse mesh can be used in the first phase to determine the load location; then in the second phase a finer mesh can be used in the reduced CB model to reconstruct the load magnitude.

To apply the solution procedure described in Fig. 7.5 for a cantilevered beam, two cases were implemented. The first case is based on acceleration measurements and the second case is based on strain measurements. Both cases were compared by calculating

the RMS error values between the actual and the predicted magnitudes of the applied load for the same number of sensors and retained modes. In both cases a point load is applied on the middle node of the free end.

7.3.1 Case I: Displacement transmissibility for load identification using optimum location of accelerometers and frequency-based Craig-Bampton reduced model

Phase I: Load location prediction.

This phase starts by building the FE model of the beam, as suggested earlier. A coarse mesh is implemented along with modal analysis using ANSYS software to get [M], [K], and $[\phi]$. For this example, the beam is meshed using SOLID45 elements. All degrees of freedom at the left end of the beam are constrained. The model consists of 30 free nodes with three degrees of freedom per node; i.e., the total number of degrees of freedom in the FE model is 90. A harmonic point load is applied on the middle of the beam's free end on node number 31 and is given as: $F(t) = 500\ \sin(3\pi t)$. (See Fig. 7.6).

Using the D-optimal algorithm described previously for 10 modes retained, the optimum locations for five accelerometers (I_{opt}) are identified to be node numbers [3,4,15,17,28]. Then the DFRF at optimum locations for all possible load locations and directions for a given range of frequencies are calculated using a MATLAB program to get $[H^d(\omega)]_{opt}$. Based on these optimum locations, the accelerometers' data $\{D(t)\}_{I(opt)}$ are obtained from ANSYS. A MATLAB program is used to get the acceleration data in frequency domain $\{D(\omega)\}_{I(opt)}$ using (fft) command. For the accelerometers data at J

coordinates $\{D(\omega)\}_J$, it is assumed to be the same as $\{D(\omega)\}_{I(opt)}$. (See Table 7.3). Then the procedure described in subsection 4.4.1 is implemented to calculate the accumulated errors for all possible applied load locations and directions as given in Eqn. (4.31) and plotted as shown in Fig. 7.7. For this case where the load direction is unknown a priori, the total number of combinations explored for one applied load is 90. The applied load location at node 31 on the Y direction corresponds to combination number 77. It can be seen from Fig. 7.7 there is a minimum value at this combination number that corresponds to the load location and direction being predicted correctly. Another minimum value is shown at combination number 62 that corresponds to the applied load on node 26 on the Y direction, which makes sense since node 31 lies above node 26.

Phase II: Load reconstruction using the D-optimal algorithm and the CB reduced model.

In this phase load magnitude is reconstructed using a smaller number of modes retained. To achieve a good accuracy, the model is built and re-meshed in ANSYS software using a SOLID45 element type (see Fig. 7.8). This model has 200 free nodes, and each node has three degrees of freedom; i.e., the total number of degrees of freedom in the FE model is 600. The updated node number of the applied load is 149 and the DOF of the applied load on the Y direction is 425. This DOF will be used as one of the boundary degrees of freedom in the CB reduction method as discussed earlier. For a small number of modes retained (m=7), a modal analysis is implemented to get the updated modal

matrix. After eliminating the degree of freedom at which the load is applied from the updated modal matrix, the D-optimal algorithm is used to identify ten optimum accelerometers locations. Additional inputs for the load reconstruction problem are tabulated in Table 7.5. By using Eqn. (7.20), the modal participation factor of the retained modes can be calculated from the acceleration measurements at optimum locations.

The system response for the full model can be identified and then transformed to match the CB reduced system matrices as in Eqn. (7.10). The applied load is finally recovered by using Eqn. (7.12). The applied and recovered loads using the technique of model reduction are plotted in Fig. 7.9. It can be seen that a good agreement is achieved in the applied and recovered loads when the CB model reduction is applied to the load recovery procedure. The RMS error value between the applied and the recovered loads is calculated and it is found to be 6.25.

7.3.2 Case 2: Strain transmissibility for load identification using optimum location of strain gages and frequency-based Craig-Bampton reduced model

In this case the two-phase procedure for the load identification problem is implemented based on the strain measurements and the strain modal analysis as follows:

Phase I: load location prediction.

Following the same procedure described in the first phase of case 1, the D-optimal algorithm described previously is applied for the 10 modes retained. Nodes [9,22,30,45,83] are identified as optimum locations for the five strain gages (l_{opt}). Then

the SFRF at the optimum locations for all possible load locations and directions for a given range of frequencies are calculated using a MATALB program to get $[H^{\varepsilon}(\omega)]_{opt}$. Based on these optimum locations, the strain data $\{\varepsilon(t)\}_{I(opt)}$ are obtained from ANSYS and a MATLAB program is used to get the strain data in frequency domain $\{\varepsilon(\omega)\}_{I(opt)}$ using (fft) command. For the strain data at *J* coordinates $\{\varepsilon(\omega)\}_J$, it is assumed to be same as $\{\varepsilon(\omega)\}_{I(opt)}$. (See Table 7.6). Then the procedure described in subsection 5.3.1 is implemented to calculate the accumulated errors for all possible applied load locations and directions as given in Eqn. (5.18) and plotted as shown in Fig. 7.10. As in case 1, the total number of combinations explored for one applied load is 90. The applied load location at node 31 on the Y direction corresponds to combination number 77. It can be seen from Fig. 7.10 there is a minimum value at this combination number, which corresponds to the load location and the direction being predicted correctly. Another minimum value is shown at combination number 62, which corresponds to the applied load on node 26 on the Y direction, which make sense since node 31 lies above node 26.

Phase II: Load reconstruction using D-optimal locations and CB reduced model.

In this phase the load magnitude is reconstructed using a smaller number of modes retained. For the same purpose mentioned in phase II of case 1 the model is built and re-meshed in ANSYS software using SOLID45 element type (see Fig. 7.8). Using the updated node number of the applied load (149) and knowing that the DOF of the applied load on the Y direction is 425, this DOF will be used as one of the boundary degrees of

freedom in the CB reduction method as discussed earlier. For a small number of modes retained (m=7), a modal analysis along with a strain modal analysis are implemented to get the updated modal matrix and the strain modal matrix. After eliminating the degree of freedom at which the load is applied from the updated modal matrices, the D-optimal algorithm is used to identify ten optimum strain gages locations. Additional inputs for load reconstruction problem are tabulated in Table 7.6. By using Eqn. (7.21), the modal participation factor of the retained modes can be calculated from the strain measurements at optimum locations.

The system response for the full model can be identified and then transformed to match the CB reduced system matrices as in Eqn. (7.14). The applied load is finally recovered by using Eqn. (7.15). The actual applied load and the recovered load using the technique of model reduction are plotted in Fig. 7.11. It can be seen that a good agreement is achieved in the applied and recovered loads when the CB model reduction is applied to the load recovery procedure. The RMS error value is calculated, and it is found 2.46. Comparing this value with RMS value using the accelerometers, it can be concluded that using the strain measurement improves the accuracy by about 60% for this example.

Finally, comparing these results with the results obtained for the same problem but without using model reduction technique. (See Table 6.2), it can be seen that for the same number of sensors (accelerometers or strain gages) the load prediction needed 20 retained modes such that the RMS error values are 101.2 and 48.41 in case of using

accelerometers and strain gages respectively. By using model reduction technique, the number of retained modes reduced to 7 and the RMS error values to 6.25 and 2.46 in case of using acceleration and strain measurements respectively. It can be concluded that using the model reduction technique improved the accuracy of load prediction and saved computational time.

7.4 Conclusions and Summary

A computational method is presented that allows for load component prediction (number, direction, location, and magnitude) of dynamic loads applied on a structure based on model reduction technique. This is achieved by using the response measurements at optimum sensor locations along with response transmissibility concept retaining a small number of modes. The Craig-Bampton reduction model technique is proposed to reduce the size of the system matrices. Implementing the model reduction in the load magnitude reconstruction phase results in significant improvement in the dynamic load estimates while simultaneously reducing the computational times. Numerical example results illustrate the effectiveness of the proposed approach in recovering dynamic loads that induce significant levels of vibrations in the structure. The robustness of the approach has been demonstrated through two cases wherein the applied loads are recovered accurately despite the presence of simulated measurement errors in acceleration and strain measurements.

The proposed approach is also implemented for two different types of sensors, accelerometers and strain gages. A comparison between these cases has been presented by comparing the RMS error values between the applied and predicted loads. Based on that comparison, it can be concluded that both cases show accurate results for load location prediction, but better results have been shown for the load magnitude reconstruction phase when strain gages are used.

Table 7.1 Input Data for the Horn bracket with CB Reduction Case 1

Variable	**Value**
Total DOF (*n)*	1398
Retained modes (*m)*	5
CB constrained modes ($\mathcal{R}$)	3
Boundary DOF (*b)*	[214 403 425 753]
Optimum locations for 7 accelerometers	[6 14 18 23 50 75 209]

Table 7.2 Input Data for the Horn bracket with CB Reduction Case 2

Variable	**Value**
Total DOF (*n)*	1398
Retained modes (*m)*	5
CB constrained modes ($\mathcal{R}$)	3
Boundary DOF (*b)*	[58 425 713 1313]
Optimum locations for 7 strain gages	[14 75 106 134 193 221 237]

Table 7.3 Displacement Transmissibility Data for Cantilevered Beam Case 1

Optimal *I* coordinates	[3,4,15,17,28]
J coordinates	[3,4,15,17,28]
P coordinate	[31]

Table 7.4 Input Data for a Cantilevered Beam with CB Reduction Case 1

Variable	**value**
Total DOF (*n)*	600
Retained modes (*m)*	7
CB constrained modes ($\mathcal{R}$)	3
Boundary DOF (*b)*	[12 173 425 480]
Optimum locations for 10 accelerometers (I_{opt})	[3,13,55,73,124,129,130,172,177,189]

Table 7.5 Strain Transmissibility Data for Cantilevered Beam Case 2

Optimal *I* coordinates	[9,22,30,45,83]
J coordinates	[9,22,30,45,83]
P coordinate	[31]

Table 7.6 Input Data for CB Reduced Model of Cantilevered Beam Case 2

Variable	**Value**
Total DOF *(n)*	600
Retained modes *(m)*	7
CB constrained modes ($\mathcal{R}$)	3
Boundary DOF *(b)*	[64,137,353,425]
Optimum locations for 10 strain gages (I_{opt})	[3,20,45,51,113,115,125,190,200,201]

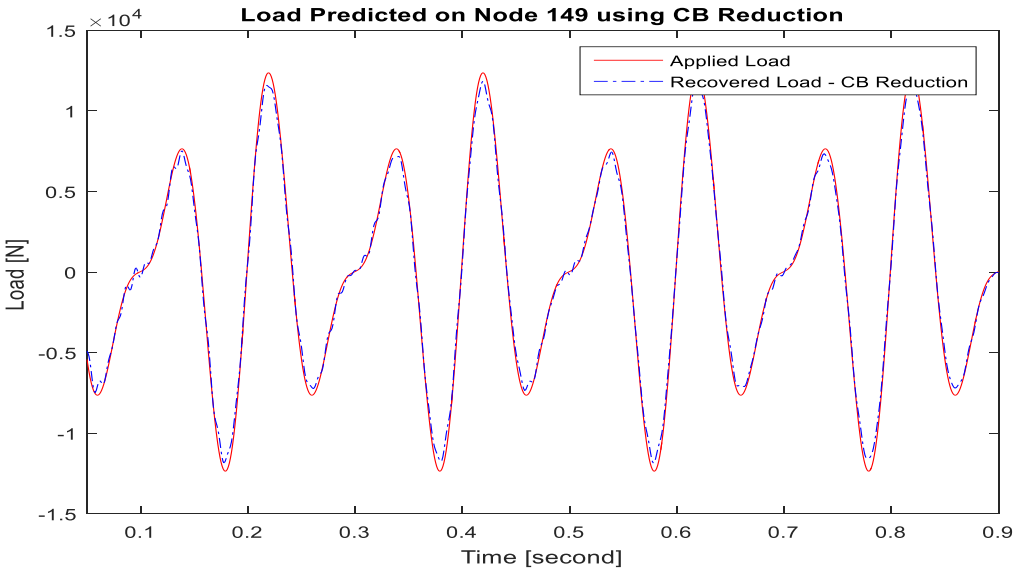

Figure 7. 1 Applied and Recovered Loads Using Acceleration Measurements

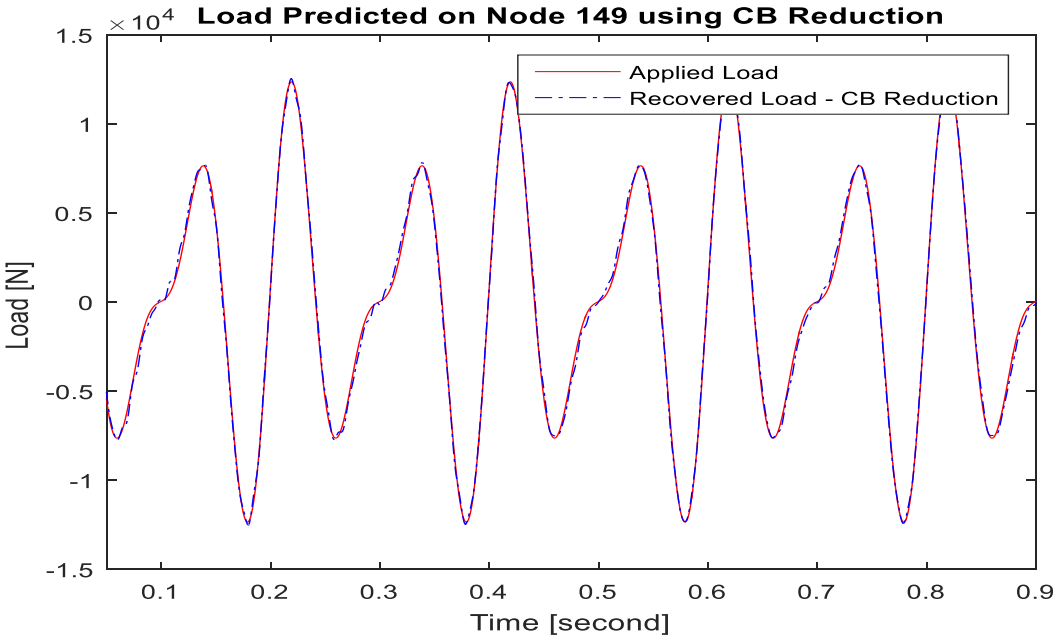

Figure 7.2 Applied and Recovered Loads Using Strain Measurements

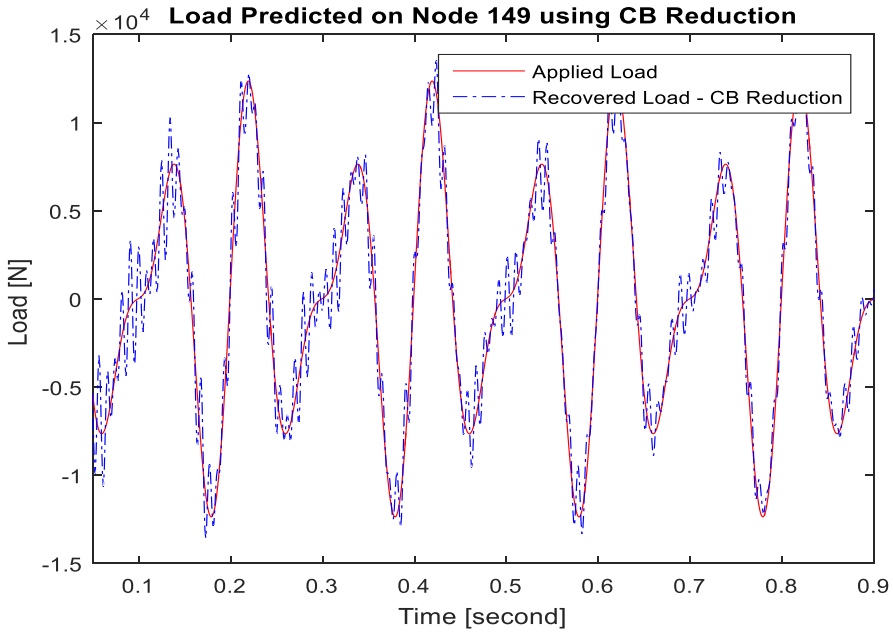

Figure 7.3 Applied and Recovered Loads Using Accelerometers with Measurement Errors

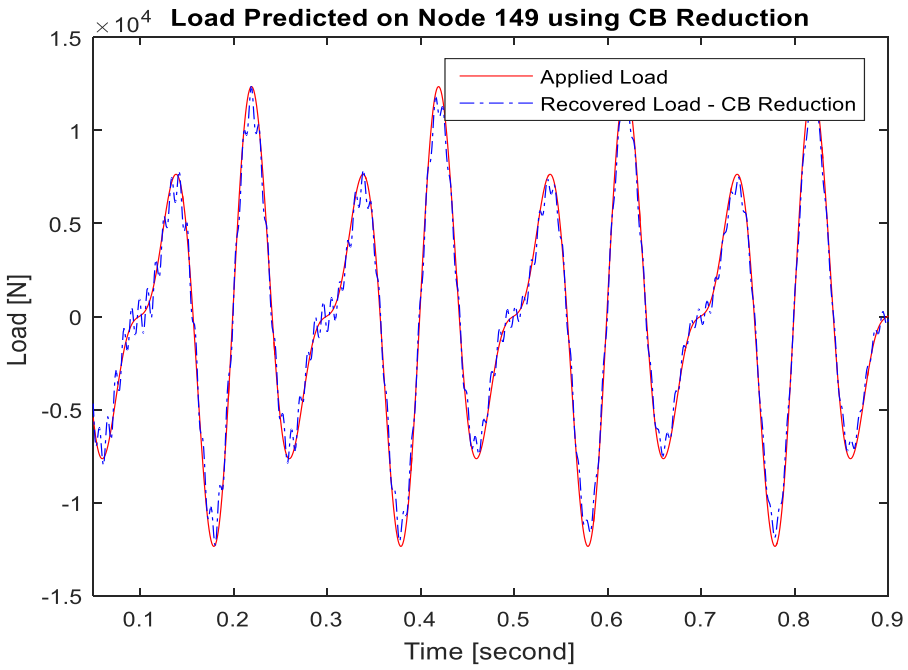

Figure 7.4 Applied and Recovered Loads Using Strain Gages with Measurement Errors

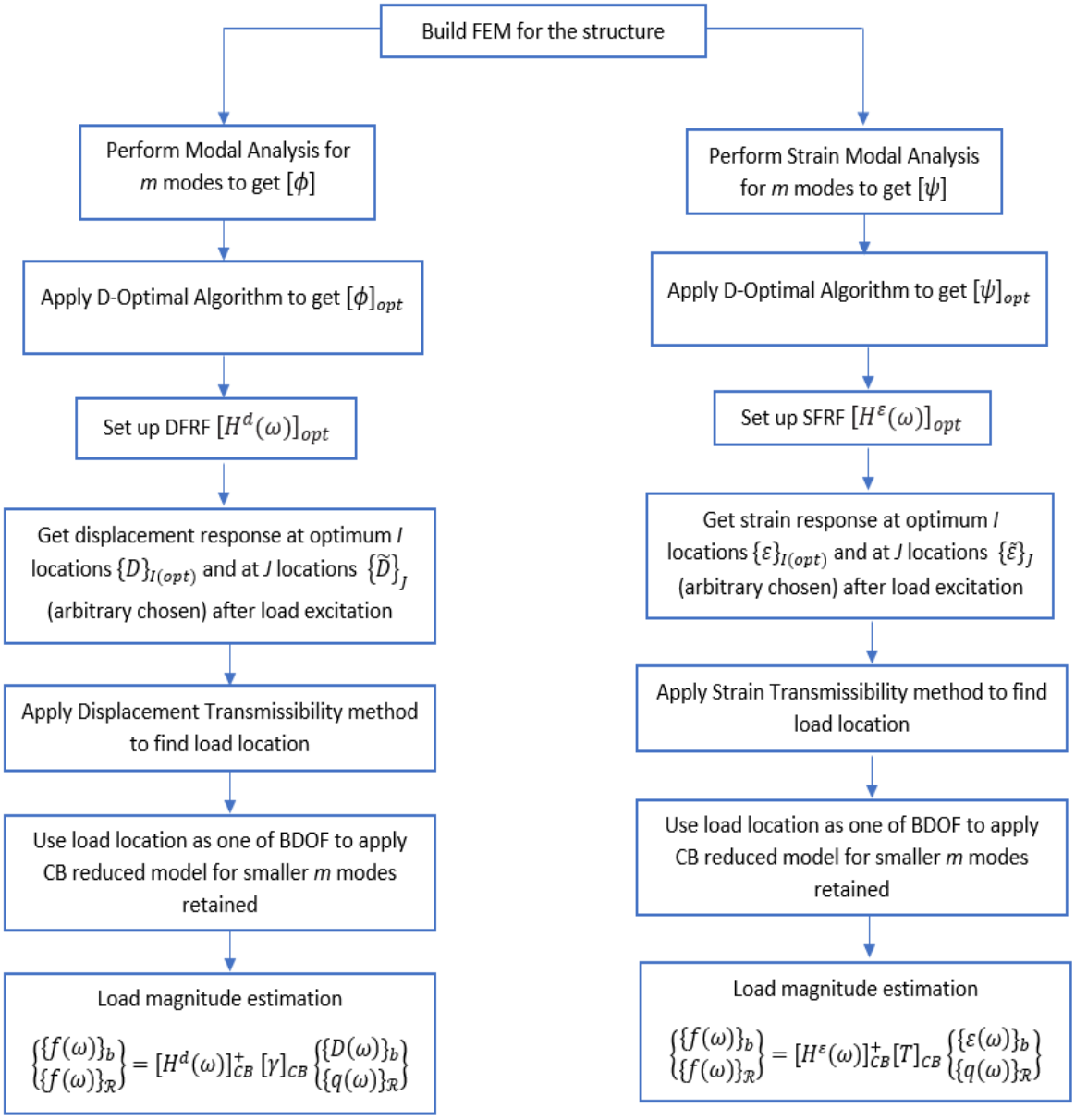

Figure 7.5 Flow Chart for Two Cases Load Identification

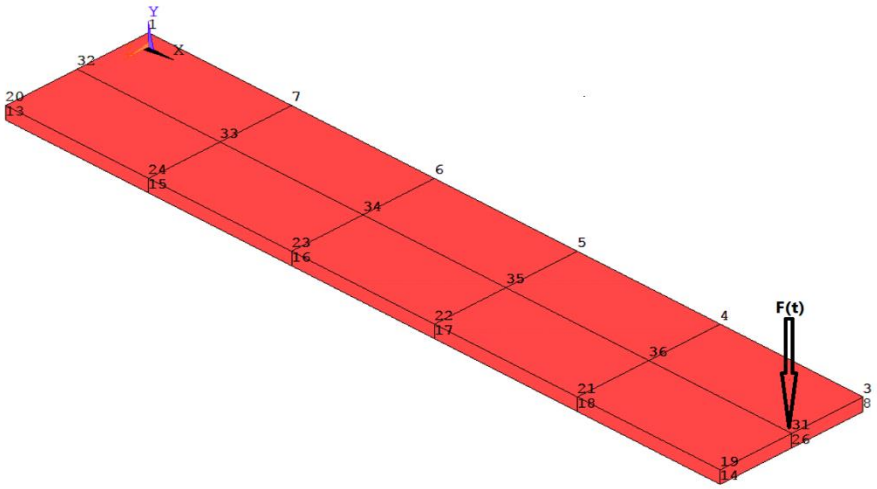

Figure 7.6 Finite Element Model of a 3D Cantilevered Beam (Coarse-mesh) for Phase1

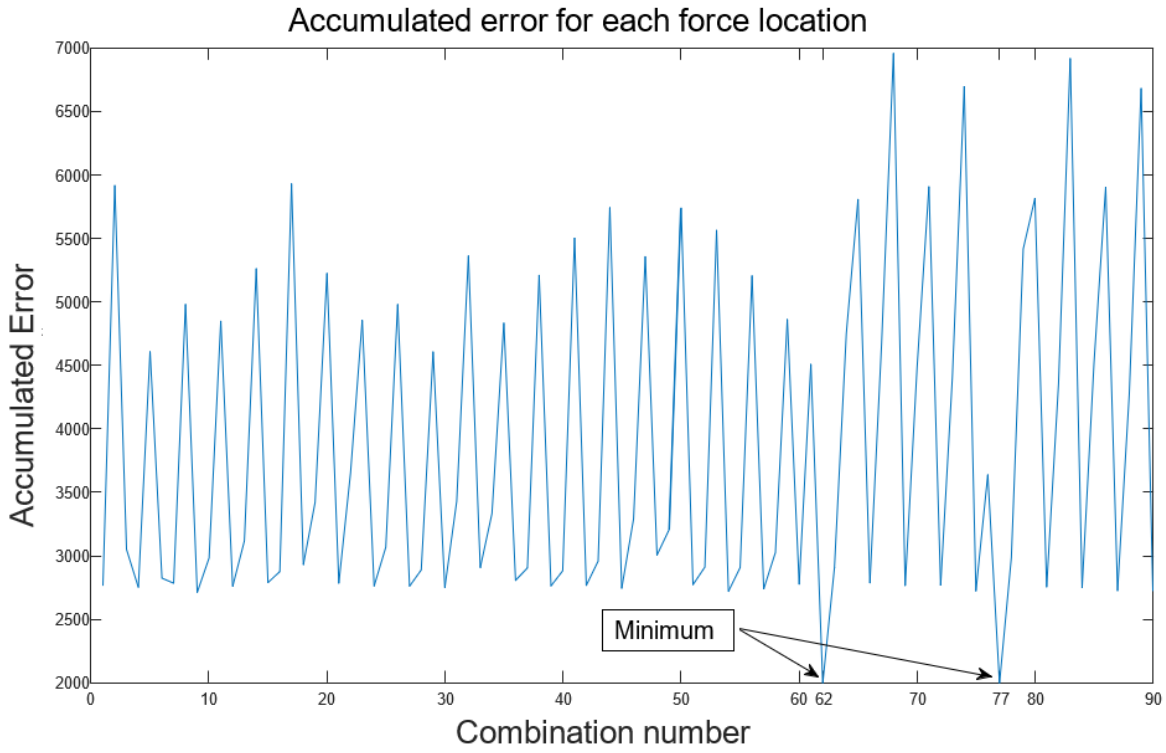

Figure 7.7 Accumulated Error for Cantilevered Beam-Case 1

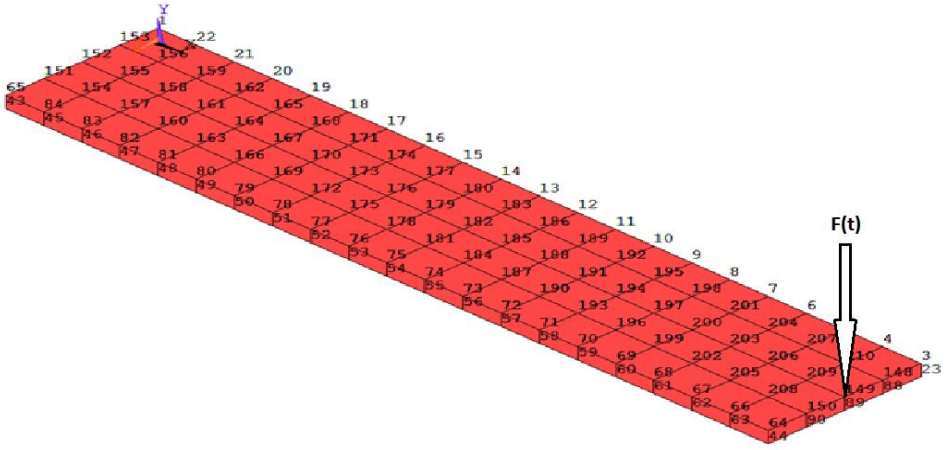

Figure 7.8 Finite Element Model of a 3D Cantilevered Beam (Fine-mesh) for Phase II

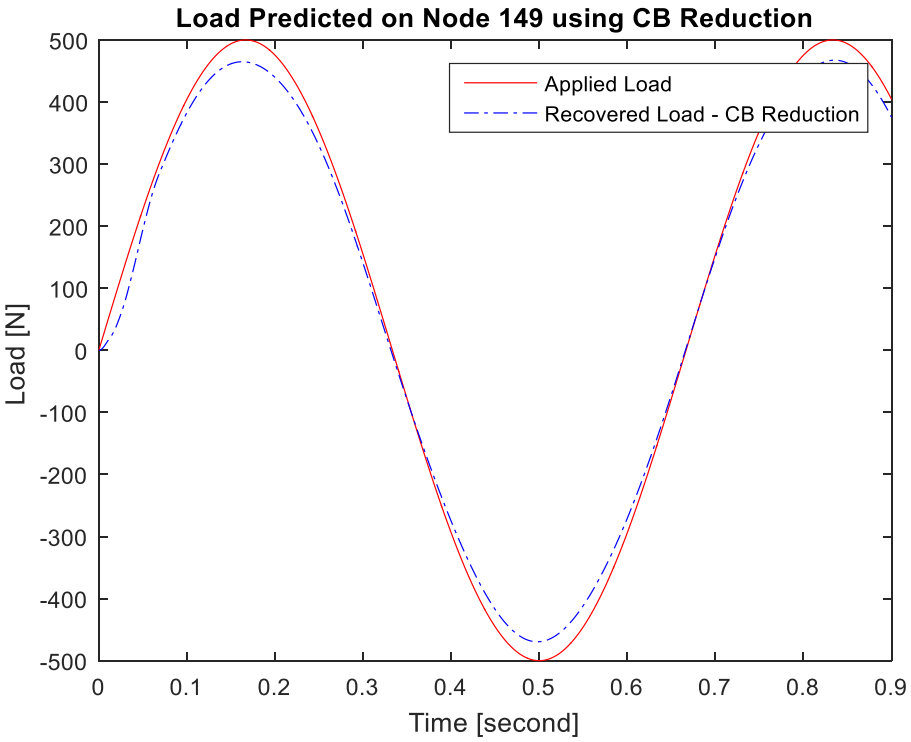

Figure 7. 9 Applied and Recovered Loads on Node 149 with Optimum Accelerometer Placements

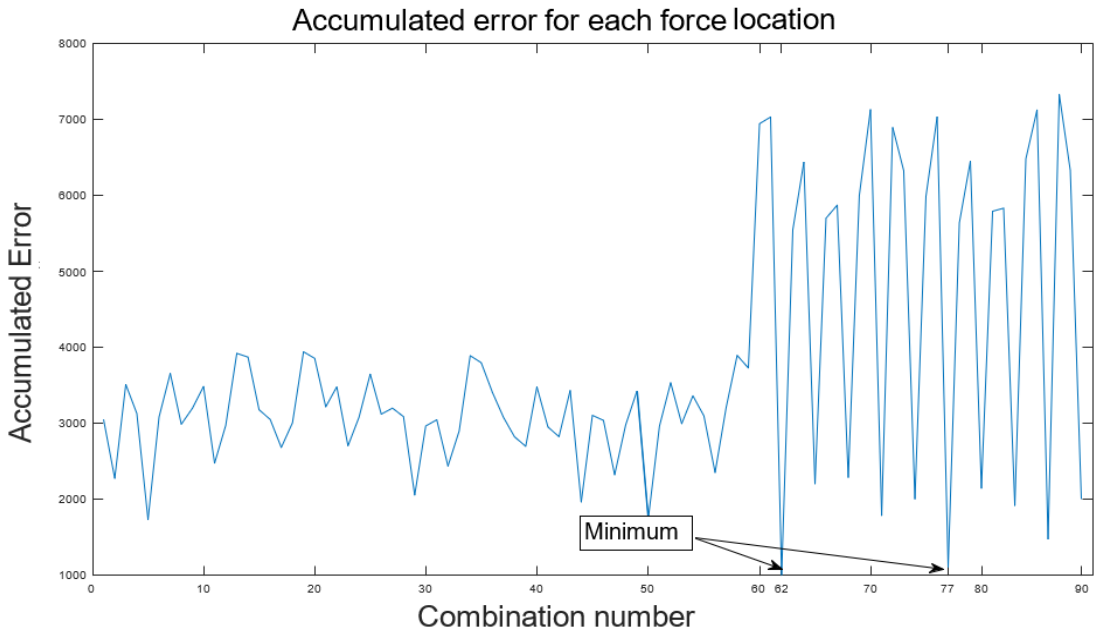

Figure 7.10 Accumulated Error for Cantilevered Beam-Case 2

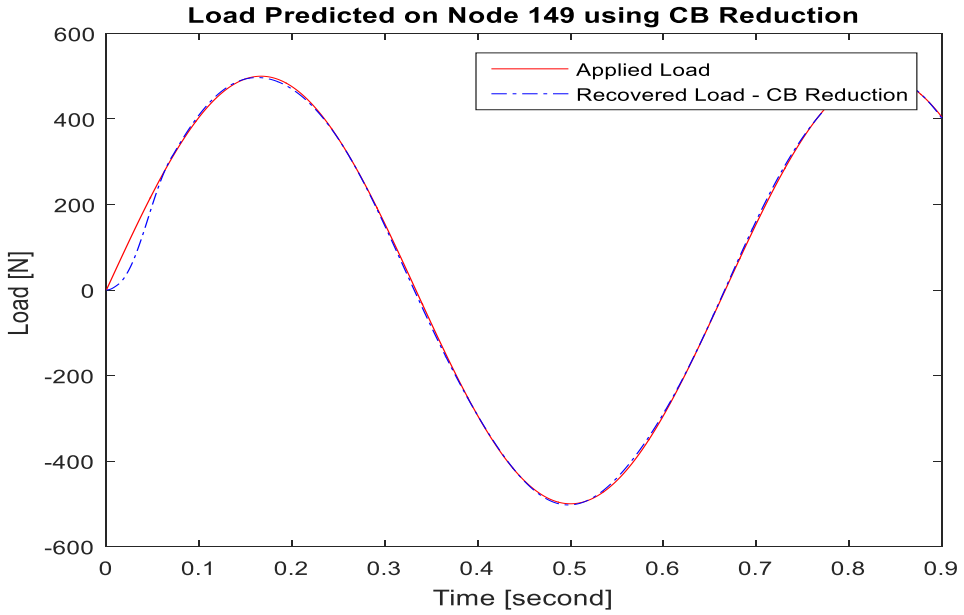

Figure 7.11 Applied and Recovered Loads on Node 149 with Optimum Strain gages Placements

Chapter 8 - Summary and Future Research

The primary goal of this dissertation was to develop as well as bring together efficient algorithms and novel techniques to identify dynamic loads acting on a structure from measured structural response (strain, acceleration, etc.). Chapter 1 described the problem statement and the requirements of this dissertation in detail. Load identification through output response measurement is an inverse problem in which a structure itself is converted into a transducer or so-called “self-transducer”. Solving inverse problems is challenging not only due to the ill-conditioning, but, in general, leads to multiple solutions. Therefore, additional information such as the number and the locations of the imposed loads must be provided ahead of time in order to allow for a unique solution. This dissertation focuses on cases where such information is not readily available. Identification of the accurate location, direction, and magnitude of a dynamic load are important for an optimized design solution.

A discussion of several former methods is provided in chapter 2. Some studies work on load magnitude identification only, assuming load location is known in advance, which makes these methods limited to certain applications. Other studies work on more challenging cases where neither the load location or the magnitude are known. Chapter 3 presented one of these methods to predict the location and magnitude of a harmonic load. The approach is based on a direct search complex algorithm to solve the general optimization problem for the force amplitude and its location index. This method is limited

for one kind of harmonic loads with fixed amplitude and one excitation frequency. To deal with the aforementioned shortcoming, an alternate algorithm is presented in chapter 4 for identifying dynamic loads acting on the structure from acceleration responses using the motion transmissibility concept for MDOF systems. The reconstruction of loads is done in two successive phases. In the first phase, the location and the number of applied loads are estimated by using a transmissibility model. In the second phase, the load vector is reconstructed by multiplying the inverse of the structural FRF matrix with the system's measured response. This approach uses system response, such as accelerations, to predict the load magnitudes and locations. While this technique provides promising results, the question of sensor placement was not addressed and was left as the user's choice.

In previous as well as recent works that use the concept of transmissibility for load prediction, the number of sensors used was addressed, but little attention was paid to their locations. The placements of sensors were left to the engineering experience or judgement of the user. The accuracy of load estimation is strongly influenced by the location of sensors and a random placement of sensors increases problem ill-conditioning whereas a proper selection of sensor locations decreases problem ill-conditioning and improves the accuracy of the load estimation.

The motivation of this dissertation lies in the fact that using the concept of motion transmissibility, a solution procedure is presented for the load identification problem wherein all three load components, the number of applied loads, the load locations, and

the load magnitudes, are unknown. The solution also provides an answer to the question of sensor placement for improved load prediction. This is especially important when multiple loads are applied. It is seen that the efficacy of load estimation is improved when sensors are placed at optimum locations. These optimum sensor locations are determined using the D-optimization technique.

Using optimum locations of accelerometers as determined by the D-optimal algorithm allows for improvement in the identification for the unknown loads especially when multiple loads are applied. In this dissertation it has been verified numerically that even in the presence of simulated measurement errors, the proposed method was able to achieve promising results.

Another approach has been proposed in chapter 5 using the strain transmissibility concept for MDOF system in conjunction with the D-optimal algorithm for strain gages locations. The approach is based on the fact that the measurements of strain may lead to more accurate results than measurements of acceleration for a beam-like structure. This is explained by the fact that, for such structures, there are generally more vibrational eigen modes significantly contributing to the strain response than to the acceleration response. Using strain gages in strain transmissibility has been verified numerically for its effectiveness in load identification as using the motion transmissibility.

A computational comparison in frequency domain for load magnitudes identification using two different types of sensors i.e., accelerometers and strain gages,

is presented in chapter 6. The concepts of strain frequency response function and displacement frequency response function are explained and used along with the optimum sensors' locations determined by the D-optimal algorithm. The similarities and differences between acceleration-based load identification and strain-based load identification are discussed through numerical examples. A use of mixed strain-acceleration measurements is also considered in this chapter. The results of numerical examples using SFRF, DFRF and SDFRF in conjunction with optimum sensor placement form a powerful set of tools for load identification applications. Other important observations can be concluded from this comparison study and can be summarized as:

- Using strain gages, in general, gives better results than accelerometers alone; hence, their use as sensors for load identification is attractive.
- The condition number of a SFRF matrix is several order magnitudes lower than the condition number of the DFRF matrix. Therefore, the SFRF matrix poses a less ill-conditioned inverse operation for the loading cases than would be the case for the DFRF matrix.
- Strain modal analysis provides an improved force estimation ability compared to displacement modal analysis.
- The combined SDFRF approach yields results that are as good as, if not better than, those obtained using pure SFRF or DFRF approaches. This method has a better identification accuracy than using SFRF or DFRF even while retaining a limited number of modes.

An investigation on the number of retained modes and the number of sensors used on the accuracy of recovered loads is also presented. It was found that acceptable load estimates may only be obtained by retaining a high number of modes in the analysis, which is not often possible in real world problems. To overcome this restriction, a different approach, which uses the technique based on Craig-Bampton model order reduction is proposed in chapter 7. It is observed that the load recovered using the reduced model shows an initial discrepancy, but later follows the applied load closely. It is inferred that with the introduction of model order reduction and without compromising the quality of load estimates, the computation time can be reduced significantly.

To present a complete procedure for load identification problems using response transmissibility along with the frequency-based CB reduction method and the D-optimal algorithm for sensors location, two cases have been implemented with explanation for all steps required to achieve better accuracy for load identification problem. The first case is based on using accelerometers' measurements and the second case is based on using strain measurements. In both cases; the solution procedure is divided into two phases. The first phase uses the transmissibility concept in conjunction with the D-optimal algorithm to determine the optimum location of sensors, so the most accurate predictions of load location and direction are achieved. Based on the results, both cases show a good accuracy for load location and direction prediction. The second phase is load magnitude reconstruction in which the CB reduction model in conjunction with the D-optimal technique is implemented. Based on the results, both cases show a good agreement

between the load applied and the load reconstructed. Comparing the RMS errors between the magnitudes of the applied and the predicted loads for both cases and using same number of sensors and modes retained, it can be concluded that a better result has been shown in the load magnitude reconstruction phase when strain gages are used.

Finally, the load identification techniques developed and proposed in this dissertation using the response transmissibility concept rely on so many factors:

- The description of the structure in terms of the degrees of freedom where usually a finite element tool is used. Although using fine mesh for FEM is recommended to get the best accuracy in load identification, it will increase the computational time for the search process to cover all possibilities for load locations and directions. So to avoid this, it is suggested to use coarse mesh for FEM in the first phase and fine mesh in the second phase of load identification process.
- The D-optimal algorithm for the determination of optimum sensor locations such that accurate load location and magnitude are obtained. Additional improvement in the quality of the load estimates is achieved through the Craig-Bampton model order reduction. The sequential exchange D-optimum design algorithm is efficient and quite popular among the design optimization community. However, it suffers from the restriction of often getting stuck in local optima, which may not yield the best possible locations for sensor placements. Future research in this area will focus on experimenting with more efficient and

robust optimization techniques that can be applied to determine optimal sensor locations on the structure.

- Although the Craig-Bampton model order reduction technique worked well when applied in the context of load identification schemes, experimenting with several other well-established model order reduction techniques and studying their effect on the load estimates is further suggested.
- Application of the load identification techniques developed in this dissertation has been studied numerically using discrete systems such as the Spring-mass system and continuous systems as cantilevered beam, all and other simple geometries, where one or two sinusoidal loads are exciting the structure. All are assumed to be undamped linear systems. The real interest of the proposed techniques lies in the case of complicated structures (non-linear, composite, and damped structures) where complex loads are acting. Implementation and testing of the proposed approaches on complicated structures towards identification of multiple complex loads forms another potential area of research.
- Finally, the solution techniques developed are based on the assumption of harmonic excitation applied force. Other types of non-harmonic excitation forces (Impulse or Random) can be considered as future works.

References

[1] Adams, R., & Doyle, J., 2002, "Multiple Force Identification for Complex Structures," *Experimental Mechanics,* 42 (1), pp. 25-36.

[2] Akbar, E., and Masoud, S., 2010, "Finite Element Model Updating Using Frequency Response Function of Incomplete Strain Data," AIAA J., 48(7), pp. 1420–1433.

[3] Atkinson, A.C., Donev, A.N., and Tobias, R.D., 2007, *Optimum Experimental Designs*, New York: Oxford University Press, ISBN-13: 978-0199296606, 2007.

[4] Bateman, V. I., Carne, T. G., Gregory, D. L., Attaway, S.W., Yoshimura, H.R., 1991, "Force Reconstruction for Impact Tests of an Energy Absorbing Nose," *Transaction of ASME, Journal of Vibration and Acoustics,* 113, pp. 192-200.

[5] Boukria, Z., Perrotin, P., and Bennani, A., 2011, "Experimental Impact Force Location and Identification Using Inverse Problems: Application for a Circular Plate," *International Journal of Mechanics, 5* (1), pp. 48-55.

[6] Carne, T. G., Mayes, R. L., and Bateman, V. I., 1992, "Force Reconstruction Using a Sum of Weighted Accelerations Technique," *Proceedings of the 10th International Modal Analysis Conference (IMAC)*, San Diego, CA. pp. 291-298.

[7] Chatterjee, S., and Hadi, A. S., 1988, *Sensitivity Analysis in Linear Regression.* New York: John Wiley.

[8] Choi K., Chang F.K., 1996, "Identification of Impact Force and Location Using Distributed Sensors," *American Institute of Aeronautics and Astronautics (AIAA) Journal,* 34 (1), pp. 136-142.

[9] Craig, R.R., and Bampton, M.C.,1968, "Coupling of Substructures for Dynamic Analysis," *American Institute of Aeronautics and Astronautics (AIAA) Journal,*6 (7), pp. 1313-1319.

[10] Daraji, A. H., Hale, J. M., and Ye, J., 2017, "New Methodology for Optimal Placement of Piezoelectric Sensor/Actuator Pairs for Active Vibration Control of Flexible Structures," *ASME J. Vib. Acoust*., 140(1), p. 011015.

[11] Desanghere, G.,1983, “Identification of External Forces Based on Transfer function Measurements: Frequency Response Method,” *Proceedings of the 8th International Seminar on Modal Analysis*, Leuven, Belgium, 144, pp. 1-28.

[12] Desanghere, G., and Snoeys, R., 1985, “Indirect Identification of Excitation Forces by Modal Coordinate Transformation,” *Proceedings of the 3rd International Modal Analysis Conference (IMAC)*, Orlando, FL., pp. 685-690.

[13] D’Cruz, J., Crisp D.C. and Ryall T.G., 1992, “On the Identification of a Harmonic Force on a Viscoelastic Plate from Response Data,” *ASME Journal of Applied Mechanics,* 59, pp. 722–729.

[14] Doyle, J.F.,1994, “A Genetic Algorithm for Determining the Location of Structural Impacts,” *Experimental Mechanics*, 34 (1), pp. 37-44.

[15] Ewins, D.J.,2000, *Modal Testing: Theory, Practice, and Application.* Baldock, England: Research Studies Press Ltd.

[16] Fabunmi, J.A., 1986, “Effects of Structural Modes on Vibratory Force Determination by Pseudo-Inverse Techniques,” *AIAA Journal* 24, pp. 504-509.

[17] Galil, Z., & Kiefer, J., 1980, “Time- and Space-Saving Computer Methods, related to Mitchell’s DETMAX, for Finding D-Optimum Designs,” *Technometrics,* 22 (3), pp. 301-313.

[18] Genaro, G., & Rade, D. A. ,1998, “Input Force Identification in the Time Domain,” *Proceedings of the 16th International Modal Analysis Conference (IMAC)*, Santa Barbara, CA. pp.124-129.

[19] Govers, Y., and Jelicic, G., 2016, “The Use of Strain Sensors for Modal Identification of Aeroelastic Structures,” *International Conference on Noise and Vibration Engineering*, Leuven, Belgium, Sept. 19–23, pp. 2207–2216.

[20] Gupta, D. K., 2013, “Inverse Methods for Load Identification Augmented by Optimal Sensor Placement and Model Order Reduction. *Ph.D. Dissertation*, University of Wisconsin Milwaukee. U.S.A.

[21] Guyan, R.J., 1965, “Reduction of Stiffness and Mass Matrices,” *American Institute of Aeronautics and Astronautics (AIAA) Journal,* 3 (2), pp. 380.

[22] Han, M.C., and Wicks, A. L., 1990, “Force Determination with Slope and Strain Response Measurement,” *The Eighth International Conference on Electronic*

Measurement and Modal Analysis Conference (IMAC), Kissimmee, FL, Feb. 8–11, pp. 365–372.

[23] Hashemi, R., and Kargarnovin, M. H., 2007, "Vibration Base Identification of Impact Force using Genetic Algorithm," *International Journal of Mechanical Systems Science and Engineering,* 1 (4), pp. 204-210.

[24] Hillary, B., 1983, "Indirect Measurement of Vibration Excitation Forces," *PhD Thesis, Imperial College*, Department of Mechanical Engineering, London.

[25] Hillary, B., and Ewins, D.J., 1984, "The Use of Strain Gauges in Force Determination and Frequency Response Function Measurements," *Proceedings of the 2nd International Modal Analysis Conference (IMAC)*, Orlando, FL., pp. 627-634.

[26] Hui, Z., Xia, C., and Xianjun, W., 2017, "A Review of the Methods for Solving the Ill Conditioned Problem in Frequency Response Domain Identification of Load," *24th International Congress on Sound and Vibration (ICSV24)*, London, July 23–27, pp. 6614.

[27] Hurty, W.C., 1965, "Dynamic Analysis of Structural Systems Using Component Modes", AAIA Journal, 3(4), pp. 678-685.

[28] Irvine, T., 2015, "Effective Modal Mass and Modal Participation Factors," *Vibrationdata*, no. 1, pp. 1-36, http://www.vibrationdata.com/tutorials2/ModalMass.pdf

[29] Johnson, M., and Nachtsheim, C.J.,1983, "Some Guidelines for Constructing Exact D-optimal Designs on Convex Design Spaces," *Technometrics,* 25 (3), pp. 271-277.

[30] Karlsson S. E. S., 1996, "Identification of External Loads from Measured Harmonic Responses," *Journal of Sound and Vibration,* 196 (1), pp. 59–74.

[31] Kammer, D.C., 1998, "Input Force Reconstruction Using a Time Domain Technique," *Journal of Vibration and Acoustics,* 120 (4), pp. 868-874.

[32] Kammer, D. C., 1991, "Sensor Placement for On-Orbit Modal Identification and Correlation of Large Space Structures," *Journal of Guidance, Control and Dynamics,* 14 (2), pp. 251-259.

[33] Khoo, S. Y., and Ismail, Z., 2014, "Impact Force Identification with Pseudo- Inverse Method on a Lightweight Structure for Under-Determined, Even- Determined and Over-Determined Cases," *Int. J. Impact Eng.,* 63, pp. 52–62.

[34] Lage, Y. E., Maia, N. M., M., and Neves, M. M., 2013 “Force Identification Using the Concept of Displacement Transmissibility,” *Journal of Sound and Vibration*, 332, pp. 1674-1686.

[35] Lage, Y. E., Maia, N. M., M., and Neves, M. M., 2014 “Force Magnitude Reconstruction Using the Force Transmissibility Concept,” *Shock and Vibration*, vol. 2014, Article ID 905912.

[36] Lee, H., and Park, Y., 1995, “Error Analysis of Indirect Force Determination and a Regularization Method to Reduce Force Determination Error,” *Mechanical Systems and Signal Processing* 9(6), pp. 615-633.

[37] Liu, G. R., and Han, X., 2003, “Recent Progress on Computational Inverse Techniques in Non-Destructive Evaluation,” *Proceedings of the Second MIT Conference on Computational Fluid and Solid Mechanics*, June 2003, pp. 418-422.

[38] Liu, J.J., Ma, C.K., Kung, I.C., and Lin, D.C., 2000, “Input Force Estimation of a Cantilever Plate by using a System Identification Technique,” *Computer Methods in Applied Mechanics and Engineering,* 190 (11), pp. 1309-1322.

[39] Liu, W., and Ewins, D.J., 1998, “Transmissibility Properties of MDOF Systems,” *Proceedings of the 16th International Modal Analysis Conference,* vol. 3243, Santa Barbara, California, USA, 1998. pp. 847–854.

[40] Lu, Z.R., & Law, S.S., 2007, “Identification of System Parameters and Input Force from Output Only,” *Mechanical Systems and Signal Processing*, 21 (5), pp. 2099-2111.

[41] Ma C. K., Lin D.C., 1997, “Force Estimation of An Equipment-Isolator System Excited by Base Motions,” *Journal of the Chinese Society of Mechanical Engineering* 14, pp. 244–250.

[42] Maia N.M.M., Silva J.M.M., Ribeiro A.M.R., 2001, “The Transmissibility Concept in Multi-Degree-of-Freedom Systems,” *Mechanical Systems and Signal Processing* 15 (1) pp. 129–137.

[43] Manzato, S., and Santos, F., 2014, “Combined Accelerometers-Strain Gauges Operational Modal Analysis and Application to Wind Turbine Data,” *Ninth International Conference on Structural Dynamics (EURODYN ’14)*, Porto, Portugal, June 30–July 2, pp. 3675–3682.

[44] Masroor, S.A., and Zachary, L.W. 1991, “Designing an All-Purpose Force Transducer,” *Experimental Mechanics,* 31 (1), pp. 33-35.

[45] Mignolet, M.P., and Choi, B.K., 2003, “Robust Optimal Positioning of Strain Gages on Blades,” *ASME Journal of Turbomachinery,* 125 (1), pp. 155-164.

[46] Mitchell, T.J., 1974, “An Algorithm for the Construction of ‘D-optimal’ Experimental Designs,” *Technometrics,* 16 (2), pp. 203-210.

[47] Moller P. W., 1999, “Load Identification Through Structure Modification,” *Transactions of the ASME Journal of Applied Mechanics* 66 (1), pp. 236–241.

[48] Nashed, M.Z., 1976, *Generalized Inverses and Applications.* Academic Press.

[49] Neves, M.M., and Maia, N.M.M., 2010, “Estimation of Applied Forces Using the Transmissibility Concept,” *Proceedings of the International Conference on Modal Analysis Noise and Vibration Engineering (ISMA 2010),* Leuven, pp. 3887-3897.

[50] Okubo, N., Tanabe, S., and Tatsuno, T., 1985, “Identification of Forces Generated by a Machine Under Operating Condition,” *Proceedings of the 3rd International Modal Analysis Conference (IMAC)*, Orlando, FL. Feb. 6-9, pp. 920-927.

[51] Paz, M., 1985, *Structural Dynamics: Theory and Computation.* New York: Van Nostrand Reinhold Company, Inc.

[52] Qu, Z.Q., 2004, Model Order Reduction Techniques with Applications in Finite Element Analysis. New York: Springer.

[53] Ribeiro A.M.R., Fontul M., Maia N.M.M., Silva J.M.M., 2005, “Further Developments on the Transmissibility Concept for Multiple Degree of Freedom System,” *Proceedings of the 11th International Conference on Vibration Engineering,* Timisoara, Romania, September 2005.

[54] Ribeiro, A. M. R., Silva, J. M. M., and Maia, N.M.M., 2000, “On the Generalization of The Transmissibility Concept,” *Mechanical Systems and Signal Processing,* 14 (1) pp.29–35.

[55] Ribeiro, A.M.R., Silva, J.M.M., Maia, N.M.M., and Fontul, M., 2004, “Transmissibility Matrix in Harmonic and Random Processes,” *Shock and Vibration*, 11(5-6), pp. 563-571.

[56] Shih, C.Y., Zhang, Q., and Allemang, R.J., 1989, "Force Identification by Using Principle and Modal Coordinate Transformation Method," *Vibration Analysis-Techniques and Applications, ASME Publication DE 18-4,* pp. 303-309.

[57] Starkey, J. M., and Merrill, G. L., 1989, “On the Ill-Conditioned Nature of Indirect Force Measurement Techniques,” *International Journal of Analytical and Experimental Modal Analysis, 4* (3), pp.103-108.

[58] Steltzner, A.D., and Kammer, D.C. ,1999, “Input Force Estimation Using an Inverse Structural Filter,” *Proceedings of the 17th International Modal Analysis Conference (IMAC)*, Kissimmee, FL. pp. 954-960.

[59] Stevens, K.K., 1987, “Force Identification Problems - An Overview,” *Proceedings of the 1987 SEM Conference on Experimental Mechanics*, Houston, TX, pp. 838-844.

[60] Szwedowicz, J., Senn, S. M., and Abhari, R. S., 2002, “Optimum Strain Gage Application to Bladed Assemblies,” *ASME Journal of Turbomachinery,* 124 (4), pp. 606-613.

[61] Thite, A., and Thompson, D., 2006, “Selection of Response Measurement Locations to Improve Inverse Force Determination,” *Appl. Acoust*., 67(8), pp. 797–818.

[62] Trujillo, D.M., and Busby, H.R., 1997, *Practical Inverse Analysis in Engineering.* CRC Press, 1997.

[63] Vakakis, A.F., 1985, “Dynamic Analysis of a Unidirectional Periodic Isolator, Consisting of Identical Masses and Intermediate Distributed Resilient Blocks,” *Journal of Sound and Vibration,* 103(1), pp. 25-33.

[64] Vakakis, A.F., Paipetis, S.A., 1985, “Transient Response of Unidirectional Vibration Isolators with Many Degrees of Freedom,” *Journal of Sound and Vibration*, 99 (4), pp.557-562.

[65] Vakakis, A.F., Paipetis, S.A., 1986, “The Effect of a Viscously Damped Dynamic Absorber on a Linear Multi-Degree-of-Freedom System,” *Journal of Sound and Vibration,* 105(1) pp. 49-60.

[66] Varoto, P.S., McConnell, K.G., 1998, “Single Point vs Multi Point Acceleration Transmissibility Concepts in Vibration Testing, *Proceedings of the 12th International Modal Analysis Conference (IMAC XVI),* pp. 83-90.

[67] Vishwakarma, R., Turner, D., Lewis, A., Chen, Y., Houghton, P., and Xu, Y., 2010, "Load Reconstruction on a Missile Structure Using the Pseudo-Inverse Methods," in *Proceedings of the 2010 International Conference on Modelling, Identification and Control*, Okayama, July 2010. pp. 100–105.

[68] Wang B.T., 2002, "Prediction of Impact and Harmonic Forces Acting on Arbitrary Structures: Theoretical Formulation," *Journal of Mechanical Systems and Signal Processing*, 16 (6), pp. 935-953.

[69] Wang B.T., Chiu C.H., 2004, "Prediction of Harmonic Force Acting on Cantilever Beam," Proceedings of the 21st International Modal Analysis Conf. (IMAC) (2004), Honolulu, HI, pp. 1230-1241.

[70] Wickham, M. J., Riley, D. R., & Nachtsheim, C. J., 1995, "Integrating Optimal Experimental Design into the Design of a Multi-Axis Load Transducer," *Journal of Engineering for Industry,* 117 (3), pp. 400-405.

[71] Wu, A.L., and Loh, C.H., 2007, "Input Force Estimation Using System Identification Techniques," *Proceedings of the 8th Pacific Conference on Earthquake Engineering (PCEE).* Singapore.

[72] Yam, L.H., Leung, T. P., Li, D. B., and Xue, K.Z., 1996, "Theoretical and Experimental Study of Modal Strain Energy," *Journal of Sound and Vibration,* 191 (2), pp. 251-260.

[73] Yang, J., and Yoshizawa, T., 2014, "Indirect Force Identification Using Strain Sensor," *21st International Congress on Sound and Vibration (ICSV21)*, Beijing, China, July 13–17, pp. 3288.

CURRICULUM VITAE

Hana'a M Alqam

Education	08/2019 Ph.D Mechanical Engineering University of Wisconsin Milwaukee
	12/2011 M.S Mechanical Engineering University of Wisconsin Milwaukee
	06/2003 B.Sc. Mechatronics Engineering Al-Balqa Applied University, Jordan
Work Experience	01/13-present Instructor University of Wisconsin Milwaukee Mechanical Engineering Department Biomedical Engineering Department **Courses Taught:** • Computational Tools for Engineers (MATLAB) • Mechanical Design • Design of Machine Elements • Introduction to Finite Elements • Introduction to Control Systems • Modeling and Analysis of Dynamic Systems. 08/08-12/12 Teaching Assistance University of Wisconsin Milwaukee Mechanical Engineering Department **Duties:** • Teach and Run the Lab of Control and Design of Mechatronic Systems

	• Teach and Run the lab of Introduction to Control Systems 11/03-02/07 Lab supervisor Philadelphia University, Jordan **Duties:** • Teach and Run Mechatronics System Design Lab • Teach and Run Automatic Control Lab • Teach and Run Microprocessor and Sensors Lab • Teach and Run Mechanics and Vibration Lab
Special Training Courses	• PLC (Programmable Logic Controller) • A+ Computer Maintenance • CISCO • MATLAB • DSP (Digital Signal Processing) • PIC (Peripheral Integrated Circuit)
Honors and Awards:	• Chancellor Awards 2008-2018
Publications	• H. M. Alqam and A.K. Dhingra (2019), "Frequency Response Based Indirect Load Identification Using Optimal Placement of Strain Gages and Accelerometers", ASME, *Journal of Vibration and Acoustics.*141(3), paper No: VIB-18-1178; doi: 10.1115/1.4042709. • H. M. Alqam and A.K. Dhingra (2019), "Motion Transmissibility for Load Identification Based on Optimum Sensor Placement", Hindawi, *Shock and Vibration,* vol. 2019, article ID 7810686.